UNIVERSITÀ DEGLI STUDI DI PARMA

Doctoral Program in Industrial Engineering

IMPROVEMENT OF METAL-TO-METAL ADHESIVE JOINT STRENGTH BY PRETREATMENT OF SUBSTRATES WITH A YB-FIBER PULSED LASER

Doctoral Dissertation by

Giovanni Chiodo

SUPERVISOR
Prof. Alessandro Pirondi

THE CHAIR OF THE DOCTORAL PROGRAM
Prof. Agostino Gambarotta

XVII CYCLE

To my family

All collected data had come to a final end.

Nothing was left to be collected.

(Isaac Asimov)

Abstract

Adhesive bonding is nowadays successfully employed in a wide range of engineering application and ensures greater design flexibility, more efficient production and improved performance compared to the traditional joining technologies. The most important applications of adhesive bonding include microelectronics devices, civil infrastructures, aerospace industry, etc. The strength and reliability of adhesive joints strongly rely on the establishment of intermolecular forces at the adhesive/substrate interface. As a consequence, substrate surface preparation before bonding plays an important role. Surface treatments, such as mechanical grinding or sandblasting, have been widely employed in order to increase surface roughness and joint strength. A viable alternative to mechanical treatments is represented by chemical etching, which promotes the formation of a surface morphology enabling an improved mechanical interlocking. On the other hand, anodizing processes affect adhesion and durability by mean of an electrochemically formed porous oxide film that improves chemical interaction between the adhesive and the adherends. Recent works have focused on laser irradiation carried out by mean of excimer, solid state or fiber lasers, e.g. ytterbium (Yb) fiber laser. Experimental data have shown that a pulsed laser surface pretreatment can induce a beneficial action on the strength of adhesive

joints. This is due to the contaminants removal and to the favorable changes in both the chemical composition and surface morphology.

The present work of thesis describes an experimental study about the shear strength and the mode I fracture toughness of adhesive joints with laser ablated metal substrates. An ytterbium-doped pulsed fiber laser was employed to perform laser ablation on AA6082-T4 aluminum alloy and on AISI304 stainless steel. Morphological and chemical modifications induced by laser irradiation were evaluated by means of surface profilometry, scanning electron microscopy (SEM) and X-Ray photoelectron spectroscopy (XPS). In addition, surface wettability was analyzed by means of the sessile drop technique. In order to assess the capability of laser ablation to improve mechanical interlocking, cross-sectional areas of the samples taken across the interfacial region were probed under an optical microscope.

Single lap shear tests (SLS) and thick adherend shear tests (TAST) were carried out on AA6082-T4 and AISI304 samples in order to assess shear strength while the mode I fracture toughness was determined using the Double Cantilever Beam (DCB) test on aluminum samples only . For comparison, control samples were prepared using classical surface degreasing and grit blasting.

The obtained results indicated that laser ablation has a favorable effect on both the shear strength and fracture toughness of Al/epoxy joints. Indeed, a +20% increase was recorded for the shear strength, while a remarkable three-fold enhancement for the mode I fracture toughness was observed with respect to control samples. On the other hand AISI304 TAST samples showed a +77% increase of the average shear stress at failure with respect to simple degreasing.

Contents

List of Figures

List of Tables

Nomenclature

a_0	Initial pre-crack of a DCB Specimen
b	Adherend Width
c	Light Velocity
D_0	Diameter of Collimated Laser Beam
E	Young Modulus
E'_a	Plain Strain Young Modulus
f	Focal Length
G	Strain Energy Release Rate
G_{Ia}	Mode I Crack Arrest Strain Energy Release Rate
G_{Ic}	Mode I Critical Strain Energy Release Rate
h	Planck Constant
h_A	Adherend Thickness
I	Intensity of Radiation
I_m	Melting Laser Intensity Threshold
I_p	Plasma Formation Laser Intensity Threshold
I_v	Evaporation Laser Intensity Threshold

L	Adherend Length
M^2	Laser Beam Propagation Factor
n	Index of Refraction
R_a	Average Roughness
$R_{R\perp}$	Reflectance Coefficient in the Plane Perpendicular to Incidence Plane
$R_{R\parallel}$	Reflectance Coefficient in the Incident Plane
R_r	Reflectance Coefficient
R_q	Root Mean Square Roughness
R_z	Maximum Excursion of Surface Profile
S_k	Kernel Roughness
t	Adhesive Thickness
α	Thermal Diffusivity
ΔH_V	Molar Heat of Vaporization
δ	Optical Penetration
δ_s	Solubility Parameter
γ_{lg}	Liquid Surface Free Energy
γ_{sg}	Solid Surface Free Energy
γ_{sl}	Solid-Liquid Interfacial Free Energy
λ	Light Wavelength
μ	Absorpion Coeffieceint
ν	Wave Frequency
ω_0	Laser Beam Waist Radius

σ	Laser Beam Divergence Angle
τ_0	Apparent Shear Stress
θ_c	Contact Angle
θ_i	Angle of Incidence of Light
$\overrightarrow{E}$	Oscillating Electric Field
$\overrightarrow{H}$	Magnetic Field

Chapter 1

Introduction

Adhesive bonding is nowadays widely employed for several structural applications, ranging from microelectronic devices and civil structures to aerospace applications. It ensures great design flexibility, more efficient production and, in many cases, improved performances compared to other well known joint techniques. It is also considered a key technology to build complex lightweight structures that are able to fulfill the required functions for a desired lifetime. [2]

> *"An adhesive may be defined as a material which when applied to surfaces of materials can join them together and resist separation."*

This definition was proposed by Kinloch in 1987 [3]. The key to a successful structural bonding is the correct design of the bonded area, based on the material properties of the substrates, the expected load and the required stiffness of the bonded structure but it is also important to assess how the adhesive can contribute to the structure and durability under the expected operating conditions.

The main component of an adhesive is an organic polymer, or two compound that can chemically react to create a polymer. During the application the adhesive is liquid, and this can allow intimate molecular contact with the adherends. After application the adhesive must be hardened (cure) to become a cohesive solid. An exception is represented by pressure-sensitive adhesives because they do not harden and remain permanently sticky.

Adhesive and sealants can be classified by the manner in which they harden that can be by loss of solvent, loss of water, cooling or chemical reaction. Once hardened the polymer in the adhesive can be linear or cross-linked. All structural polymers are cross-linked. Nowadays a large selection of structural adhesives is available to the engineer, but considering a number of key parameters the selection can be simplified. The major key parameters include:

- ◇ adhesive form/structure
- ◇ mode of adhesive cure
- ◇ substrate compatibility and operating environment
- ◇ joint design

Depending upon the application, each parameter can have different priority and it is not uncommon for an iterative approach to be taken.

1.1 Adhesive structure

Adhesives exist in a wide variety of physical forms including two-parts liquid adhesives, single-parts liquid adhesives, single or double sided tapes, films with or without carrier, single-part solid. [4]

The key influence of chemistry over the form supplied is based upon the curing mechanism. Two-parts adhesives are made up by two liquids at room temperature which react chemically when they are brought into contact. The level of mixing required is dictated by the chemical reaction mechanism.

Single-part adhesives either have both components mixed together but in a non reactive state or are single component systems which use an external agent to initiate cure (e.g., moisture cure, UV cure).

Pressure sensitive tape are in general non-chemically curing adhesives and the tape carrier provides the most convenient means of dispensing such system.

Adhesive films are often solid or semi-solid version of single-part liquid adhesives made up by a carrier in the form of a woven or non-woven substrate used to support the film. The carrier provide additional levels of toughness and acts as a bond-line thickness control layer.

However, although chemistry is very important, the types of application that the adhesive has been formulated for dominate the final physical form. Adhesives are, in the majority of cases, complex mixtures of different materials, including reactive agents which provide structural adhesion, rheology modifiers, fillers to control shrinkage, thermal expansion and bond-line control, adhesion promoters, toughening agents, cure initiators and so on. For this reason some adhesives, most notably the epoxies, can contain the same basic chemistry but exist in many different forms depending upon what is required with regard to the method of application, joint type, dimensions, cure type and so on.

1.2 Adhesive cure

The method by which an adhesive is cured is extremely important for selecting the most suitable one. For example, some applications require fast curing adhesives, perhaps a two-parts toughened acrylic system over an epoxy with similar mechanical performances. However, if the bond area is large, a rapid cure system may require a rate of mixing and dispensing that may not be possible. In this case a slower curing formulation or one in which it can be controlled in other way may be more appropriate (e.g., by heat, radiation, pressure). On the other hand, when small joints are produced in very high volumes, the adhesive used may require a rapid cure , for example through the use of cyanoacrylate or a UV cure adhesive.

In other applications there may be a need to apply a very specific amount of adhesive, in terms of bond-line thickness and coverage, over a large bond area, i.e., in composite bonding. If this is the case, a film adhesive would be the best solution owing to the fact that it can be cut precisely to shape and easily placed in position. The adhesive will not cure until the joint is assembled and necessary pressure and temperature applied.

However it is important to recognize that the type of substrate to be bonded can greatly influence the range of curing mechanism that could be applied (e.g., transparent substrates, thermally sensitive substrates).

Finally, the economics of manufacturing can have an important impact on the choice of cure mechanism and type of adhesive. A room temperature curing system normally requires little more

than investment in the appropriate mixing dispensing equipment, whereas additional equipment is required to cure other systems (e.g., UV source, ovens, autoclaves).

1.3 Substrate compatibility

The nature of substrate may have a great influence on the type of adhesive that can be applied. The influence may be positive or negative depending on the type of sensitivity. In the case of some polymeric materials that are susceptible to stress cracking, such as polycarbonates, polystirene or ABS, adhesives that contain low molecular weight components (e.g, cyanoacrylates, toughened acrylics) may act as solvents, causing whitening or blooming of the polymer in contact with the adhesive. Sensitivity can also influence the cure mechanism, for example for cyanoacrylates, a low pH and the presence of adsorbed water can promote cure. On the other hand epoxy adhesives are much less substrate sensitive. Anaerobic adhesives require contact with metal to facilitate cure and although any metal will promote it, some will enhance the rate of curing (e.g., copper), whereas other, such as zinc, may require a secondary catalyst or primer. Bonding to non-metal materials will require the application of an appropriate primer or catalyst on the substrate to reach an adequate bonding strength.

1.4 Joint design

What the joint has to do in service play a key role in the selection of the correct adhesive. Sometimes it has to tolerate adverse environment (e.g., wet, acid, alkaline, solvent) or high temperatures, survive high loading levels or impact conditions. Some or all of these factors may control the form or type of adhesive that should be considered. For example a brittle, high strength adhesive would not be suitable for a structure that has to suffer impact loading, whereas an opaque adhesive may not be considered for a glass bonding application.

The design of the joint may also influence selection of adhesive. A small joint area or bond-line thickness may require very different forms of adhesive with respect to a large bonding area. Where very high levels of joint tolerance are present, as in composite-metal or composite-composite bonding, a film adhesive may be more suitable

than a paste system. In some cases the joint may have a very complex geometry and the access to all areas could be difficult. An appropriate adhesive may have to be one that can be injected into the joint from a particular position, thereby eliminating solid or semi-solid adhesives or pastes.On the other hand, joint surfaces may be in vertical or overhead positions, requiring tixotrophic adhesive formulations.

1.5 Mechanism of adhesion

The generation of intrinsic adhesion forces across the interface, and the nature and magnitude of such forces are extremely important. They must be sufficiently strong and stable to ensure that the interface does not act as the "weak link" in the joint, either when the joint is initially made or throughout its subsequent service life. The various types of intrinsic forces which may operate across the adhesive (or primer)/substrate interface are commonly referred to as the *mechanism of adhesion.*

The molecular forces in the surface layers of the adhesive and substrate greatly influence the attainment of intimate molecular contact across the interface and such molecular forces are now frequently the main mechanism of adhesion, and this is called the adsorption theory of adhesion. However, this is only one of the four main mechanism of adhesion which have been proposed, namely:

- ◇ mechanical interlocking
- ◇ diffusion theory
- ◇ electronic theory
- ◇ adsorption theory

Some years ago many workers searched for "the mechanism of adhesion", but more recently it has become generally accepted that, whilst the adsorption theory has the widest applicability, each of the others may be appropriate in certain circumstances and often make a contribution to the intrinsic adhesion forces which are acting across the interface. Much of the confusion that has arisen in the literature concerning the mechanism of adhesion has undoubtedly been caused by the methods commonly employed to measure

the strengths of adhesive joints not being well suited to ascertaining the magnitude of the intrinsic adhesion forces which are acting across the adhesive/substrate interface. They introduce geometrical and loading factors which are difficult to analyze, and the measured joint strength typically includes contributions from from rheological energy losses in the adhesive and substrates. Thus, although the intrinsic adhesion forces influence the joint strength they are usually completely obscured by other contributions. Information about the magnitude of such forces may therefore usually only be obtained indirectly, or by the use of especially developed continuum fracture mechanism approaches.

1.5.1 Mechanical interlocking

This theory essentially proposes that mechanical keying, or interlocking, of the adhesive into the irregularities of the substrate interface is the major source of intrinsic adhesion. However, the attainment of good adhesion between smooth surfaces exposes the mechanical interlocking theory as not being of wide applicability. For example, Tabor [5] studied the adhesion between two perfectly smooth mica surfaces and Johnson [6] examined the adhesion to optically smooth rubber surfaces, clearly demonstrates that adhesion may be attained with smooth surfaces. Also, detailed examination of surfaces roughened by typical industrial pretreatment methods, for example, grit-blasted metallic substrates (Fig.1.1 and Fig.1.2), usually reveals little indication of cavities such as "ink-bottle" pits which would enable mechanical interlocking to be the major mechanism of adhesion.

in the case of the anodization of aluminum alloys a deep porous topography is produced and, with many of the more open porous structures, the adhesive (or primer) typically penetrates to virtually the bottom of the pores, and so a "composite" interfacial region is created. This composite region will have a modulus and strength intermediate between that of the polymeric adhesive and the oxide and this would be expected to be beneficial from the viewpoint of joint strength and toughness. However, considering the role of mechanical interlocking really does occur [7] and secondly, even if it does, to asses its contribution to the strength and stability of the interface. There is much work to be found in literature which convincingly demonstrates that increasing the surface roughness of

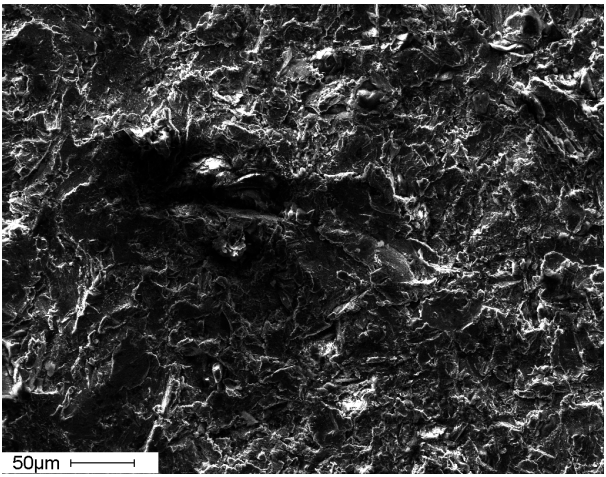

Figure 1.1: Scanning electron micrograph of an abraded stainless steel surface.

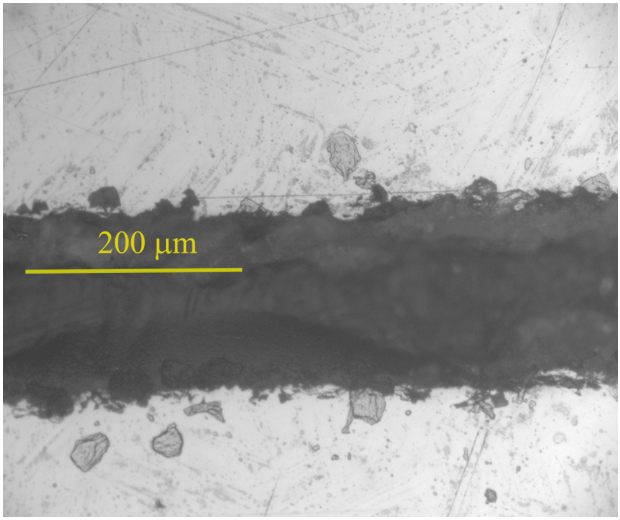

Figure 1.2: Cross-sectional view of a grit blasted steel/epoxy joint.

the substrate may increase the measured strength of the adhesive joint.

1.5.2 Diffusion theory

Voyutskii [8, 9, 10] is the chief advocate of the diffusion theory of adhesion which states that the intrinsic adhesion of polymers to themselves (autoadhesion), and to each other, is due to mutual diffusion of polymer molecules across the interface. This requires that the macromolecules, or chain segments of the polymers (adhesive and substrate) possess sufficient mobility and are mutually soluble. this requirement may be restated by the condition that they possess similar values of solubility parameter. The solubility parameter, δ_s, may be defined by:

$$\delta_s = \left(\frac{\Delta H_V - RT}{V} \right)^{1/2} \tag{1.1}$$

where ΔH_V is the molar heat of vaporization, R is the gas constant, T is the temperature $[K]$ and V is the molar volume. Hence, the solubility parameter is an index of the compatibility of two components, e.g. if an amorphous polymer and a solvent have similar values the they should form a solution. (The added need for the polymer to be amorphous is included since if the polymer possess a significant degree of crystallinity then the free energy of crystallization makes it more resistant to dissolving in the solvent. The concept of a solubility parameter does not take this aspect into account.)

1.5.3 Electronic theory

If the adhesive and substrate have different electronic band structures there is likely to be some electron transfer on contact to balance the Fermi levels which will result in the formation of a double layer of electrical charge at the interface. The electronic theory of adhesion is due primarily to Deryaguin [11, 12, 13] and he has suggested that the electrostatic forces arising from such contact or junction potentials may contribute significantly to the intrinsic adhesion. The controversy of this theory is due to this final statement

that such electrostatic forces are an important *cause*, rather than merely a *result*, of high joint strength

1.5.4 Adsorption theory

The adsorption theory of adhesion is the most widely applicable theory and proposes that, provided sufficiently intimate molecular contact is achieved at the interface, the materials will adhere because of the interatomic and intermolecular forces which are established between the atoms and molecules in the surfaces of the adhesive and substrate. The most common such forces are van der Waals forces and these are referred to as secondary bonds. Also in this category may be included hydrogen bonds. In addition, chemical bonds may sometimes be formed across the interface. This is termed chemisorption and involves ionic, covalent, or metallic interfacial bonds being established; these types of bonds are referred to as primary bonds. The terms primary and secondary are in a sense a measure, although somewhat arbitrary, of the relative strengths of the bonds. This may be appreciated from Table 1.1 [14, 15, 16], where the various types of bonds are shown together with estimates of the range of magnitude of their respective bond energies. Also, it has been proposed that donor-acceptor interactions may occur across an interface and these are typically intermediate in strength between secondary and primary bonds. Finally, it has also been suggested that interfacial molecular complex structures may, in certain circumstances, be established.

1.6 Epoxy adhesives

Epoxies are the best known and most used structural adhesives and they have the widest range of application of the various classes of adhesives arising principally from their broad set of performance properties. They bond well a wide range of materials, especially metals, ceramics and most polymers. They exhibit good chemical resistance, do not produce volatiles during curing and have very low shrinkage values. Therefore they have the capability to form extremely strong and durable bonds with most materials in well-designed joints. For these reasons epoxy adhesives can be successfully employed in place of traditional joint techniques (e.g., welding, bolts, rivets).

Type	Bond energy $[kJ/mol]$
Primary bonds	
Ionic	600-1100
Covalent	60-700
Metallic	110-350
Donor-acceptor bonds	
Bronsted acid-base interactions	Up to 1000
Lewis acid-base interactions	Up to 80
Secondary bonds	
Hydrogen bonds	
Hydrogen bonds involving fluorine	Up to 40
Hydrogen bonds excluding fluorine	10-25
van der Waals bonds	
Permanent dipole-dipole interactions	4-20
Dipole-induced dipole interactions	Less than 2
Dispersion (london) forces	0.08-40

Table 1.1: Bond types and typical bond energies. [14, 15, 16]

Structural epoxy adhesives have been used in numerous industries including construction, electrical and electronic, medical and all branches of transportation segment. For most structural applications, cure at high temperatures is required to achieve ultimate strength. However, the construction industry, in particular, most often must work with adhesives that cure entirely at ambient temperature.

Fields such as electronic and medicine or dentistry have other special restrictions. In electronics, ionic impurities must be severely limited and and, due to the particular chemical reaction further purification of the product epoxy resin is required.

The mechanism of curing is always the same. This mechanism requires precise quantities of resin and hardener and without the correct ratio between the two components curing will be affected resulting in lower strength and stiffness and reduced environmental resistance.

Two-part epoxy adhesives start to react under ambient conditions once the two components have been mixed together. However the reaction rate is strongly influenced by temperature and it approximately doubles for every 10°C rise.

Single-part epoxy adhesives require heat to cure. The resin and hardener are premixed but curing does not occur at room temperature because the catalyst is in an inactive form. It can become reactive only above a certain temperature level and the higher the temperature, the faster the reaction becomes.

1.7 How to assess surface modifications

As already said in the previous sections adhesive bonding relies on the establishment of intermolecular forces between a substrate and the polymeric adhesive itself. To this end it is necessary to pretreat the substrate in some manner so as to confer the required surface properties; this may be a simple abrasion treatment or a more sophisticated method such as acid anodizing. In a similar vein, chemical methods such as a corona discharge treatment used on polyolefins, or the application of a primer solution based on an organosilane adhesion promoter, may be used to ensure the required durability of an adhesive joint. In all cases, the performance of the adhesive joint is directly related to the successful application of such a pretreatment, and an important part of the development of a new pretreatment procedure or the quality assurance of an established process is the assessment of the surface characteristics, both in terms of topography and chemistry.

The methods that are commonly used by the adhesive bonding technologist for the assessment of the surface characteristics of solid substrates prior to bonding are several. Surface topography is generally investigated by stylus profilometry, electron microscopy and scanning probe microscopy, the assessment of the wetting and spreading of liquids on solid surfaces and the surface chemical analysis of surfaces by X-ray photoelectron spectroscopy (XPS), Auger electron spectroscopy (AES) and time-of-flight secondary ion mass spectroscopy (ToF-SIMS).

The need to assess the surface properties of an adherend is most likely related to one of two rather fundamental questions: on the one hand, there is a need to know the condition of the surface as delivered (from internal or external sources): this encompasses the need to be aware of the presence of temporary protective coatings that may give rise to weak boundary layers in the eventual adhesive joint. But also, there is a requirement to determine the chemical and phys-

ical changes that have been brought about by specific pre-treatment applied as part of the adhesive bonding system. In the latter category, the need may be related to a quality assurance requirement, but it is more likely to be encountered during the development of a new or improved pre-treatment process.

There is a wide variety of reason that leads one to assess the properties of a substrate for adhesive bonding. These range from ensuring it is clean, through the need to assess the quality of a pre-treatment, or perhaps to relate it to performance, to the forensic examination of failure surfaces either from a laboratory test or an in-service failure. The variety of possible methods that can be used is equally as broad, ranging from a simple water break test to a sophisticated method such as surface chemical analysis. The choice of test method will depend on many factors, not least the test environment, financial constraints, and the aim of making the analysis. Quality assurance and research activities will have very different requirements.

Therefore, to obtain a clear, concise, and accurate picture of a surface it will be essential to use more than one method and the best combination is probably to use SEM and stylus profilometry for surface topography, contact angle measurements to deduce the surface free energy, and XPS to provide surface chemical analysis. This will enable quantitative comparison of the important characteristics of the surface and enable the changes brought about by, for example, surface treatment, to be related to adhesive bond performance. All these techniques will be described in detail in Chapter 3.

1.8 Basic Mechanical testing of adhesive joints

The successful use of adhesives in load-bearing engineering structures relies critically on a correctly balanced interaction between design, testing, and experience. First, it is necessary at the design stage to know what loads are likely to occur in practice and in the lifetime pattern over which these loads will act. Knowing the lifetime loading pattern, the designer can initially introduce safety factors to reduce the problem to one of short-term loading. Experience, rather than an understanding of the fundamental mechanics, is usually the guide regarding the factor to be applied. In short, the

development of a successful design methodology can be achieved only by underpinning it with a testing program.

Often it is not necessary to test a whole component or structure in order to ascertain the likely behavior under load. For instance, if aluminum sheet, which is made to recognized standards, is bonded into a structure, it is usually only the quality of the adhesive bond that needs to be assessed.

1.8.1 Single-lap shear test

Despite all its obvious weaknesses, the lap-shear test is the most widely used method for producing in-situ shear strength data of an adhesively bonded joint. The test consists essentially of two rectangular sections bonded together with an overlap length of l. The single-lap specimen is easy to prepare and test. A fixture is used to ensure correct overlap and accurate alignment of the adherend. This may include control of the fillet. Testing can be conducted using standard tension/compression mechanical test equipment. The average shear stress (τ_m) for the single-lap joint shown in Fig. 1.3 is given by:

$$\tau_m = {}^{P}\!/_{bl} \tag{1.2}$$

where P is the applied load, b is the joint width, and l is the joint length. Many designers analyzing stresses find this simple equation, which is the definition of adhesive shear strength used in standard tests such as ASTM D 1002, to be sufficient. The equation is, of course , rather simplistic and does not take into account the flexibility of the adhesive and the adherends.

Figure 1.3: Single lap joint specimen.

Volkersen [17] tried to analyze the stresses in riveted panels, but could deal only with the case of an infinite number of tiny rivets, which effectively created a continuum, for which he developed his

well known shear lag equations. The continuum is, of course, identical to the case of an adhesive layer. Volkersen assumed that the adhesive deformed only in shear and that the adherends deformed only in tension. The equation he developed for the shear stress distribution at any position x along the length of a single-lap joint is:

$$\bar{\tau} = \frac{\omega}{2}\frac{\cosh \omega X}{\sinh \omega/2} + \left(\frac{\psi - 1}{\psi + 1}\right)\frac{\omega}{2}\frac{\sinh \omega X}{\cosh \omega/2} \tag{1.3}$$

where $\omega^2 = (1 + \psi)\phi$, $\psi = {}^{t_1}/_{t_2}$, $\phi = {}^{Gl^2}/_{(Et_1t_3)}$, $X = {}^{x}/_{l}$, and $-{}^{1}/_{2} \leqq X \leqq {}^{1}/_{2}$. In addition, G is the shear modulus of the adhesive, E is the Young's modulus of the adherends, l the length of the bonded region, t_1 and t_2 are the thicknesses of the adherends and t_3 the thickness of the adhesive. $\bar{\tau} = {}^{\tau_x}/_{\tau_m}$, where τ_m is the average applied shear stress as defined in Eq.1.2.

But Volkersen ignored the fact that the directions of the two forces in Fig.1.3 are not collinear, which creates a bending moment applied to the joint in addition to the in-plane tension. The ad-

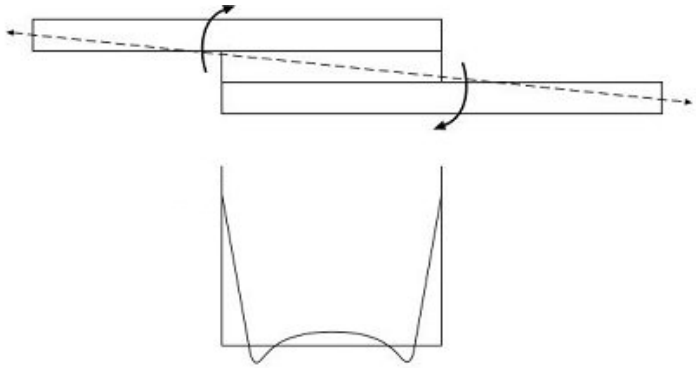

Figure 1.4: Transverse (peel) stresses in a single-lap joint according to Goland and Reissner.

herends bend, and the rotation alters the direction of the load line in the region of the overlap in such a way that the joint displacements are no longer directly proportional to the applied load. Goland and Reissner [18] took this effect into account by using a bending moment factor (k), which relates the bending moment on the adherend at the end of the overlap (M_0) to the in-plane loading, by

the relationship:

$$M_0 = {}^{kPt}/_2 \tag{1.4}$$

where t is the adherend thickness. If the load on the joint is very small, no rotation of the overlap takes place; thus, $M_0 = {}^{Pt}/_2$, and $k = 1.0$. As the load is increased, the overlap rotates, bringing the line of action of the load closer to the centerline of the adherends, thereby reducing the value of the bending moment factor. Goland and Reissner gave a similar shear stress distribution to that of Volkersen, but also gave the transverse (peel) stresses σ_y, in the adhesive layer as:

$$\begin{aligned}\sigma_y &= \frac{\sigma t^2}{C^2 R_3}\left[\left(R_2\lambda^2\frac{k}{2} - \lambda k^{'}\cosh\lambda\cos\lambda\right)\cosh\frac{\lambda x}{C}\cos\frac{\lambda x}{C} + \right. \\ &\left. + \left(R_1\lambda^2\frac{k}{2} - \lambda k^{'}\sinh\lambda\sin\lambda\right)\sinh\frac{\lambda x}{C}\sin\frac{\lambda x}{C}\right] \end{aligned} \tag{1.5}$$

where σ is the mean tensile stress in the adherends, t is the adherends thickness, x is the position along the glue line, $C = {}^{l}/_2$, $\lambda = {}^{C}/_{t\left({}^{6E_3 t}/_{Et_3}\right)^{1/4}}$, $k^{'} = k\left({}^{C}/_{t}\right)\left[3\left(l-\nu^2\right){}^{\sigma}/_{E}\right]^{1/2}$, $R_1 = \cosh\lambda\sin\lambda + \sinh\lambda\cos\lambda$, $R_2 = \sinh\lambda\cos\lambda - \cosh\lambda\sin\lambda$, $R_3 = {}^{(\sinh 2\lambda + \sin 2\lambda)}/_2$and ν is the Poisson's ratio. The shear and peel stresses were both assumed to be uniform across the adhesive thickness, and it can also be seen from Fig.1.4 that the maximum values of peel stress occur at the ends of the overlap.

Therefore, the eccentricity of the load path causes out-of-plane bending moments, resulting in high peel stresses and non-uniform shear stresses in the adhesive layer. This effectively reduces the structural efficiency of the joint.

The main problem with the single-lap shear test is that the average shear strength determined using this method does not correspond to a unique material property of the adhesive and therefore cannot be used as a design parameter. [19]

1.8.2 Thick adherend shear test

An alternative approach for determining the shear properties of an adhesive is to apply uniaxial tensile or compressive load to a specimen consisting of thick, rigid adherends, with a short overlap length. This test geometry was developed to overcome the inherent weaknesses of the single lap shear test.

The specimen can be produced by one of two methods:

- ◇ Bonding two pre-shaped bars together;
- ◇ Bonding two sheets together and then milling two parallel slots.

UNI EN 14869–2, Fig.1.5, specifies a specimen with an overall length of 110 mm, a width of 25 mm and an overlap length of 5 mm. The adherend thickness is 6 mm and the bondline thickness is typically 0.5 mm. Load is introduced to the specimen via two 12.7 mm diameter pins inserted in holes 80 mm apart. Care is needed to ensure

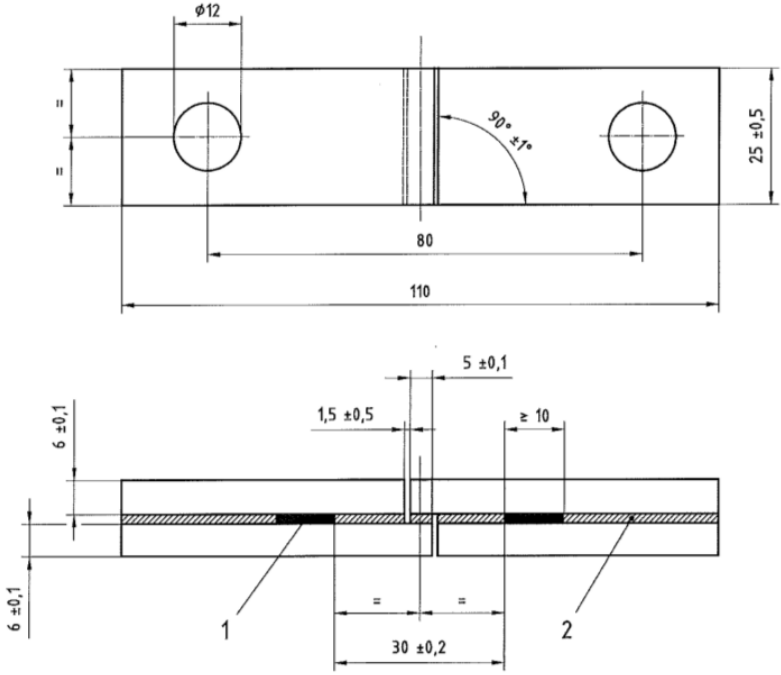

Figure 1.5: TAST specimen with flat-ended adherends according to UNI EN 14869–2 .

that the holes are accurately drilled in the center of each adherend, since small misalignments can result in unwanted rotation and uneven loading of the joint, thus compromising the test data. Testing

can be conducted using a standard mechanical test machine. It is important to ensure that no coolants are used when machining the two parallel slots, as the coolant may react with the adhesive or penetrate the adherend-adhesive interface. Localized increases in temperature may also result in thermal degradation of the adhesive properties.

The stress distribution along the overlap length is predominantly shear with large peel stresses present at the corners of the overlap. The large peel stresses may cause premature failure. However, adding a fillet to the end of the bondline may reduce the high concentration of peel stresses.

The average shear stress τ_m is given, in the same manner as in single-lap shear test, by Eq.1.2. [19]

1.8.3 Mode I double cantilever beam test

The crack growth in adhesive bond specimens can proceed in two ways:

- ◇ Slow-stable extension where the crack is dictated by the displacement rate.
- ◇ Run-arrest extension where a stationary crack abruptly grows at a rate that exceeds the cross-head speed.

Terms associated with run-arrest crack growth are given below:

- ◇ Opening mode fracture toughness, G_{Ic}: The value of G_I just prior to the onset of rapid fracture is determined from the load required to initiate crack growth.
- ◇ Opening mode crack arrest toughness, G_{Ia}: The value of G_I just after arrest of a run-arrest segment of crack extension is determined from the load required for crack arrest.

Although, this test has attracted considerable academic interest, it is not widely used in industry. The method is covered in ASTM D 3433 [20], Fig.1.6. The test is used to measure the initiation and propagation values of G_I under static and cyclic loading conditions. A tensile load is applied to a specimen with an embedded through-width insert (i.e. debond) at the specimen mid-plane. The tensile force acts in a direction normal to the crack surface. Specimens are typically 25 mm wide and 356 mm long. The adherend thickness

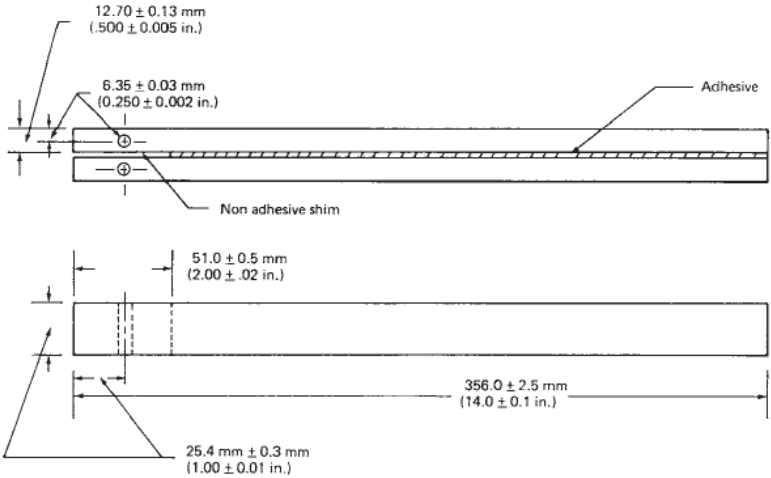

Figure 1.6: DCB flat adherend specimen according to ASTM D 3433-99. [20]

is typically 6.35 mm (0.25 inches). Crack length is measured using either a travelling microscope, a crack gauge or video camera. The use of a crack gauge enables crack measurement to be automated.

The critical strain-energy release rate or fracture toughness G_I is calculated as follows:

$$G_{Ic} = \frac{4P^2\left(3a^2 + h^2\right)}{Eb^2h^3} \tag{1.6}$$

where P is applied load, E is the flexural modulus of adherend in the longitudinal direction, b is the specimen width, a is the crack length and h is the adherend thickness. The analysis assumes linear elastic behavior and no large displacement effects. To determine G_{Ic} and G_{Ia} values, the corresponding applied load values P_{MAX} and P_{MIN} are substituted into the above equation.

Experimental compliance method equation for G_{Ic} is:

$$G_{Ic} = \frac{P^2}{2b}\frac{dC}{da} \tag{1.7}$$

Non-linear load-displacement response may result from inelastic material behavior and/or sub-critical damage formation in front of the

planar crack (i.e. micro-cracking and extensive deformation) or by large beam deflection. The latter can be associated with materials with low flexural stiffness or loss in flexural stiffness resulting from substantial crack growth. Fabrication and testing of DCB specimens is straightforward and relatively inexpensive. Testing can be conducted using standard mechanical test frames. Specimen fabrication is identical to that employed for wedge cleavage specimens. Reusable aluminum loading blocks are recommended. Both static and fatigue loading can be used with these specimens. Tests may also be conducted under simulated service environments such as hot humid environments. [21]

1.9 Surface pretreatment

Normally it is recommended that the adherend surface is adequately prepared prior to bonding. Many pretreatment are available ranging from a simple solvent wipe to a more complex process such as chemical etching, anodizing, sandblasting or laser treatment.

The method chosen depends on the nature of the substrate, the conditions to which the adhesive joint will be subjected, environmental factors and cost. A pretreatment can act by removing potential weak boundary layers, by altering the surface topography, by modifying the chemistry of the substrate or by a combination of all these mechanisms.

If a cohesively weak layer is present in an adhesive joint then failure will occur at a low applied load. This kind of layer is often named weak boundary layer. Typical examples include lubricant layers, polymer additives and weak metal oxides.

Topography affects the level of adhesion because it will determine the degree of contact between the adhesive and the substrate and it may lead to a good mechanical keying. Surface chemistry is important because it affects the wetting of surface and the degree of interaction across the substrate-adhesive interface where wetting has occurred.

Surface treatments can be classified into physical and chemical methods. Physical methods include solvent degreasing and grit blasting. These treatments are able to remove cohesively weak layers from a substrate and they can also modify topography. Chemical include flame or plasma treatment of polymers, anodizing and laser

procedures for metals (laser treatments are actually able to modify both the topography and the chemistry of the substrate). All these processes cause chemical modification to the substrates.

A satisfactory performance of adhesive joints in service can be achieved only by a careful selection of a substrate pretreatment.

To understand the effect of pre-treatments on joint performance, it is necessary to have information on the physical and chemical nature of surfaces. This can be achieved by means of modern instruments such as scanning electron microscopes and X-ray photoelectron spectroscopy XPS. Other techniques employed to provide useful information about topography and surface energy include profilometry and sessile drop technique. Normally information on the physical and chemical states of substrates are acquired before and after pre-treatments. Primers can provide several advantages. They have low viscosities and can therefore achieve great contact with the substrate achieving better interaction between adhesive and substrates and inhibiting corrosion of metals. Depending on the nature of substrate, different surface pretreatment are employed.

Inorganic materials (e.g., glasses, ceramics, concrete), although very different, are affected by the same adhesion factors, namely surface chemistry, topography and cohesive strength of surface regions. Glass has been the subject of the most research within this group of materials. Glass has a high surface energy if it is not covered by an organic layer, and under dry conditions it is easy to obtain high joint strengths. However, under wet conditions joint strengths may be greatly reduced due to the strong interaction between glass and water. This led to an extensive programme to improve bond durability. The result was a range of silane "coupling agents" that can greatly increase the resistance of the glass-polymer interface in water acting as a bridge between the glass and the polymer and reducing the loss of mechanical properties [22].

On the other hand, plastics and elastomers have much lower surface energies than metals or glass. Therefore the interaction between polymers and adhesives is generally lower than between metal (oxides) and polymers. However surface energies can vary considerably from one polymer to another. The wetting of PTFE by an adhesive is less complete than that between nylon 66 and the same adhesive. Also the magnitude of the interaction across the interface will be considerably greater in the case of nylon 66.

To achieve satisfactory bonding with PTFE, PE, polypropylene

and other similar plastics it is usually necessary to chemically modify the surfaces of these polymers.

For plastics containing suitable chemical functionality, i.e., the amide group in the case of nylon 66, it may be possible to achieve a good adhesion without pretreatment. In case of weak cohesive layer on nylon 66 a physical method to remove it may be suitable; hence solvent degreasing or grit blasting are often used for such plastics.

Polyolefins such as PE and PP can be treated using several methods, i.e., flame, corona discharge, chromic acid immersion and exposure to chlorine gas activated by UV.

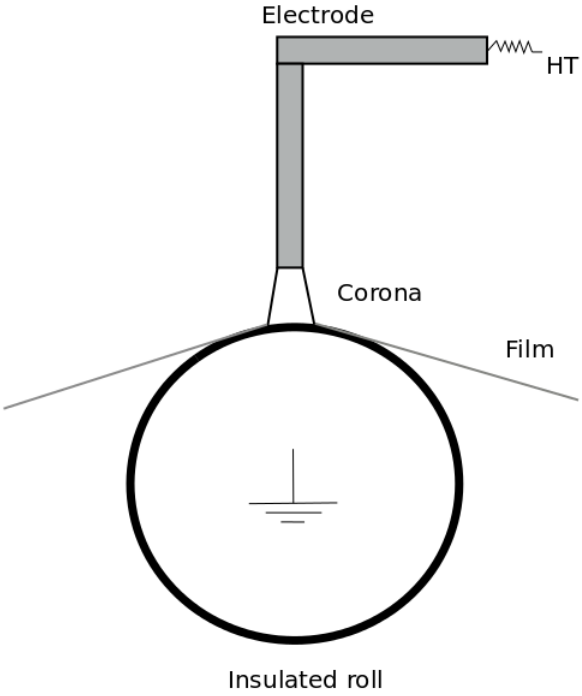

Figure 1.7: Schematic representation of the corona discharge treatment.

The corona discharge method involves decomposing air into active species by the application of a high voltage and it is still preferred for treating film for the packaging industry. Treating speed is

normally set to 3 m/s over an earthed metal electrode at a distance of about 1-2 mm. A high frequency generator and step-up transformer produce a high voltage causing the electrical breakdown of the air with the formation of atoms, ions, electrons and other active species (Fig.1.7).

	Concentration*	
Group	Initial	Water-washed
Peroxide	1.2	0.9
Hydroxyl	1.7	1.1
Carbonyl	1.8	0.9
Epoxide	2.3	1.1
Carboxylic Acid	1.6	0.8
$-NO_3$	0.8	0.4

*Moles of functional species per initial unreacted carbon atom $(\times 10^2)$

Table 1.2: Concentration of different chemical groups after corona discharge treatment of polyethylene. [23]

Surface analysis has shown that the corona discharge treatment introduces various groups, into the polymer surface (Table 1.2) [23]. It is known that some additives, i.e, slip agents, antioxidants, can adversely affect corona treatment if this is not made immediately after processing. If the additives migrate to the surface before the treatment is carried out, the poor adhesion may result because of the tendency to chemically modify the additives rather than underlying polymer chains [23].

Flame treatment (Fig.1.8) involves exposing the plastic for a fraction of a second and it is employed for treating cylindrical objects and also for non regular shapes such as car bumpers. The object to be treated is passed over one or more burners, each of which contains a large number of closely spaced jets, for a very limited time (0.04-0.1 seconds). In one of the first detailed studies of the flame treatment of a polyolefin has been found that higher peel strength were achieved with an excess of air over the stoichiometric ratio required to burn all the alkane gases used. it was concluded that the optimum treatment time was about 0.02 seconds and the optimum distance between substrate and flame inner cone was about $10mm$ [24].

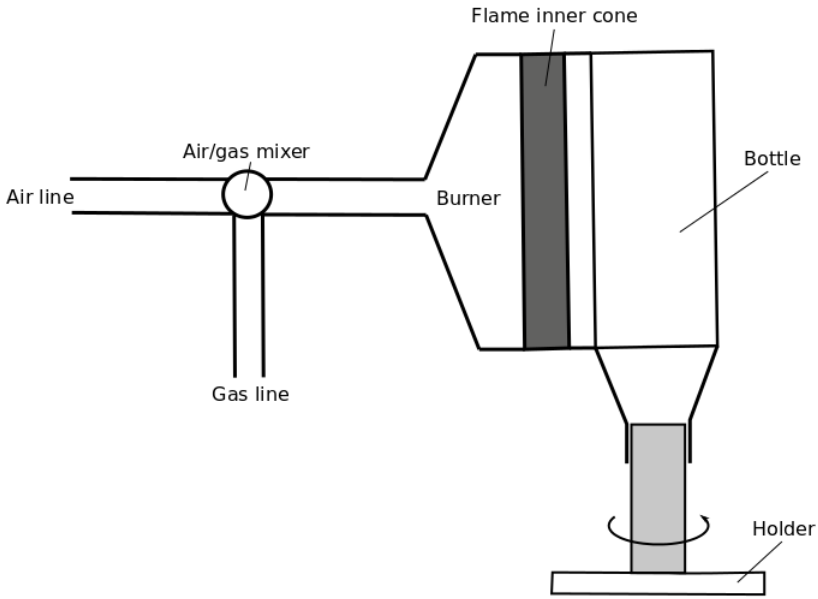

Figure 1.8: Schematic representation of the flame treatment.

Since 1960s, the use of low-pressure plasmas to improve the bondability of polyolefins and other plastics was studied. In this method, power is applied to a gas at low-pressure forming a plasma consisting of ions, electrons, atoms and free radicals. Several parameters control the effect on polymers, including the nature of gas, pressure, flow rate, discharge power, excitation frequency, the nature of polymer and the temperature. The improvement of adhesion may be due to different mechanism such as the removal of surface contaminants, cross-linking of polymers chains, grafting of monomers to a polymer surface and introduction of functional groups. The improvement of adhesion has been demonstrated for a wide variety of polymers. [25][26]

1.10 Metal substrates pre-treatments

Pre-treatments of metal substrates consist of a combination of physical and chemical methods. Physical methods include solvent de-

greasing, abrasion and grit blasting. In case of demanding operating conditions, for example moist environment or high stresses, it is likely that a chemical treatment will b necessary. Pretreatment of metal substrates has been the main subject of many researches. This is especially true for aluminum widely employed for aerospace applications. Methods to pre-treat aluminum have been reviewed by Critchlow and Brewis [27].

1.10.1 Surface treatment of aluminum alloys

Aluminum alloys are generally considered to be difficult to bond. Indeed without a proper surface treatment of the aluminum surface before the bonding, the strength and the retention of the strength during the lifetime of the joint will be poor. This issue has been recognized in the early stages of the application of adhesives metal bonded structures resulting in surface treatments that are very well adapted to the specific demand in this industry. By anodizing, long term durability of bonded joints is obtained, even under extreme environmental and chemical exposure. In Table 1.3 is given an overview of the most well-known surface treatments for metals.

Degreasing is the basic step for all treatments and should be performed in all cases. This can be done either by wiping or by immersing the material in a tank with an alkaline degreasing agent. The process may increase the bond strength but it is generally not able to achieve a good improvement. In fact the natural oxide layer that is still present on the surface has irregular properties and the mechanical strength can be relatively low. In some cases, when certain types of adhesives are used and when the adhesive is not exposed to hostile environment, only degreasing would be enough.

In most cases it is necessary to perform more treatment to achieve good adhesion. Etching treatment is employed in the aerospace industry to remove the natural oxide layer of the aluminum, leaving only a thin but close oxide. Bonding soon after the etching treatment can lead to a good strength of the joint. This process is based on a mixture of chromic and sulphuric acid (CSA) and shows good adhesion and durability properties in combination with phenolic adhesives. Etching process will result in surface microstructures and enhanced initial adhesion. On the other hand the durability of the etched surface in combination with epoxy adhesives is limited. The etched surface treatments showed poor long-term durability with

Category	Surface treatment
Chemical and electrochemical	Degreasing
	Etching/pickling
	Anodizing
	Conversion coatings (e.g., chromate, titanate)
Mechanical	Grinding, scouring brushing
	Grit blasting with corundum
Laser	Laser patterning
Application of adhesion promotors	Application of silanes, sol-gels, primers

Table 1.3: Overview of surface treatments for aluminum alloys.

epoxy adhesives in operational use, especially on clad alloys.

In order to improve the durability of the joint, the etching process has to be followed by an anodizing treatment. This is an electrochemical method carried out to the purpose of creating a surface structure suitable for adhesion. The created oxide layer consist of a porous structure (Fig. 1.9) in which the adhesive is able to penetrate before it cures completely. This is called mechanical interlocking or hooking of the adhesive in the substrate. Another effect of the porous structure is the growth of the total bonding area.

Several different anodizing process are available. One of the most common method is the chromic acid anodizing process (CAA), which is used extensively by the aerospace industry in Europe [28] and has a proven track record of long-term durability in combination with both clad and bare aluminum alloys. In the United States, another CAA process was used for adhesive bonding with partial sealing in a chromate containing rinse after anodizing [29]. The major disadvantage of this process is that hexavalent chromium is used, which is toxic and corrosive.

The sulphuric acid anodizing (SAA) process is not suitable for structural adhesive bonding with rigid adhesives because of the narrower pores on the resulting surface ($10nm$). The adhesive is therefore not able to penetrate resulting in a relatively low strength interfaces. SAA is successfully employed in combination with flexible adhesives.

The above-mentioned CAA anodizing treatment for aluminum

generally results in a good initial strength of the joint and in an excellent durability due to the resulting surface topography and oxide stability. On the other hand, the anodizing process of the aluminum is a relatively complex and expensive process. This has often led to the conclusion that the adhesive bonding of aluminum is not economically viable in applications different from the aerospace industry. However, there are continuous developments in aluminum surface treatment aimed to reduce costs without sacrificing bond strength and durability.

As an alternative to the CAA treatment, a new process is currently under development, the phosphoric-sulfuric acid anodizing (PSA) treatment [30][31]. This results in an oxide layer with the some adhesion performance of the CAA treatment without the environmental penalty of the chromium. Current research aims to find the proper process parameters to obtain the optimal oxide layer for a wide range of aluminum alloys.

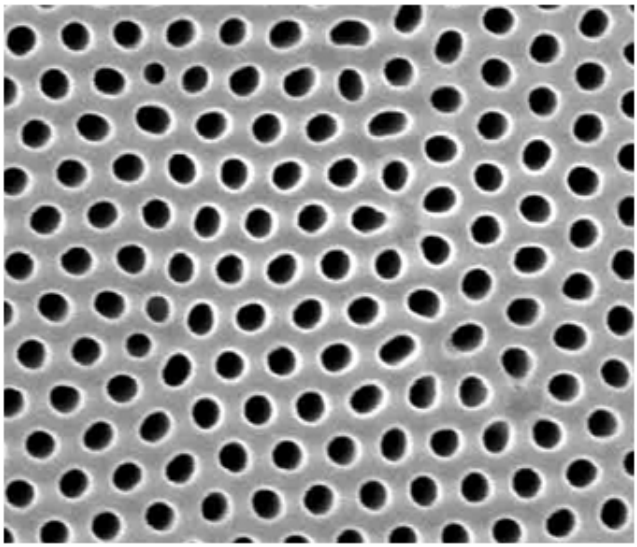

Figure 1.9: SEM image of CAA oxide. [32]

1.10.2 Surface treatment of steel

Steel is generally used in more mundane applications than aluminum and cost considerations demand relatively simple pre-treatments. Grit blasting is often used with mild steel. Stainless steel is likely to be used in more demanding applications and more complex pre-treatments are often necessary. Nowadays in many applications steel is adhesive bonded instead of welded because of improved corrosion resistance, joining of dissimilar materials, increased joint stiffness and fatigue resistance, less heat distortion and, often, more cost effectiveness. In the case where the adhesive joint experience no environmental or chemical exposure, a surface treatment for degreasing and cleaning thoroughly may be sufficient to provide a medium strength bonded joint.

In contrast to aluminum alloys, where the surfaces are usually treated by chemical methods, etching procedures for different types of steel are not recommended [33].

Good bonding results are usually obtained by using abrasive or mechanical roughening techniques like grinding or grit blasting. The best results are obtained using alumina grit (Al_2O_3, corundum) with a particle size between $150 - 250\mu m$. It has to be performed on a clean dry surface in order to prevent contamination of the grit-blasting medium with organic material. For this reason the grit-blasting equipment should be fed with clean compressed air and therefore oil and water separators are necessary.

Abrasive treatments of thin sheet metal may result in warping. In which case an acid-etch solution may be more suitable. Generally a nitric-phosphoric acid solution is employed at room temperature for 5-7 minutes to produce a micro-rough surface morphology and good adhesion and durability on carbon steels.

Stainless or corrosion resistant steels (CRES) are steel alloys containing over 11% of chromium. They are applied in several types of instruments and appliances ranging from automotive and aerospace to food industry and construction materials in large buildings for their chemical and corrosion resistance. Abrasive treatments used for carbon steel do not lead to good results with stainless steel. Grit blasting with alumina improves adhesion but it is also detrimental to the passive layer that protects the stainless steel against corrosion. It sometimes can be used for applications that are not exposed to moisture or corrosive environment.

A number of chemical and electrochemical process improve adhesion on stainless steel. Various strong acid are sometimes used to improve adhesion, resulting in carbon smut layers on the surface of the stainless steel. By brushing off the black deposit or by desmutting in a passivation solution, high strength bonds can be obtained. However, the peel strength of passivated layers is sometimes low.

Another method is the nitric acid anodizing process. After degreasing, the anodizing is performed at a current density of 0.5 A dm^{-2} in a 45-50 vol% nitric acid solution at 50° for 60 minutes. The adhesion and durability of bonded joins on surfaces formed in this process are excellent. The surface of the stainless steel has a microporous morphology and is chromium enriched.

Chapter 2

Laser surface treatments

Laser is an acronym for *Light Amplification by Stimulated Emission of Radiation*. Laser light is essentially a coherent, convergent, and monochromatic beam of electromagnetic radiation with wavelength ranging from ultraviolet to infrared [34].

Light has a dual behavior and can be treated either as a wave according to Maxwell's theory, or as a quantum mechanical stream of particles called photons. Electromagnetic radiations consist of propagating waves associated with the oscillating electric field $\left(\overrightarrow{E}\right)$ and magnetic field $\left(\overrightarrow{H}\right)$. These components oscillate at right angles to each other and also to the direction of propagation of wave.

Since the magnetic field vector is perpendicular to the electric field vector, the description of the propagation of the wave generally considers the oscillation of the electric field vector only. When the oscillations of the electric field vector are in particular order, the light is said to be polarized. In Fig.2.1 a schematic of a plane-polarized wave is shown: the electric field varies in space and time along the x axis sinusoidally, according to the following equation [35, 36]:

$$E = A \sin 2\pi \left(\frac{x}{\lambda} - \nu t\right) \tag{2.1}$$

where A is the amplitude, λ is the wavelength and ν is the frequency of the wave.

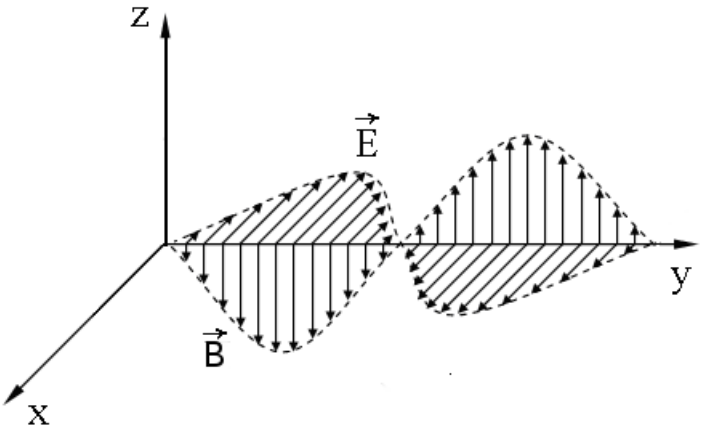

Figure 2.1: Propagation of a plane electromagnetic wave. [34]

From the point of view of quantum mechanic, the electromagnetic radiation is thought of as a stream of particles (photons). Each photon is associated with an amount of energy, which is proportional to its frequency and can be expressed as:

$$E = h\nu = h\frac{c}{\lambda} \tag{2.2}$$

where h is the Planck constant $\left(6.63 \times 10^{-34 J/s}\right)$ and c is the light speed. The shorter the wavelength of the light is, the higher the energy of the photon results; therefore, ultraviolet light is more energetic than infrared light because it has longer wavelength.

The light emitted by laser devices differs from that produced by common light sources with respect to some unique properties, which arise from the stimulated emission process providing the amplification mechanism. These properties are *monocromaticy* and *collimation.* The first one is related to the very narrow finite bandwidth of laser light, which makes it highly monochromatic. The latter is related to the capability of the laser light to propagate with very small *divergence*, that is with approximately constant beam radius. For this reason laser light can be focused on a small area at long distances.

A laser beam is defined *diffraction-limited* when its potential to be focused to small spots is limited only by the effects of diffraction.

For a given optical power and wavelength, a *diffraction-limited* beam

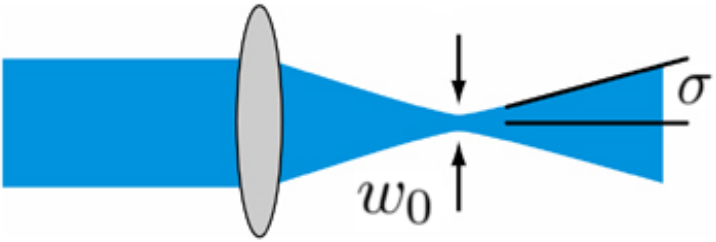

Figure 2.2: Schematic representation of a Gaussian beam described by the divergence angle.

has the highest brightness, i.e. its beam quality is ideal. The degree of collimation of such a laser beam is related to the beam divergence angle, which can be expressed as:

$$\sigma = \frac{\lambda}{\pi\omega_0} \tag{2.3}$$

where ω_0 is the beam waist radius.

Even for distinctly non-Gaussian beams, there is a generalization of Gaussian beam propagation that can be widely used; therefore Equation 2.3 can be generalized to any laser beam by means of the beam propagation factor M^2, defined as the ratio of the divergence of a beam to that of a perfectly coherent beam [37]:

$$\sigma = M^2 \frac{\lambda}{\pi\omega_0} \tag{2.4}$$

M^2 is commonly used as an index of the beam quality of a laser, since a higher beam divergence for a given beam radius is related to an lower beam quality, and therefore to a lower potential focusing capability of the beam to a very small spot.

Another property of lasers is the *coherence*, related to the strong correlation (fixed phase relationship) between the electric field values at different locations (*spatial* coherence) and at different times (*temporal* coherence) [38].

2.1 Industrial lasers

Since the development of the first lasers, several of materials have been investigated as lasing active medium. However, only a limited number of them have found application in commercial laser systems. A description of the main categories of laser media is given in this section.

Gas lasers use a gas as active lasing medium: electric current is discharged through the gas to produce laser light. Laser gas sources have the advantages of using a high volume of a relative inexpensive, not damageable active material, but they are usually larger in size than solid-state laser, due to the low density of the gas medium. The most common example of gas laser is the CO_2 laser, which is widely used in material processing application.

Solid-state lasers use a crystalline or glass rod which is doped with impurity ions, where the population inversion is generated and maintained. The doped materials are pumped optically by a radiation with shorter wavelength than the lasing wavelength. $Nd:YAG$ laser are the most common example in the field of material processing.

Excimer lasers are based on diatomic molecules that are stable in the excited state and unstable in the ground state (excimer). Highly inert noble gases are used: when in an excited state, they can form temporarily-bound molecules, which soon release the excess energy by undergoing spontaneous or stimulated emission. The resulting strongly-repulsive ground state molecule is unstable and therefore disassociates into two unbound atoms, creating a population inversion between the two states. Excimer laser are typically excited with electrical discharges.

Liquid dye lasers use an organic dye as active lasing medium. Since the dye molecules efficiently absorb and emit radiation over a broad range of wavelengths, dye laser can be tuned to operate over a wide range of frequencies. *Semiconductor lasers* are electrically pumped diodes. Under an applied current, electrons and holes are forced into the depletion zone of a $p-n$ junction. When electrons recombine with holes, they fall into a lower energy level and release energy in the form of photons. Under the right condition, stimulated emission may take place, resulting in optical gain. A resonator cavity around the active region completes the laser.

2.1.1 Fiber lasers

Fiber laser are lasers in which the active gain medium is an optical fiber doped with rare-earth elements such as erbium(Er^{3+}), ytterbium(Yb^{3+}), neodymium(Nd^{3+}), praseodymium(Pr^{3+}), and thulium(Tm^{3+}). They are related to doped fiber amplifiers, which provide light amplification without lasing (Fig.2.3) [39]. Fiber nonlinearities, such as stimulated *Raman* scattering or four-wave mixing can also provide gain and thus serve as gain media for a fiber laser.

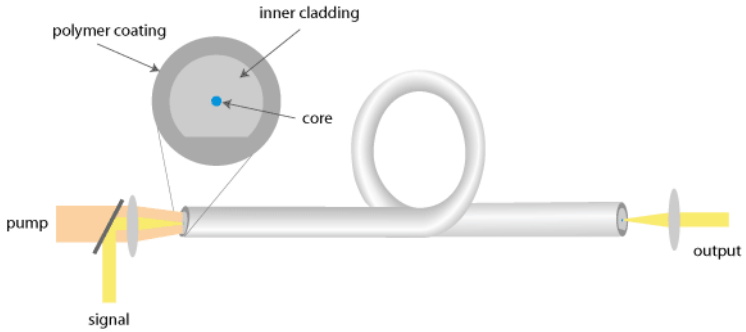

Figure 2.3: Schematic of a *double-clad* fiber laser setup. [39]

The use of a doped optic fiber as lasing medium offers several advantages when compared to bulk solid-state laser. First of all, the rugged and compact setup of fiber lasers that usually consist of a monolithic combination of fiber-based components, with no need for optical alignment and no potential for external contamination.

The simplified thermal management is another pro of fiber lasers. Specifically the much larger surface-to-volume ratio of fiber-based lasing media, compared to the traditional bulk media used in solid-state laser, reduces issues related to over-heating of the cavity and material integrity. The low operating temperature also avoid optical distortions to the output beam due to thermal lensing and birefringence effects in the gain media, which may be produced by temperature gradients in the laser cavity because of the temperature-sensitive nature of the refractive index.

Fiber lasers can operate on the lowest-order transverse mode,

leading to excellent output beam quality. They have no strict pump requirements: indeed fiber lasers are based on rare-earth ions, which exhibit broad spectral regions with good absorption, making the pump wavelength uncritical and thus enabling the use of high power low beam quality laser diodes for the pumping process.

Finally, it is remarkable the high efficiency of operation (up to 80%), due to the high gain efficiency of doped fibers.

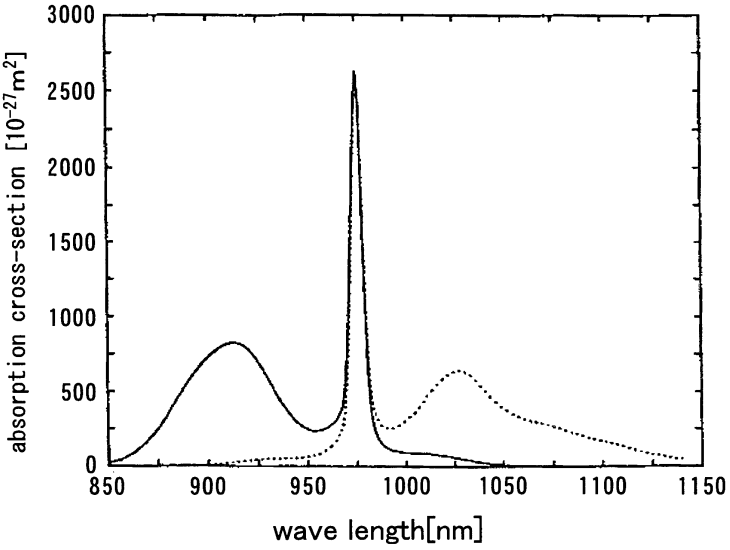

Figure 2.4: Wavelength dependences of emission (dashed) as well as absorption (solid) cross sections of (Yb^{3+}) ion in germano-silicate glass. [40]

As already described previously, in fiber lasers the gain medium is usually a fiber doped with rare earth ions. The ytterbium(Yb^{3+}) ion is the most commonly used ion in fiber lasers. The broad absorption spectrum of ytterbium permits wide flexibility in the choice of pump source wavelengths. Moreover, the absorption spectrum peaks at $915nm$ and $976nm$, very close to the peak of emission at $1030nm$ (Fig.2.4) [40].

The small quantum defect allows efficient energy conversion from

pump radiation to laser output; this also reduces heating in the laser crystal, improving prospects for power scaling. In comparison to ytterbium, both neodymium (Nd^{3+}) and erbium (Er^{3+}) ions have much larger quantum defects, coupled with inferior maximum dope levels into silica fibers. For these reasons, ytterbium is usually preferred in high power laser application.

2.1.2 Design of doped fibers

Optical fiber comes in two common types: *single-mode* and *multi-mode*, each with their own advantages and drawbacks. *Single-mode* fiber allows for higher beam quality with low propagation loss, but requires *single-mode* pump sources, which tend to be lower power and more expensive. *Multi-mode* fiber allows the use of higher power and less expensive *multi-mode* pump sources. However they sacrifice beam quality and propagation losses occur in the process.

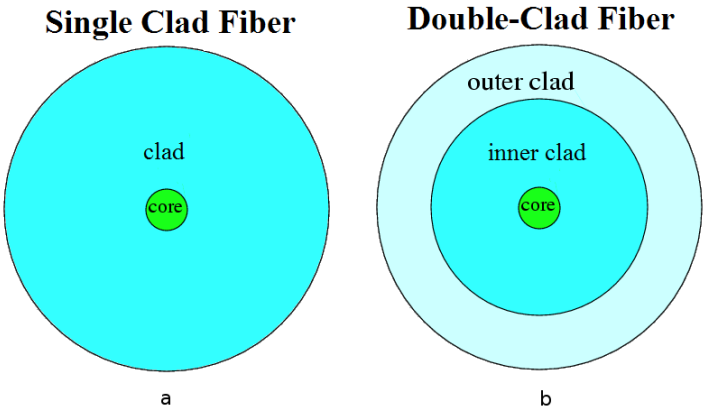

Figure 2.5: Single-mode, single clad and double-clad fibers. [41]

Doped fiber, in its simplest case, is made up of an optical fiber consisting of a transparent core surrounded by a transparent cladding material with a lower index of refraction (Fig.2.5a) [41]. This structure causes the fiber to act as a waveguide, supporting a single propagation mode for a given wavelength. Single mode fiber can generate laser output with diffraction-limited beam quality, but they require to be pumped by radiation with the same high beam quality, which

can be generated only by low power pumping source.

Double-clad fiber (Fig.2.5b), however, offers the best of both *single-mode* and *multi-mode* fibers. Like its name suggest, double-clad fiber has two claddings, along with *single-mode* core. Double-clad fiber offers high beam quality with low propagation loss of the signal in the core, but supports higher power and less expensive *multi-mode* pumping of the inner cladding. The design of the double-clad optic fiber allows the medium to be pumped by relatively low brightness sources to generate a laser beam with brightness of orders of magnitude higher, effectively acting as brightness converters.

2.2 Laser material processing

Over the last decades, laser light has found several application in material processing, such as drilling, milling, grooving, welding, cladding and thermal treatments. [42]

Lasers have some others unique properties which make them suitable for surface treatments. The electromagnetic radiation of a laser beam is absorbed within the first few atomic layers for opaque materials, such as metals and there are no associated hot gas or eddy currents and there is even no radiation spillage outside the optically defined beam area. In fact the applied energy can be placed precisely on the surface only where it is actually needed. The ability to focus laser radiation on micron-sized spots enables the production of a wide variety of geometries with reduced Heat Affected Zone (HAZ). Moreover, being a non-contact technique, laser does not suffer from tool wear and no cutting forces are exerted, thus enabling the processing of traditionally hard-to-cut materials. In particular, the high quality and high energy beam of fiber lasers operating in the nanosecond and femtosecond regimes makes such class of lasers an ideal tool for micromachining application [43]. Thus, laser is a unique tool for surface engineering.. The range of possible processes with laser are illustrated in Figure 2.6. Common advantages include: [44]

- ◇ chemical cleanliness
- ◇ controlled thermal penetration and therefore distortion
- ◇ less after-machining, if any, is required

- ◇ remote non contact processing is usually possible
- ◇ relatively easy to automate

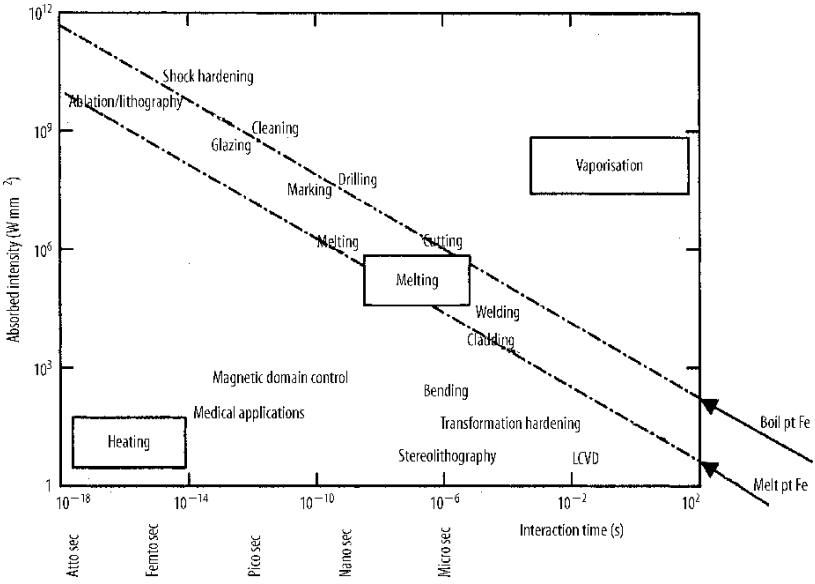

Figure 2.6: Different laser material processing. [44]

Surface treatment is therefore a subject of considerable interest at present because it seems to allow improved components with idealized surfaces and bulk properties. These ambitions are real and possible. However, if great areas are required to be covered other kind of surface treatments could be more suitable; for discrete areas the laser has few competitors and can give a wide variety of treatments. Currently the uses of lasers in surface treatment include:

- ◇ surface melting for homogenization, microstructure refinement, generation of rapid solidification structures and surface sealing
- ◇ surface alloying or cladding for improved corrosion and wear resistance
- ◇ laser marking

- ◇ micromachining
- ◇ surface cleaning
- ◇ surface texturing and roughening for enhanced glue adhesion

It can be seen that these process range from low-power-density to process involving substrate melting requiring high power densities to overcome latent heat effects and larger conduction heat losses (e.g. laser cladding, laser glazing, laser cleaning). If very short pulses of great power intensity strike a surface, they are able to cause instant ablation.

The interest in ablation as a process has recently become important with the introduction of very powerful, ultrashort laser pulses. Such pulses can deliver energy at a rate that the material can only absorb by evaporating or flying apart. Thus, material is removed leaving very little heat-affected material. These lasers have become a form of machine tool, which can operate on very fine structures causing very little chemical or mechanical damage.

The applications for such a tool are slowly being recognized. It has never been possible before to work with such cleanliness and precision except via chemical etching which can hardly be described as clean. Therefore laser ablation has a growing niche market in surgical applications, lithography, micro-optical and electronic device, manufacture, marking, cutting and surface cleaning.

2.3 Material removal mechanism

2.3.1 Energy transfer

Absorption of light can be explained as the interaction of the electromagnetic radiation with the electrons (either free or bound) of the material. When light strikes the surface of a material, a portion will be reflected from the interface between the atmosphere and the material due to the discontinuity in the index of refraction. The fraction of the incident power that is reflected from the interface is given by the r*eflectance coefficient* R_r. The reflectance coefficient R can be calculated from the Fresnel equations:

$$R_{R_{\text{II}}} = \left(\frac{n_1 \cos\theta_i - n_2 \cos\theta_t}{n_1 \cos\theta_i + n_2 \cos\theta_t} \right)^2 \tag{2.5}$$

$$R_{R\perp} = \left(\frac{n_1 \cos\theta_t - n_2 \cos\theta_i}{n_1 \cos\theta_t + n_2 \cos\theta_i} \right)^2 \tag{2.6}$$

Equation 2.5 is valid for light polarized in the incidence plane whereas Equation 2.6 for light polarized in the plane perpendicular to the incidence plane. ϑ_i represents the angle of incidence of the light and n_1 and n_2 are the the indexes of refraction of atmosphere and of material, respectively.

The reflectivity depends on the wavelength of the incoming light through the relation of the wavelength with the index of refraction of the material. Since generally the reflectivity increases with increasing wavelength, materials are strong absorbers at shorter wavelengths. In addition, the reflectivity of a surface decreases when the temperature increases. Hence, a material which is strongly reflective at low temperature may become strongly absorbing at high temperature.

While the transmitted radiation propagate within the material, its intensity is attenuated according to the Beer-Lambert law:

$$I_{(z)} = I_0(1 - R)e^{\mu z} \tag{2.7}$$

where $I_{(z)}$ is the intensity at depth z, I_0 is the incident intensity and μ is the absorption coefficient of the material. The reciprocal of the absorption coefficient $\delta = 1/\mu$ is defined *optical penetration* or *absorption depth* and it represents the depth at which the intensity of the transmitted light drops to $1/e$ of its value at the material-atmosphere interface. Since absorption depths at typical laser wavelengths are in the order of nanometers, energy can be concentrated on the surface material without affecting the bulk material. While the absorption coefficient depends on the wavelength of the laser, the specific mechanism of absorption depends on the type of material. In general, the incident laser beam excites electrons within the metal to states of higher energy. Such electrons then return to equilibrium, releasing energy to the material lattice (thermalization) on a time scale ranging from $10^{-12} - 10^{-10}s$ for metals to $10^{-6}s$ for non-metals. When the electron excitation rate is low in comparison to the thermaliza- tion rate, the absorbed laser energy can be considered as being directly transformed into heat. Such processes are called photothermal. For metals, laser processing with laser pulse length above the nanosecond range is based on photothermal mechanisms. On the other hand, when the material thermalization rate

is relatively low, a large amount of energy can accumulate in the intermediary states and directly breaks bonds, without a significant change in the temperature of the material. This non-thermal process is referred to as photochemical and it is typical of irradiation of polymers with short wavelengths and of processing of metals with ultrafast pulsed lasers (femtosecond range). [38]

2.3.2 Thermal effect

When a laser beam of intensity I_0 is irradiated on the surface of material, it results in the excitation of free electrons (in metals), vibrations (in insulators), or both (in semiconductors). As mentioned in the previous paragraph, this excitation energy is rapidly converted into heat (time duration in the range $10^{-13}s$ for metals, 10^{-12} to $10^{-6}s$ for nonmetals). This is followed by various heat transfer processes such as conduction into the materials, and convection and radiation from the surface. The most significant heat transfer process being the heat conduction into the material. The generation of heat at the surface and its conduction into the material establishes the temperature distributions in the material depending on the thermo-physical properties of the material and laser parameters. If the incident laser intensity is sufficiently high, the absorption of laser energy can result in the phase transformations such as surface melting and evaporation. Generally, these phase transformations are associated with threshold (minimum) laser intensities referred to as melting and evaporation thresholds (I_m and I_v). Melting and evaporation are the efficient material removal mechanisms during many machining processes. In this section, we will deal with the simplified analysis of laser heating, melting, and evaporation of materials. More detailed analyses are presented in the following chapters with reference to specific applications.

The most simplified thermal analysis is based on the solution of one-dimensional heat conduction equation with simplified assumptions such as:

- ◇ Homogeneous material and thermo-physical properties independent of temperature.
- ◇ Constant initial temperature of the material.
- ◇ Heat input constant during irradiation time.

◇ Negligible convection and radiation losses from surface.

The temperature profile resulting from laser irradiation is therefore governed by the following equation for the onedimensional heat transfer:

$$\frac{\partial T(z,t)}{\partial t} = \alpha \frac{\partial^2 T(z,t)}{\partial z^2} \tag{2.8}$$

where T is the temperature at a location z after time t and α is the thermal diffusivity.

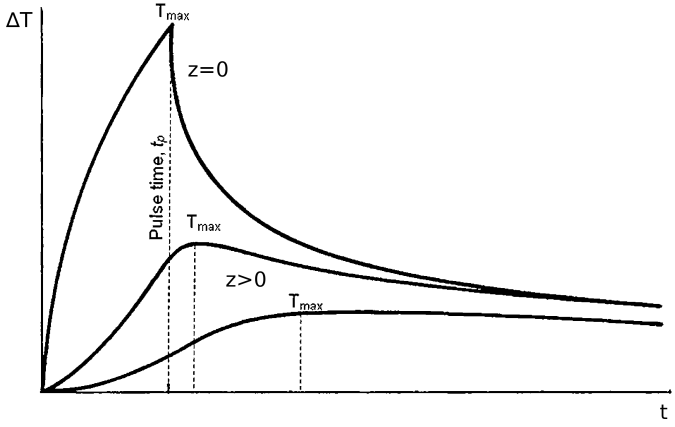

Figure 2.7: Variation of calculated temperature increases with time at various depths (z) during laser irradiation. [34]

Fig.2.7 [34] shows typical temperature changes at various depths during laser irradiation of metals. The important characteristics of the temperature changes in a material during laser irradiation are:

◇ At the surface ($z = 0$), the temperature increases with increasing irradiation time, reaches maximum corresponding to pulse time (t_p), and then rapidly decreases. Thus, the heating and the cooling parts of the curve are clearly separated at a time corresponding to pulse time.

◇ At certain depths below the surface ($z > 0$), the temperature increases with increasing irradiation time, reaches maximum, and then decreases. However, the maximum temperature does not reach exactly at the pulse time (t_p), but at the longer time

($t > t_p$). The time ($t > t_p$) to reach the maximum temperature increases as we go further into the depth below the surface of the material.

The incident laser power density leads to an increase of surface temperature and however it can reach the melting or the boiling point if the laser power densities are sufficiently high. The corresponding laser power densities are often referred to as the melting and boiling thresholds.

If the surface temperature of the material exceeds the melting point upon irradiation with laser (without surface evaporation). It is important to analyze the temporal evolution of depth of melting during laser irradiation. Figure 2.8 [34] presents the various steps for the determination of the depth of melting during laser irradiation. As indicated in Fig. 2.8a, the temperature of the surface ($z = 0$) increases with increasing irradiation time (t), reaches maximum temperature (T_{max}) at pulse time (t_p), and then decreases. Various heating and cooling steps in this temporal evolution of surface temperature are:

- ◇ Temperature reaches $T_1(T_1 < T_m)$ at time $t_1(t_1 < t_p)$.
- ◇ Temperature reaches melting point (T_m) at time $t_2(t_2 < t_p)$.
- ◇ Temperature reaches maximum, $T_{max}(T_{max} > T_m)$ at time t_p.
- ◇ Temperature decreases to melting point Tm at time $t_3(t_3 > t_p)$.
- ◇ Temperature reaches $T_1(T_1 < T_m)$ at time $t_1(t_1 > t_p)$.

The corresponding temperature profiles in the depth of the material are presented in Figure 2.8b for various times during laser irradiation. By tracing the melting point in the temperature verses depth plots, the positions of the solid–liquid interface can be located. at time t_p , the position of solid–liquid interface corresponds to $z = z_{max}$. Similarly, at times t_2 and t_3, these positions can be located at $z = 0$. These positions are schematically plotted in Figure 2.8c. The figure indicates that during laser irradiation, the melting initiates at time t_2. Below time t_2, the material is simply

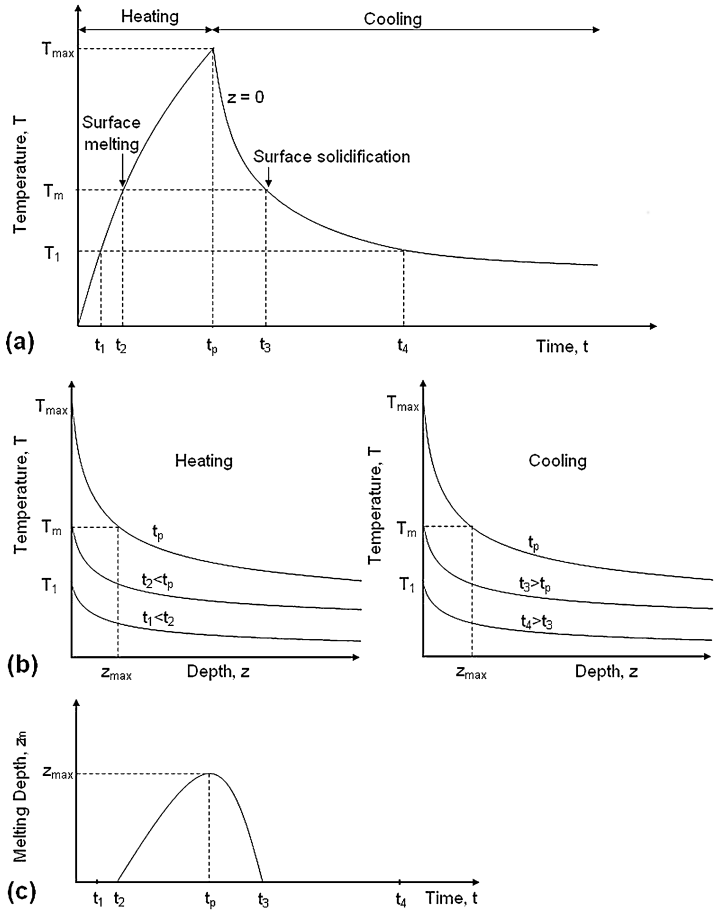

Figure 2.8: Temporal evolution of depth of melting: (a) surface temperature as a function of time, (b) temperature as a function of depth below the surface during heating and cooling, and (c) depth of melting as a function of time. [34]

heated without melting. Beyond t_2, the depth of melting increases with continued irradiation and reaches maximum (z_{max}) at pulse time t_p. This means that the solid–liquid interface moves away from the surface during heating phase ($t \leq t_p$). In the cooling

phase ($t > t_p$), the surface temperature starts decreasing rapidly and the solid–liquid interface moves towards the surface of the material (start of solidification). Beyond t_3 , the material simply cools down. Thus, each laser irradiation is characterized by the maxi-

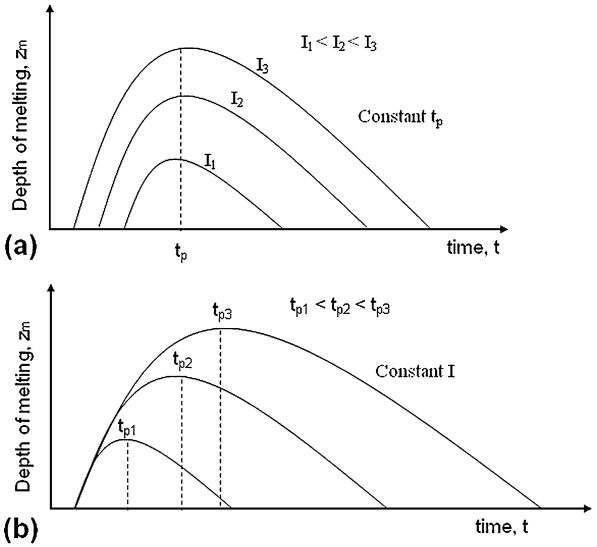

Figure 2.9: Schematic variation of melting depths during laser irradiation: (a) laser power density at constant pulse time, and (b) laser pulse time at constant laser power density. [34]

mum depth of melting z_{max} corresponding to the cessation of laser power. Figure 2.9 [34] shows the schematic of the influence of important laser processing parameters on the temporal evolution of depths of melting. At constant pulse time, the maximum depth of melting increases with increasing laser power density (Fig. 2.9a). In addition, at constant laser power density, the maximum depth of melting increases with increasing pulse time (Fig. 2.9b). It should be noted that the above generalized trends are valid for the case of laser melting before initiation of surface evaporation.

However the depth of melting cannot increase to infinitely large value with increasing laser power density and pulse time because the

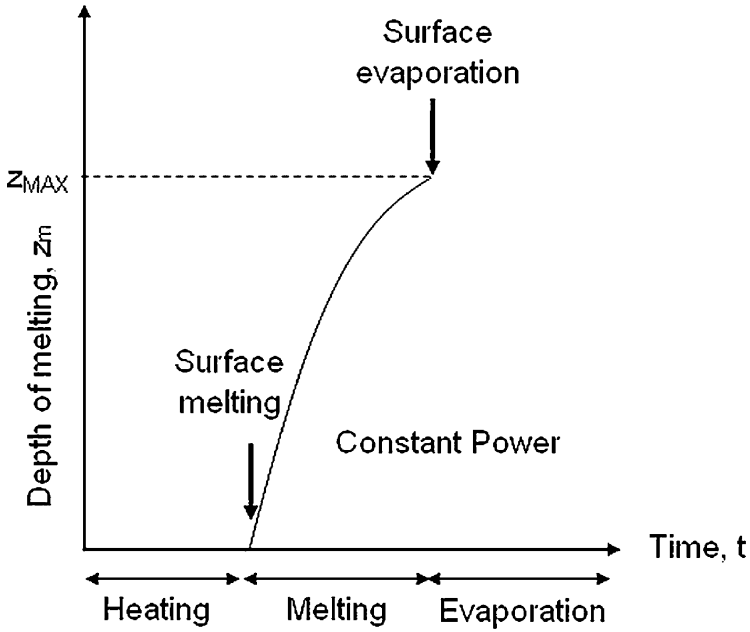

Figure 2.10: Variation of depth of melting with laser irradiation time and power. The arrows indicate the initiation of surface melting and evaporation during continued laser irradiation. [34]

location of the melting point in the temperature verses depth plot is limited by the maximum achievable surface temperature. Once the surface temperature reaches the boiling point, the depth of melting reaches the maximum value z_{MAX} (Note that z_{max} introduced earlier correspond to the cessation of power where the surface temperature has not yet reached the boiling point). Further increase in the laser power density or the pulse time cause the evaporative material removal from the surface without further increase in the depth of melting as shown in Fig.2.10 [34].

2.3.3 Plasma formation

When the material is irradiated with sufficiently larger laser intensity (I_v), significant surface evaporation takes place as explained in the previous sections. Once the vaporization is initiated, the in-

teractions between the resulting vapor and the incident laser beam become important in determining the overall effect of the laser irradiation on the material.

The generation of plasma can greatly influence (or interfere with) the interaction of laser radiation with the material. It is convenient to define the laser power density (I_p) at which the significant ionization of the vapor resulting in the formation of plasma takes place. The plasma is generally considered to form near the evaporating surface of the target and remain confined to this region during laser irradiation with intensities just above I_p. This confinement of the stationary plasma near the evaporating surface is generally referred to as plasma coupling (Fig.2.11a). Plasma coupling plays an im-

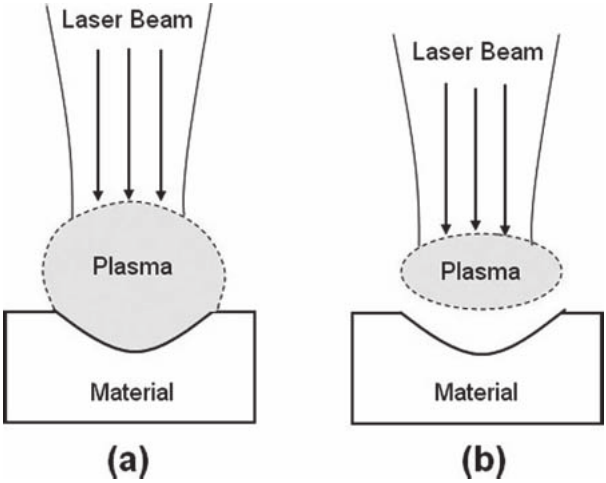

Figure 2.11: Schematic of (a) plasma coupling and (b) plasma shielding effects. [34]

portant role in transferring the energy to the dense phase. The energy transfer may be due to normal electron heat conduction, short-wavelength thermal plasma radiation, or condensation of vapor back to the surface [45]. The plasma coupling is particularly important in conditions where normal laser irradiation is not strongly absorbed by the target material. Such conditions exist during irradiation of highly reflecting materials with infrared (longer wavelength) laser radiation. Plasma coupling results in the significant increase in the absorptivity of laser radiation by the material. When the laser

power density is increased significantly beyond I_p, the dynamic interaction of the plasma with the laser radiation causes the rapid expansion and propagation of the plasma away from the evaporating surface Eventually, the plasma gets decoupled from the surface and transfer of energy to the dense phase ceases. The laser radiation is then essentially absorbed in the plasma. This condition is referred to as plasma shielding where the decoupling of the plasma ceases the interaction of the laser radiation with the target material via plasma (Fig.2.11b). The propagating plasma is often referred to as laser supported absorption wave (LSAW). The LSAWs are generally classified into laser supported combustion waves (LSCWs) and laser supported detonation waves (LSDWs) depending on the speed at which they propagate with respect to gas. The LSAW propagating at the subsonic speed is termed as LSCW, while, it is termed as LSDW when propagating at supersonic speed [46].

2.4 Laser pre-treatments

Adhesive bonding, in conjunction with state-of-the-art surface pretreatments, can provide by itself good strength of the joint [3][47][48]. Surface conditions are a crucial factor in the strength of adhesive joints and several kind of substrate preparation have already been developed mainly for steel and aluminum [3][49]. In particular, mechanical grinding or sandblasting resulted to be very effective in controlling surface roughness and therefore joint strength (thanks to an improved mechanical interlocking) [47]. Chemical treatments such as etching are successfully employed in the aircraft and automotive industries providing superior performance in comparison to a simple sandblasting [48]. On the other hand anodizing process affect adhesion and durability of the joint because it is able to produce a porous oxide film which can promote chemical interaction between adhesive and substrate.

Usually chrome-based surface preparation techniques are successfully employed for aluminum substrates to prepare adherends before bonding. These techniques requires their replacement for environmental reasons till 2007 international legislation and other procedures, such as the SACO^{TM} are expensive with no possibility of integration in serial production. Therefore laser based surface treatments can avoid the disadvantages of existing methods and

they are becoming increasingly employed [50].

An environmental friendly alternative to chemical treatments is represented by laser ablation technology. Several researches demonstrated the effectiveness of this kind of treatment on the strength of adhesive joints.

Laser radiation allows to treat the substrate surface selectively (in contrast to conventional chemical etching process) with high flexibility. In addition, compared to other surface pretreatments, laser ablation has the advantage that only the required surface needs to be processed. The fast and easy change of laser parameters makes the pretreatment of a wide variety of materials possible using only one laser equipment [50].

A pulsed laser surface pretreatment, employed on "as produced" substrates, can cause surface melting and the removal of contaminants, producing favorable changes in both chemical composition and surface morphology. As a result it is able to improve the joint strength due to the increased mechanical interlocking between the adhesive and the substrate and due to an improvement of chemical interaction of the adhesive molecules with the metal oxide layer lying on the substrate surface. in addition to the ecological advantage, it is is important to underline that laser surface pretreatment can be easily adapted to a wide variety of materials [49]. It was successfully employed to improve the adhesion of different adhesive bonded interfaces, e.g., ceramic/ceramic [51], ceramic/steel [52], titanium/titanium [53], steel/steel [54], glass-fiber/polyester [55] and aluminum/magnesium [49].

Since the invention of laser technology in the sixties, a number of attempts have been made to employ it for useful purposes. Nd-lasers and CO_2-lasers in particular are considered suitable for material processing [56]. Nowadays Nd-lasers are widely employed for the welding and cutting of small components and for the texturing of body panels in the automotive industry [44][57].

Generally, laser irradiation is used for cleaning, structuring, chemical and morphological modification and curing of material surfaces. As a pretreatment for adhesive bonding laser irradiation generates a dirt-and-grease free surface with structural and chemical modifications that can considerably influence the strength and the toughness of adhesive bonded joints. Laser ablation is noiseless and works

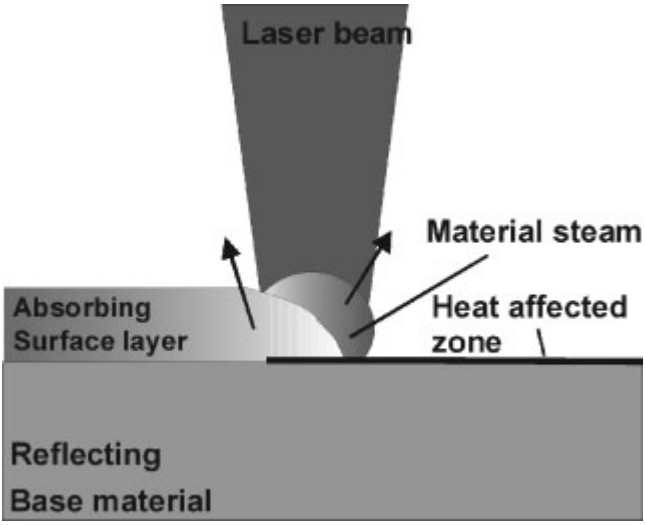

Figure 2.12: Laser surface pretreatment. [50]

touch-free with small operating cost. In addition, a precise controlling makes the integration in serial process possible.

Figure 2.12 shows the functional principle of removing dirt by laser radiation. The coating layer is removed by vaporization through absorbing the laser spot. The blank base material reflects the laser radiation. Very short laser pulses can treat the substrate causing very little thermal influence. Therefore it is possible to treat the metal without damaging or melting the base material.

One of the main outcome of the previous scientific works on this subject is that laser treatment promoted an in-layer cohesive fracture of the joints, whilst untreated samples failed adhesively (i.e., interfacial fracture). In turn, joint strength improvements of up to 50% could be achieved with respect to samples with untreated surfaces.

Alfano *et al.* [49], employed pulsed laser irradiation to enhance the adhesion strength between aluminum and magnesium alloys bonded with epoxy adhesives. Specifically, the substrates employed for specimens fabrication were aluminum (AA6082-T6) and magnesium (AZ31B) sheet-metal alloys. As described previously in this chapter, during the process, a fraction of the laser beam energy was

absorbed by the material, thus promoting material melting, surface morphological microwaves and the formation of a thin oxide layer [51, 52, 53, 54, 55]. A rectangular area $A_0 = 12.5 \times 25mm^2$ for each substrate was irradiated with a ytterbium fiber laser operated in pulsed mode (IPG, YLP1-100-100). A projective optical system directed and defocused the laser radiation on the sample surface. The morphological modification of the substrate surfaces as well as the depth of the transformed zone were dependent on the adjustable laser process parameters, such as laser power (P_{av}), lasing speed (v), line spacing (Δ), etc. The laser parameters employed in this work are summarized in Table 2.1 [49].

Process parameter	Value
Laser radiation wavelength λ	1064 nm
Pulse repetition rate f_r	100 kHz
Pulse width t_p	150 ns
Pulse energy E_p	1 mJ
Average power P_{av}	100 W
Lasing velocity v	750 mm/s
Programmed line spacing Δ	0.05 mm

Table 2.1: Example of laser process parameters set employed for joint fabrication. [49]

The process was carried out at ambient temperature and in an atmospheric environment. For comparison, sample substrates were also prepared using standard grit blasting (alumina 80 grit).

The samples analyzed in the paper were single-lap joints (SLJs) fabricated following the procedures and the recommendations in the ASTM Standard D1002 [1]. Three material combinations (Al/Al, Mg/Mg and Al/Mg) were adopted for the tests.

Scanning electron microscopy qualitative observations of the grit-blasted surfaces are reported in Figure 2.13; The insets represent the SEM images of substrate surface prior to grit blasting. As expected, the process produced a substrate surface with random ridges and grooves.

Selected SEM images of the laser treated surfaces are presented in Fig. 2.14. There are several points of interest which characterize the treated surfaces. First of all, the columnar structures protruding above the aluminum and magnesium substrates. Dolgaev *et*

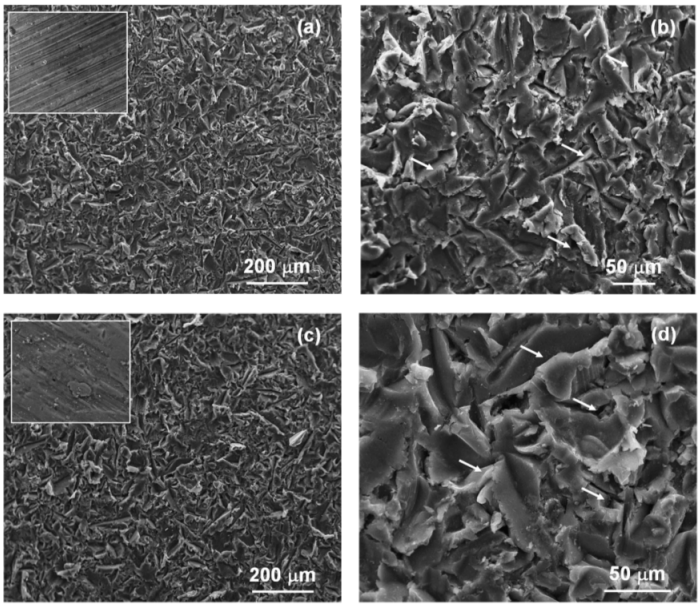

Figure 2.13: SEM images of grit-blasted substrates surfaces. (a) and (b) AA6082, (c) and (d) AZ31B. Typical grooves and ridges created by grit blasting are illustrated using yellow and white arrows, respectively. [49]

al. [58] explained the formation of the columnar structures as being due to capillary wave instabilities on the evaporating surface of melt. It has been already reported that the presence of such structures is beneficial for joint strength because of the enhancement in mechanical keying of the adhesive into the substrate and the increased surface area available for bonding [51, 52, 53, 54, 55]. such structures are more prevalent in the magnesium than in the aluminum alloy, as seen by comparing Fig. 2.14(a) and 2.14(c). This odd behavior could be a consequence of the different enthalpy of vaporization of the two alloys ($\Delta H_{AA6082} = 293.4 kJ/mol$ and $\Delta H_{AZ31B} = 127.4 kJ/mol$, respectively). In addition, it is apparent that droplets of target material formed globular micronsized oxide particles on the substrate surfaces during laser treatment; these are clearly seen in Fig. 2.14(b) and 2.14(d). These particles formed

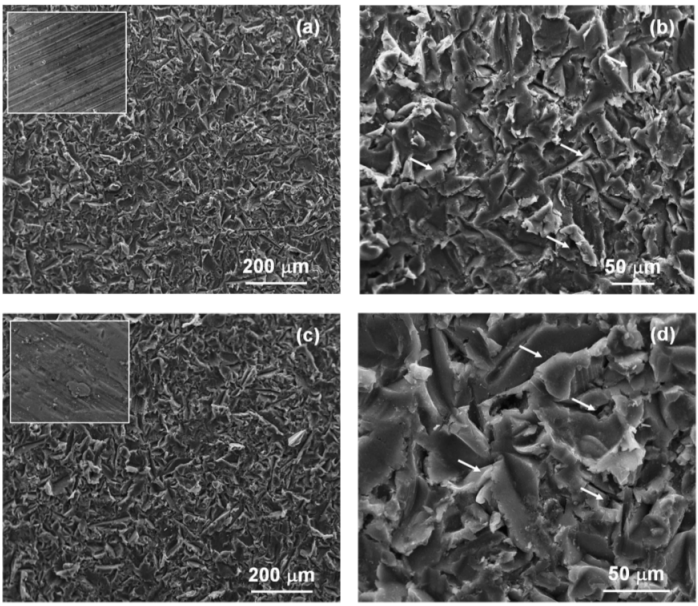

Figure 2.14: SEM images of laser treated substrates surfaces. (a) and (b) AA6082, (c) and (d) AZ31B. Column-like structures are denoted by the yellow arrows. The white arrows illustrate ridge-like features on substrate surfaces. [49][49]

through condensation of expanding gas or plasma during cooling [59]. Larger particles are attached to the top of the columnar structures in AA6082; however, the contact area seems to be quite small, as a consequence these particles are likely to be detached from the substrates under loading. The surface roughness (R_a) of treated

	Grit blasting	Laser ablation
AA6082	2.10 ± 0.36 μm	1.52 ± 0.30 μm
AZ31B	2.31 ± 0.31 μm	1.48 ± 0.24 μm

Table 2.2: Surface roughness (R_a) for grit-blasted and laser ablated aluminum and magnesium surfaces. [49]

surfaces was also examined. The measured values are reported in

Table 2.2. No difference among the values measured in the longitudinal and transverse directions was observed.

Stammen *et al.* [50] focused their attention on $Nd : YAG$ laser pretreatment of aluminum alloys. The authors showed exemplary results for laser pretreatment of AA 6040, AA 6016 and AA 6043 (anodized). The experimental setup was according to DIN EN 1465 [60] (one-side overlapped, adhesive shear tension samples). The samples where bonded together with two different adhesives: Betamate 1496 (Dow automotive) is a one part epoxy adhesive, Teromix 6700 (Henkel Teroson) is a two part polyurethan. The aluminum was treated with different laser parameters, using a workstation operating in cross-hatch handling with an optical characteristic $f - theta = 80mm$. Parameter 1 (LP 1, laser pulse frequency $8kHz$, line distance $0.2mm$, laser speed $2000mm/s$) melts the surface, Parameter 2 (LP 2, laser pulse frequency$30kHz$, line distance $0.1mm$, laser speed $4000mm/s$) only cleans the surface nearly without melting and Parameter 3 (LP 3) is a combination of 1 and 2. Additionally, a more homogenous Parameter 6 (LP 6, generated from Parameter 1 with a varied fibre-coupling; laser pulse frequency $25kHz$, line distance $0.1mm$, laser speed $1500mm/s$) was developed during the project and analyzed.

In order to analyze the influence of the surrounding medium, laser pretreatment was done in atmosphere (air), under inert gas (nitrogen), under oxygen and in combination with the Pyrosil^{TM} technique. For this, a special laser atmosphere-chamber was designed.

	Reference	LP1	LP2	LP3	LP6
6040 (air)	110.5	4.99	10.90	5.42	4.30
6016 (air)	49	6.20	13.10	6.40	10.30
6043 (air)	0.3	2.50	5.50	7.00	
6040 (N 2)		5.60	15.50	10.50	11.00
6016 (N 2)		6.30	21.20	9.80	4.30
6040 (O 2)		4.70	11.70	7.10	4.50
6016 (O 2)		4.30	8.90	7.10	3.70
6040 (Pyr)		4.20	12.70	11.00	14.00
6016 (Pyr)		5.30	11.40	11.10	12.90
6043 (Pyr)		2.10	5.30	6.50	

Table 2.3: Proportion of aluminum to oxygen. [61][50]

Table 2.3 [61][50] shows the main chemical effect on the different aluminum alloy surfaces while using process gases during the laser process.

Rechner *et al.* [62] described the pre-treatment of the wrought aluminum alloy AW 6016. The work is focused on the examina-

	LP1	LP2	LP3	LP4	LP5
pulse intensity $(W/m^2)\times 10^{11}$	1.73	2.10	2.66	3.48	4.42

Table 2.4: Laser parameter (LP) for fibre-coupled laser processing. [62]

tion of the influence of selected laser pre-treatment parameters on the strength and aging resistance of the bonded joint. The concluding tensile shear strength investigations showed the effect of the laser pre-treatment on the component strength of bonded aluminium sheets (AW 6016). The procedure has been directly compared with conventional pre-treatment and atmospheric pressure plasma pre-treatment. The tensile shear strength investigation is carried out before and after various aging procedures. A $Nd:YAG$ ($\lambda = 1064nm$) laser of the type CLA 050 manufactured by Clean-Lasersysteme GmbH was employed. It has a mean output power of 0–120 W (pulsed or cw) and a continuous frequency range of 8–40 kHz. Owing to the short pulse duration of few nanoseconds, a pulse maximum power of 120 kW can be attained. At the place of pro-

Specimen	**Elements (at%)**			
	C	O	Al	O/Al
Reference	84.1	12.1	1.3	9.1
LP1	52.8	28.8	10.3	2.8
LP2	43.0	34.0	14.3	2.4
LP3	41.0	37.6	14.1	2.7
LP4	35.2	40.5	16.8	2.4
LP5	30.1	42.7	18.7	2.3

Table 2.5: Quantitative elemental analysis. [62]

cessing, the laser beam is decoupled from the fiber and projected onto the surface through a 2D scan head with built-in F-theta lens ($f = 100mm$). The range of processing speeds is 0–$4000mm/s$. The beam profile, after having passed through the fiber, follows the continuous uniform distribution that is also called top hat distribution. The beam section is round and the beam size in the focus is $357\mu m$. The pulse frequencies and thus the resulting laser intensities were varied on the specimen surface with full power and a fixed average scan speed (Table 2.4).

Table 2.5 [62] gives a quantitative elemental analysis for the investigated parameters. Carbon contamination decreases with increasing laser intensity, while the measured oxygen content increases. Only small amounts of aluminum can be detected on the reference surface due to the heavy contamination. The laser pre-treated specimen surfaces. The quantitative elemental analysis showed an increase in aluminum percentage from 10.3% to 18.7%.

In addition, after laser pre-treatment, the visible organic and inorganic contaminations have been completely removed from the surface.

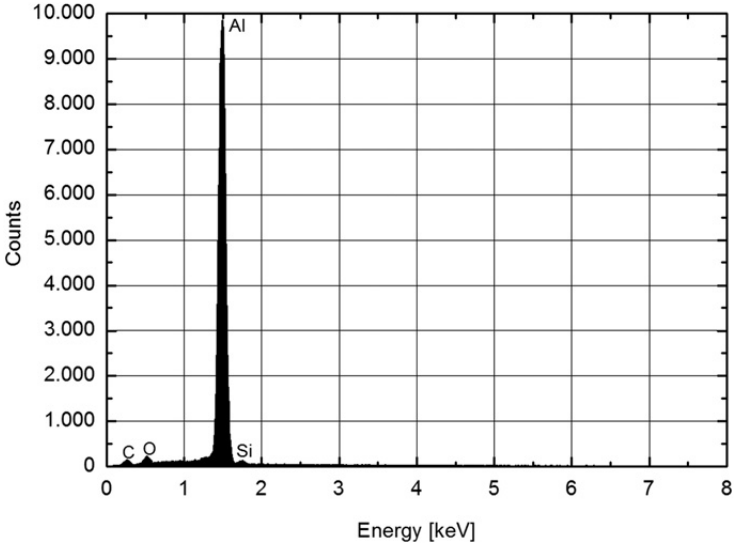

Figure 2.15: EDX analysis of LP5 pre-treated surface. [62]

The cleaning effect of the laser pre-treatment (LP5) can be seen also in the EDX analysis as the modified element composition and intensity (Fig. 2.15). The organic and inorganic contaminations on the surface are minimal. The base material can be clearly identified as a marked aluminum peak during the measurement on the cleaned surface.

2.5 Bonding strength enhancement

Alfano *et al.* [49] demonstrated with experimental tests carried out on the Al/Mg single lap joints the beneficial action of the laser treatment (described in details in the previous section) in terms of both failure stress and maximum elongation at joint failure. However, the improvement was dependent on the type of epoxy resin employed for bonding. The load–elongation (P, δ) curves recorded during the tests are reported in Fig. 2.16 [49].

In order to better understand the effect of surface treatments, the P–δ curves pertaining to grit-blasting and laser irradiation were superimposed. It is apparent, for the SLJ bonded with the toughened epoxy (i.e., Hysol 9466), that the laser treatment process is very effective because the results show that the failure loads and elongations at maximum load are in general higher than those obtained using standard sandblasting.

The scenario was quite different for the joints bonded with Hysol 9492; the failure loads relative to Hysol 9466 were essentially lower and independent of the surface treatment.

In order to compare the results pertaining to the different surface treatments, the apparent shear stress ($\tau_0 = P_{cr}/A_0$) in conjunction with the maximum elongation at joint failure, have been employed as benchmarks. In Fig. 2.17 [49], the apparent shear stress of grit-blasted and laser-treated samples is reported. For the joint bonded with Hysol 9466, a remarkable improvement in the shear strength has been observed. Specifically for the Al/Mg joints an increase of up to about 30% was registered for the apparent shear strength, with respect to the grit-blasted substrates.

The improvement in the elongation at maximum load (Fig. 2.17c [49]) was even greater as a result of the laser treatment.

For the SLJ bonded with the Hysol 9492 the apparent shear

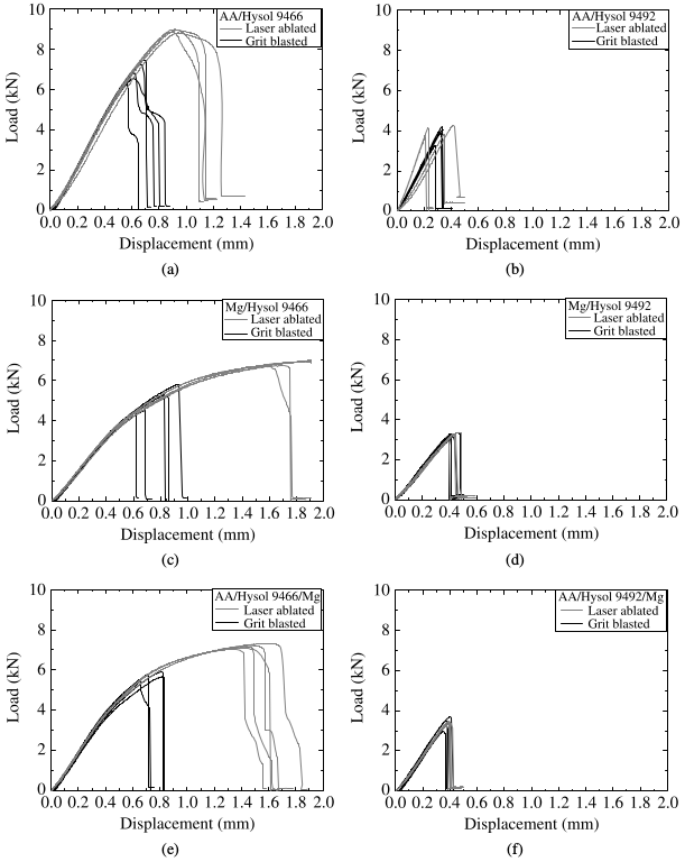

Figure 2.16: Load–elongation curves. Specimens bonded with Hysol 9466 on the left-hand side, specimen bonded with Hysol 9492 on the right hand side. [49]

strength appeared independent of the surface treatment. Accordingly, the elongation at maximum load was not affected by the surface treatment. The difference in behavior between Hysol 9466 and 9492.

Rechner *et al.* [62] demonstrated that Laser pre-treatment can successfully improve cleaning the surfaces and modify the oxide layer at the same time. The improvements resulted in better tensile shear

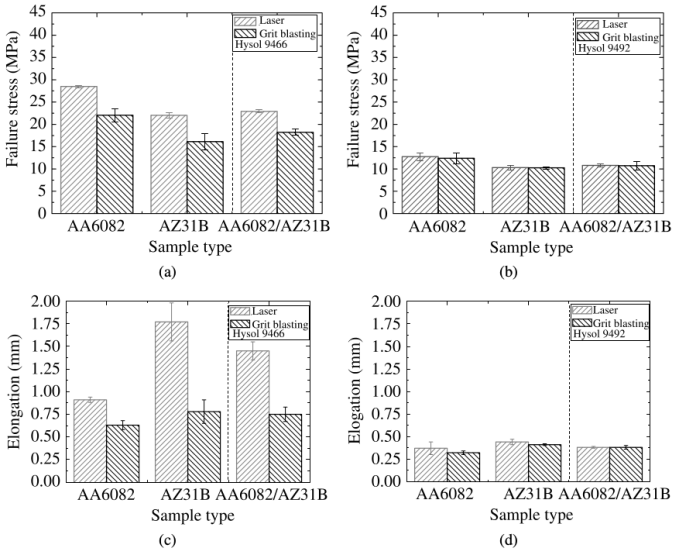

Figure 2.17: Apparent shear strength and elongation at failure for different combinations of substrates and adhesives . [49]

strength of the bonded joint before and after aging. Figure 2.18 [62] shows the results of the subsequent bonding. The drawn error bars represent the standard deviation of the tested samples. The specimens produced were tested either immediately after conditioning or after the aging procedure and subsequent conditioning. The unaged specimens, which were subjected to plasma and laser pre-treatment (LP5), displayed 14% and 20% improvement of the tensile shear strength in the test, the exact value depending on the pre-treatment process.

There is no evidence that the atmospheric pressure plasma pre-treatment improved the strength of the EPD-passivated, tensile shear specimens after 1000 and 2000 h of salt spray testing, respectively. The strength values measured were approximately the same as those for the reference samples. On the other hand, the EPD-passivated specimens showed better strength values after laser pre-treatment and after salt spray aging. The strength values obtained here were 26% and 15%, respectively, above the measured reference values. The effect of both plasma and laser pre-treatment

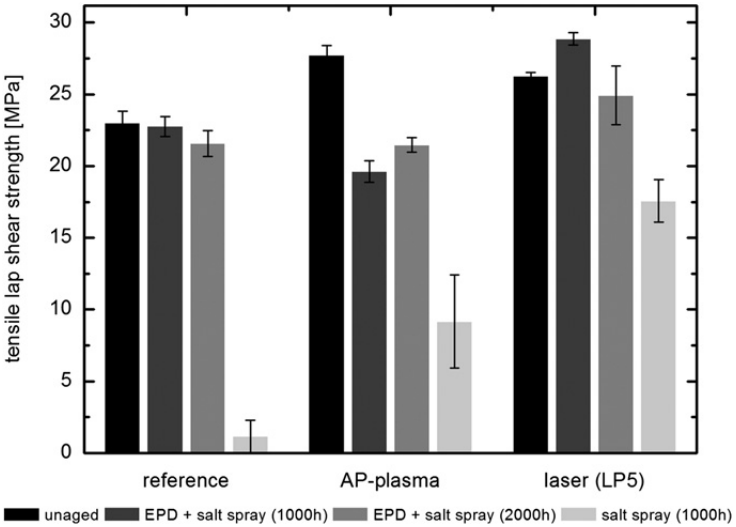

Figure 2.18: Tensile shear strength for AW 6016 bonded with Betamate 1496. [62]

was particularly obvious for specimens without the protective EPD coating which had also been subjected to lab aging in a salt spray chamber for 1000 h. While the reference specimens had only a residual strength after aging, AP-plasma and laser pre-treatment gave markedly higher values [62].

To analyze the influence of the newly established surface layer after laser irradiation, Stammen *et al.* [50] some samples were bonded not only directly after pretreatment (LP1, LP2, LP3) but also after 1 and 24 h. For industrial setups with combined pretreatment and adhesive application steps, only results for direct bonding are relevant.

The adhesive bonds were tested unaged and aged by a modified VDA 621–415 (10 weeks climate changing test in combination with a salt spray test according to DIN 50021).

Figure 2.19 [50] shows the influence of time between pretreatment and bonding for aluminum alloy AA 6016 bonded with Teromix 6700. A good aging stability is reached only when the newly established oxide surface is allowed to absorb water groups (24 h after

pretreatment).

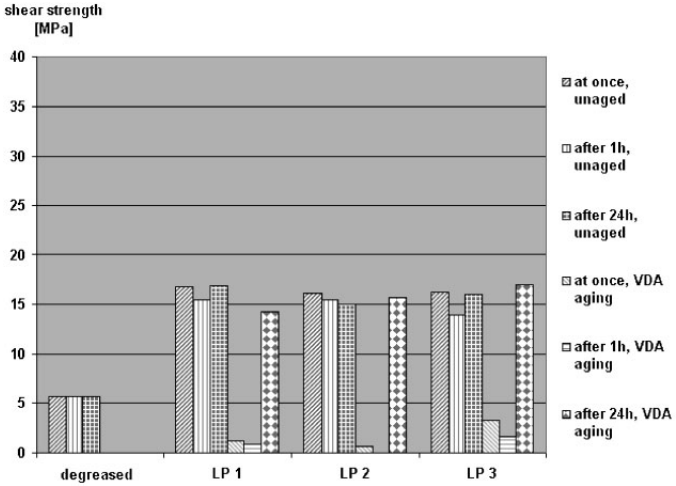

Figure 2.19: Influence of time between pretreatment and bonding, AA 6016 with Teromix 6700. [50]

Results for the epoxy adhesive Betamate 1496 show that the best aging stability is reached while bonding 24 h after pretreatment. Using a strongly roughening laser parameter like 1 or 3, the keying is able to form aging stable joints after direct/1 h bonding as well. For an industrial implementation, direct bonding is of substantial interest. Figure 2.20–2.23 [50] show results for bonding AA 6016 after a pretreatment with process gas Pyrosil TM or with air as surrounding medium. For both adhesives, LP 6 delivers good results with air and Pyrosil^{TM} . The homogeneous oxide surface established by LP 6 shows overall the best resistance against aging compared to other LPs. Especially for the polyurethane adhesive, the total removement of the weak natural oxide surface layer is extremely effective for aging stability even when bonded directly after pretreatment. Further results of the project show that the influence of the surrounding medium during the laser process is obvious and, in special cases, an enhancement of the shear strength is possible, but the main influence for the aging stability, especially for polyurethane adhesives, is the ablation of weak natural oxide while structuring the surface for possible keying, inducing the build up of

a new oxide layer. For AA 6040, the results are comparable to the shown results for AA 6016. AA 6043, the anodized aluminium alloy, showed no significant increase of initial shear strength or aging stability using a laser pretreatment.

Further literature belonging to pretreatment of pressure casting magnesia with laser irradiation [63] approves the modification of the surface structure and chemistry with the possibility of aging resistant adhesive joints.

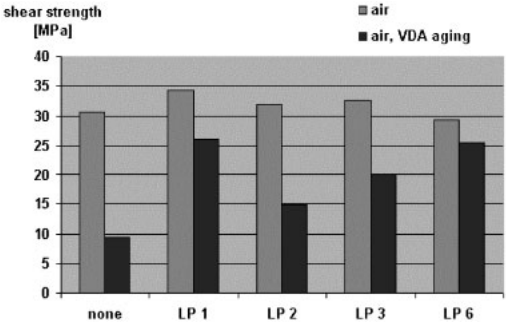

Figure 2.20: Results for AA 6016 bonded with Betamate 1496, process gas: air. [50]

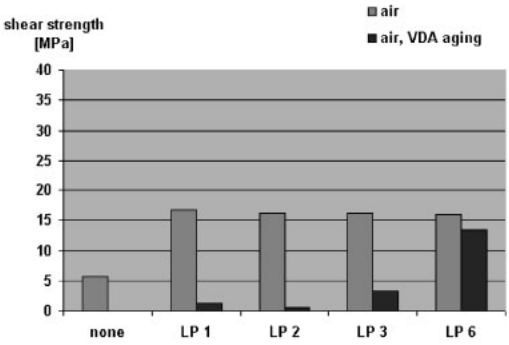

Figure 2.21: Results for AA 6016 bonded with Teromix 6700, process gas: air. [50]

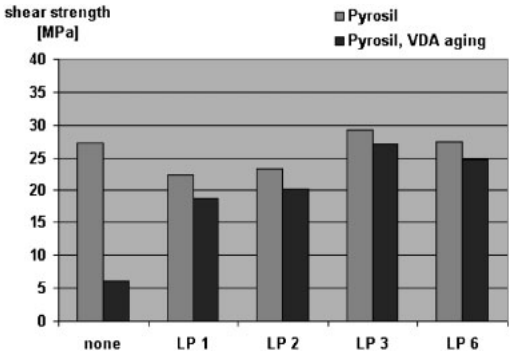

Figure 2.22: Results for AA 6016 bonded with Betamate 1496, process gas: Pyrosil^{TM}. [50]

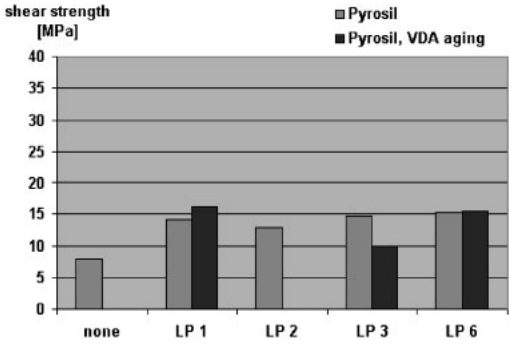

Figure 2.23: Results for AA 6016 bonded with Teromix 6700, process gas: Pyrosil^{TM}. [50]

Chapter 3

Materials and method

Recent works around adhesive bonding focused on laser irradiation of substrates in order to enhance adhesion. Laser ablation has been usually carried out using excimer [54] or solid state lasers [62, 65, 66, 67]. More recently, pulsed fiber lasers, e.g., pulsed ytterbium (Yb) fiber laser, have been also employed [49, 68, 69, 70, 71, 72, 73]. The results have shown that the pulsed Yb-fiber laser surface pretreatment can exert a beneficial action on the strength of single-lap joints. Later on, the process was also applied for the fabrication of Al/epoxy T-peel joints. A considerable increase in bond toughness was observed thanks to improved mechanical interlocking, which diverted the failure path from the near interfacial region to the adhesive layer [74, 75]. In these works, it was also reported that combining suitable process parameters, such as laser speed, line spacing, and average power, small-scale channels could be generated on the irradiated surface thereby resulting in a patterned interface. However, the implications of such surface morphology on the strength of adhesive joints were not investigated. On the other hand, a patterned interface could enhance the interlocking effect and increase the strength of adhesive joints, especially under shear loading. Previous related works carried out on the subject support the previous statement [76, 77, 78, 79]. Indeed, recent experimentations in conjunction with finite element analyses have suggested that the strength and the toughness of an interface between two materials can be enhanced by manipulating surface roughness [76, 77, 78, 79, 80]. Specifically, macroscopic scratches obtained by

mechanical cold work [76], or micro-patterns generated by means of lithographic techniques [77, 78], were able to increase the joint strength thanks to an improved mechanical interlocking. In other words, micro-patterned surfaces can improve mechanical interlocking, increasing energy dissipation and promoting the inhibition of crack propagation (i.e., interfacial toughening) [79]; moreover, simulation results indicated that surface roughness with regular patterns and reduced dimensions is in favor of mechanical interlocking and molecular bonding [80].The aim of the present work is therefore the study of the effect of laser-induced surface patterning on the strength and on the fracture toughness of adhesive joints. An advantage of laser-based patterning with respect to previous methods is that a suitable surface morphology can be created in conjunction with a deep cleaning and removal of eventual weak oxide layers. Laser ablation was therefore carried out on aluminum and stainless steel substrates using a pulsed ytterbium fiber laser. Several characterization techniques were deployed to study the effect of the surface preparation process.

3.1 Mechanical testing

Two kind of substrates were taken into account: AA6082T4 Aluminum alloy and AISI304 stainless steel. Loctite Hysol 9466 epoxy adhesive (Henkel, Düsseldorf, Germany) were selected to produce the joints used for mechanical testing. Specifically, single-lap joints were fabricated and tested according to the ASTM D 1002 standard procedure [1]. This test method covers the determination of the apparent shear strengths of adhesives for bonding metals when tested on a standard single-lap-joint specimen and under specified conditions of preparation and test. It is primarily comparative. However, it does have application as a discriminator in determining variations in adherend surface preparation parameters and adhesive environmental durability. The test method has application in controlling surface preparations, primer, and adhesive systems for determining strength properties of tested systems. In this particular case, substrates were placed into an alignment fixture and 0.2 mm diameter copper wires were employed to set the bond line thickness. A clamping force was applied over the bonding area, as shown in Fig.3.1.

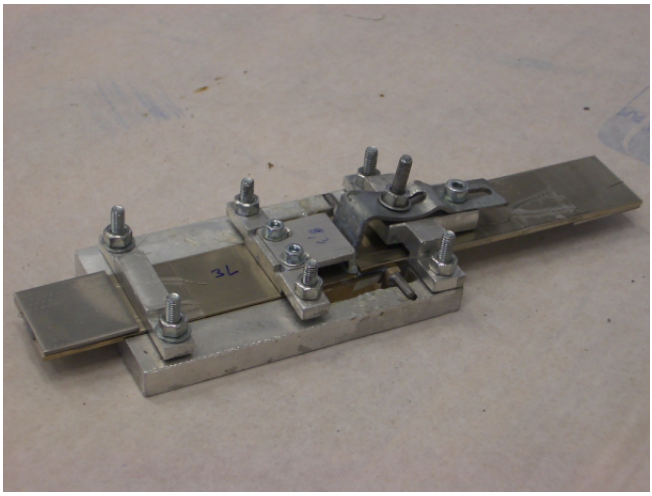

Figure 3.1: Clamping force applied in the overlap area.

Finally, the assembled samples were cured at 70° C for 30 min. The SLS test specimens conformed to the form and dimensions shown in Fig.3.2.

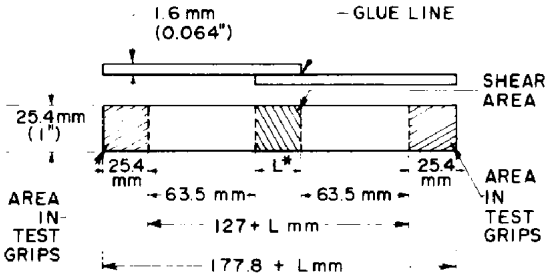

Figure 3.2: Form and dimensions of SLS test specimens according to ASTM D 1002 standard. [1]

TAST joints were fabricated and tested according to the UNI EN14869-2 standard [81]. The test is performed on specimens consisting of thick, rigid adherends, with a short length of overlap, in order to obtain the most uniform distribution of shear stresses

possible and to minimize other stress states which initiate failure. This test method is capable of providing shear modulus and shear strength values for adhesives with accuracy suitable for use by design engineers in predicting the characteristics of building assemblies bonded with nonrigid adhesives. Adhesive formulators will also find the method useful during the development of new adhesive systems or substrates preparation.

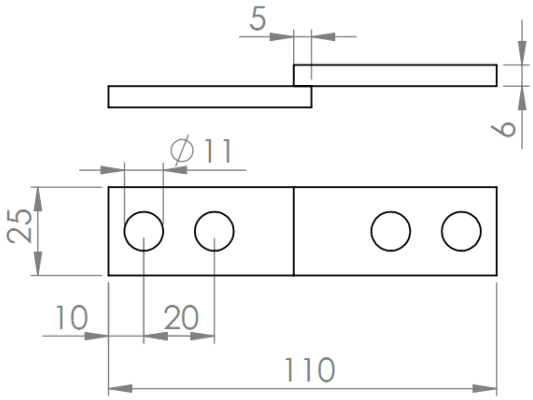

Figure 3.3: Form and dimensions of TAST specimens.

In general, the thick adherend lap-shear test is a useful tool in research during studies of both short- and long-term load-deformation properties of adhesives. Pure shear strength cannot be obtained by this test method, because some tensile and compression stresses and stress concentrations are present in the joint. The estimate of shear strength by this test method will be conservative. The specimens have been prepared by bonding metal plates to produce the configuration shown in Figure 3.3. Substrates were cut at a length L=57.5 mm, width b=25 mm and thickness h=6 mm, with an overlap of 5 mm between the adherends. The bondline thickness was set equal to t=0.25 mm using copper wires and the joints were produced using the jig shown in Figure 3.4.

To evaluate the mode I fracture toughness enhancement, double cantilever beam specimens according to the ASTM D 3433 [20] were fabricated and tested. This test method involves cleavage testing

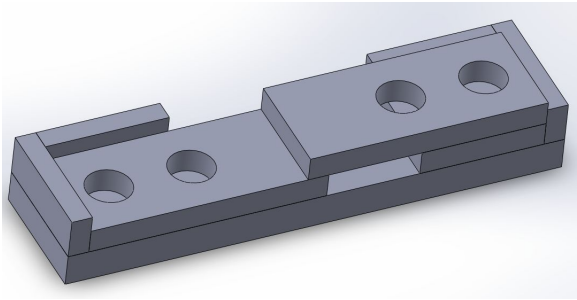

Figure 3.4: Gluing jig for controlling overlap and alignment of TAST specimens.

bonded specimens such that a crack is made to extend by a tensile force acting in a direction normal to the crack surface. This test method will measure the fracture strength of a bonded joint which is influenced by adherend surface condition, adhesive, adhesive-

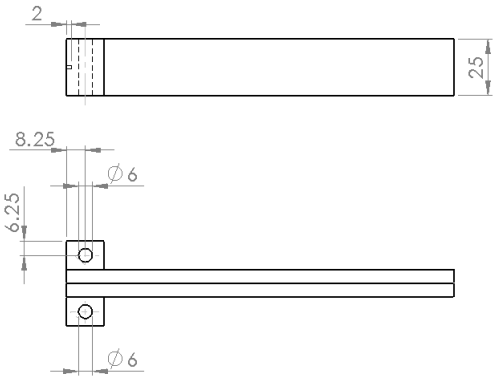

Figure 3.5: Form and dimensions of DCB specimens.

adherend interactions, primers, adhesive-supporting scrims, etc., and in which of the above possible areas the crack grows. Substrates were cut at a length $L = 120mm$, width $b = 25mm$ and thickness $h_A = 6mm$ (Figure 3.5). The two studs shown in Figure 3.5 were

also bonded to the samples using the same epoxy adhesive. Note that only aluminum joints have been taken into account because of thermal distortion problems encountered during laser process on stainless steel substrates having these dimensions.

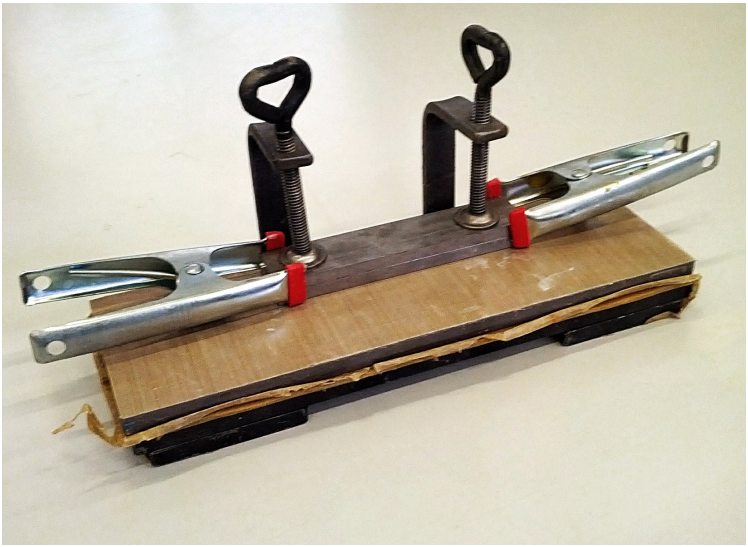

Figure 3.6: DCB joints polymerization.

The adhesive bondline thickness was set equal to $t = 0.25mm$ using brass foils as spacers. Notice that an unbonded area was introduced using a Teflon film and an initial pre-crack ($a_0 = 25mm$) was subsequently obtained by means of fatigue cycling. The specimens were produced using the equipment shown in Figure 3.6 and a clamping force were applied on the bonding area during polymerization of epoxy adhesive. Curing was carried out in temperature controlled oven at 70°C for 30 min in order to have full cure in a short time instead of waiting at least 24h at environmental temperature according to the adhesive data-sheet.

Subsequent mechanical tests were performed at room temperature using a servohydraulic universal testing machine (MTS 810) and the crack mouth opening displacement (δ) was monitored using a clip-gage. The strain energy release rate was evaluated using the

following equations [82]:

$$G = \frac{P^2}{2b}\frac{dC}{da} = \frac{(Pa)^2}{bEI}\left(1 + \frac{1}{a\lambda_\sigma}\right)^2 \tag{3.1}$$

with

$$C = \frac{\delta}{P} = \frac{2\lambda_\sigma t}{E'_a b}\left[1 + 2(\lambda_\sigma a) + 2(\lambda_\sigma a)^2 + \frac{2}{3}(\lambda_\sigma a)^3\right] \tag{3.2}$$

and

$$\lambda_\sigma^4 = \frac{4k}{EI} = \frac{6}{h^3 t}\frac{E'_a}{E} \tag{3.3}$$

where a is the crack length, P is the load, $E = 70000$ MPa is the Young's modulus and I is the second moment of area of the beam section $E_a' = 1070MPa$ is the plane strain Young's modulus of the adhesive. Therefore, Eq. 3.1 allows one to determine the fracture energy of a test sample when the evolution of crack growth is known from Eq. 3.2, which is in turn fed by compliance values measured at given points during the test by unloading-reloading. This procedure has been employed because it takes into account of the deformation and rotation of the cantilevered beam (the adherend) in correspondence of the crack tip due to the adhesive elasticity, without the need for experimental corrections of compliance as prescribed by the ASTM D 3433 standard.

3.2 Surface pre-treatment

Laser ablation of aluminum alloy and stainless steel substrates was carried out using a LaserPoint YFL 20P ytterbium fiber laser operated in pulsed mode (1055–1070nm wavelength, $20 - 80Hz$ pulse repetition frequency, $120ns$ minimum pulse Full Width at Half Maximum, FWHM). The laser beam delivery system consists of an optic fiber, a collimation device and a focusing lens.

The collimation and focusing devices are mounted on a linear translation stage to allow automated positioning of the focal plan. The z stage is motorized by a microstepper motor, which can be easily controlled by computer.

The laser is able to achieve continuous power levels up to $20W$

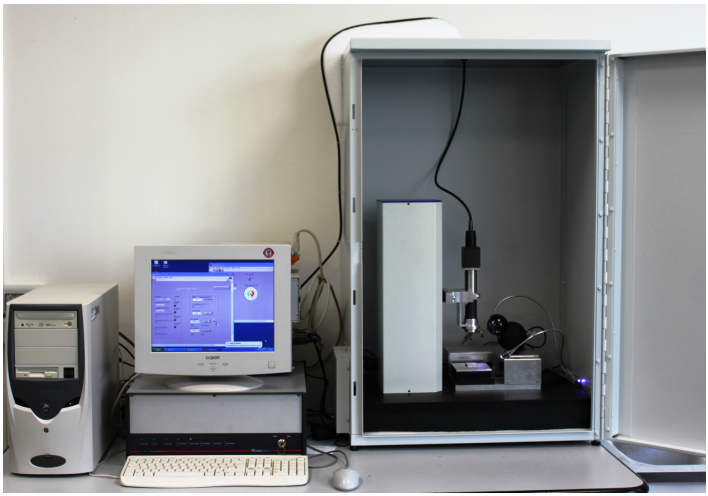

Figure 3.7: The pulsed laser equipment employed to pre-treat metal substrates. [38]

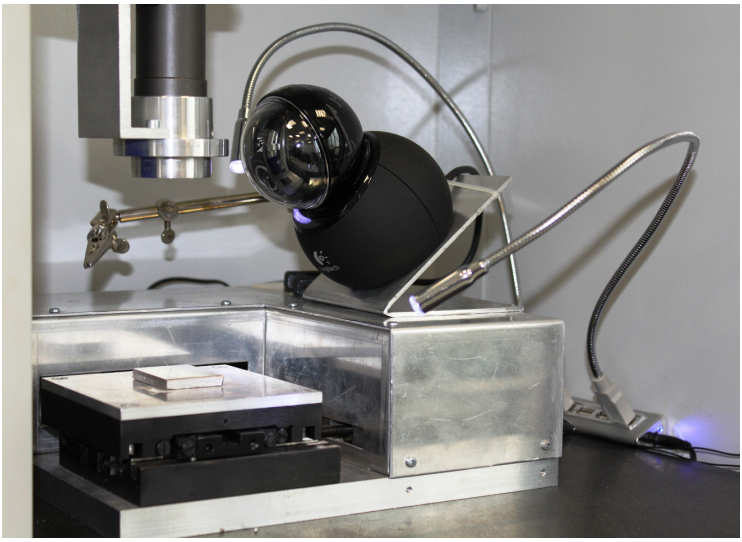

Figure 3.8: A close-up of the workpiece area. [38]

with adjustable line spacing (LS) and feed rate (V). The LS and V parameters can be adjusted by controlling the X-Y stage where the sample under treatment is placed. In this work LS and V have been set equal to $60\mu m$ (50% larger than spot size) and $5mm/s$ (maximum feed rate of the system), respectively. With these parameters, a serrated pattern can be obtained on the joining area in a reasonable time. The laser power was instead varied in the range $1-20W$. A summary of the laser process parameters employed herein is given in Tab. 3.1.

Parameter		Value
Laser nominal power	[W]	1-20
Emission wavelength λ	[nm]	1055-1070
Emission line width	$[\mu m]$	< 10
Mode of operation		pulsed
Pulse frequency range	[kHz]	20-80
Minimum pulse width FWHM	[ns]	120
Beam quality factor, M^2		1.8
Laser beam mode		TEM00
Spot size	$[\mu m]$	40

Table 3.1: Laser processing parameters. [64]

The laser beam is collimated to a diameter $D_0 = 7mm$ and then focused by a F-Theta lens with focal length $f = 100mm$. The spot size can be calculated as follows:

$$d_{spot} = \frac{4}{\pi} M^2 \frac{\lambda f}{d_0} = 350\mu m \tag{3.4}$$

The process was carried out at room temperature and pressure and in atmospheric environment. In order to assess the capabilities of the laser radiation to modify substrates morphology, additional samples were prepared using simple degreasing as well as grit blasting as surface preparation processes. Fig.3.7 and Fig.3.8 show the Laser equipment employed for substrate treatment.

3.3 Analysis of surface morphology and chemistry

3.3.1 Scanning electron microscopy (SEM)

Surface topography is one of the most important surface characteristics of metallic substrates and the usual manner of investigation is the use of scanning electron microscope to provide a high magnification image of the material under investigation.

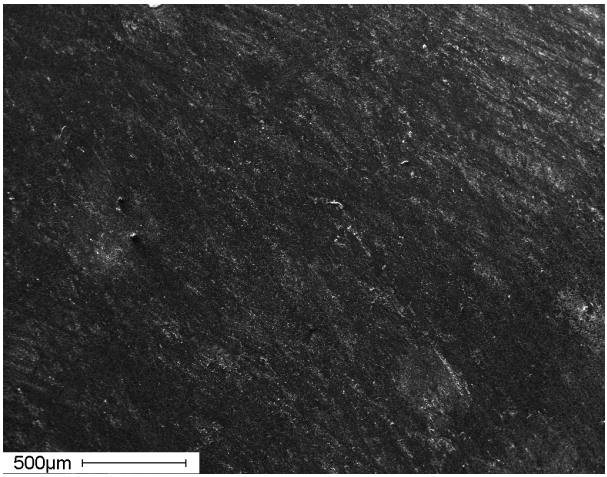

Figure 3.9: Characteristic morphology of as produced stainless steel.

Optical microscopy is not really sufficient, not because it lacks the range of magnification of a SEM, although this is an important feature, but because of its poor depth of field and depth of focus. In optical microscopy, features not in the image plane appear out of focus (i.e., blurred), whereas a SEM is able to accommodate very large depth of field.

The importance of surface topography is illustrated by the images of Fig.3.9 and Fig.3.10 where are shown steel substrates as produced and grit blasted respectively and the enhanced rugosity that is provided by such simple mechanical treatment is clearly seen.

This effectively increase the degree of interfacial contact area between the adhesive and the substrate and, at a very simplistic level, may enhance the level of adhesion and durability so obtained.

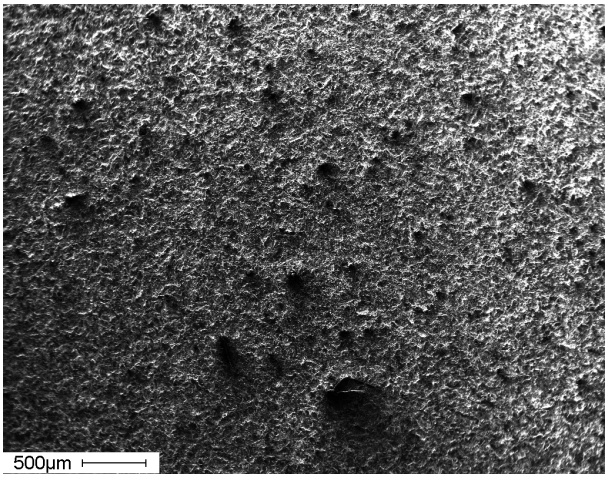

Figure 3.10: Characteristic morphology of grit-blasted stainless steel.

It is sometimes convenient to use a SEM to examine failure surfaces of joints. The micrograph of Fig.3.11 is the failure surface of an aluminum substrate bonded with a structural adhesive (Henkel Loctite Hysol 9466 epoxy adhesive). The definition of the locus of failure is a rather complex task and depends on the level of sophistication of the assessment methods available.

Some pre-treatments lead to characteristic morphologies on a very fine length scale which can be clearly defined only by high resolution SEM. The typical example of this kind of morphology is the acid anodized aluminum.

In the present work, using laser irradiation a fraction of the laser beam energy is absorbed by the material, thus promoting material ablation, i.e. removal by vaporization. In order to analyze surface morphological modifications made by the laser process, SEM analyses (Cambridge Stereoscan, 20 keV electron beam, current $\backsim 3.4\mu A$, spot size $\backsim$ 1.4 mm^2) were carried out on as-produced and surface pre-treated samples.

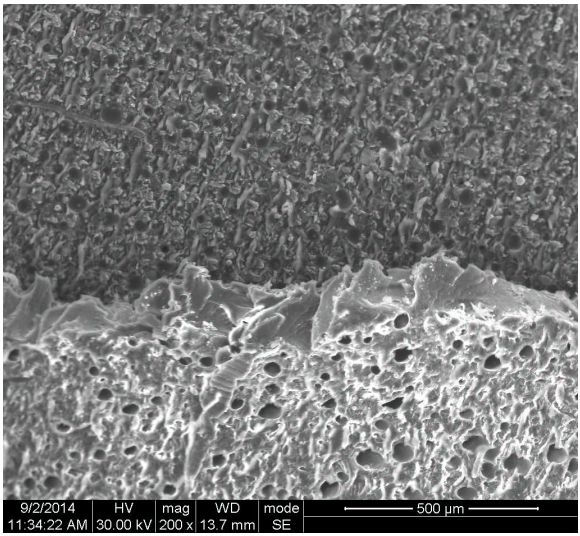

Figure 3.11: Failure surface of a grit-blasted aluminum surface bonded with a structural adhesive.

3.3.2 Stylus profilometry

In any assessment of surface roughness it is desirable to move away from the qualitative images of SEM to an approach which can provide a quantitative assessment of surface roughness. This can be achieved by a variety of techniques including the scanning probe microscopies of scanning tunnelling microscopy, but the most straightforward method is the use of stylus profilometry. This is a standard

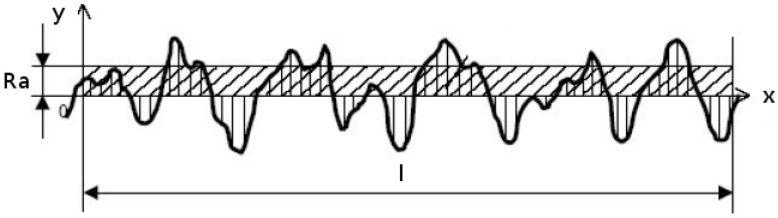

Figure 3.12: Definition of surface roughness.

metrology tool which is widely used in engineering to assess the surface profile (or roughness) of a machined component. The concept is simple in that a diamond stylus is dragged across the surface and records the short range undulations (roughness) and long range undulations (waviness) of the surface in a graphical manner, either from direct deflection of the stylus or by using an interferometric approach. The interpretation of roughness data is considered at length in the relevant national standards and international standards, but the most important terms are roughness average (also known as center line average), R_a, and RMS (root mean squared) roughness, R_q. The term R_z to define maximum excursion of the profile from the hypothetical center line is sometimes used but is not very helpful. The terms R_a and R_q can be defined, by reference of Fig.3.12 as follow:

$$R_a = \frac{1}{l}\int_0^l |y(x)|dx \tag{3.5}$$

$$R_q = \frac{1}{l}\int_0^l [y(x)]^2\,dx \tag{3.6}$$

Additional parameters are available to describe the bearing area, the autocorrelation coefficient as well as many others which are described in the standards. The main disadvantage of such an approach is that although it gives quantitative information regarding the deviation from the center line profile, it tells us nothing about the distribution of heights, the length scale of the surface profile, or the variations as a function of distance along the length of the scan. For this reason, profilometry, when used for reason other than to check the profile of a machined component for metrology purposes, should always be combined with a microscopic technique to visualize the surface (e.g., SEM, AFM).

In this work of thesis, contact profilometry was undertaken using a SM RT-150 stylus-based profilometer to have a quantitative assessment of surface morphology. Each specimen was acquired 12 times in order to obtain 12 samples for each substrate. Each resulting dataset, consisting of a height map sized 64x64 points with uniform spacing $dx = dy = 12.5\mu m$, was leveled by subtraction of the least-squares mean plane and used to evaluate the principal 3D field parameters for surface finish assessment, as defined

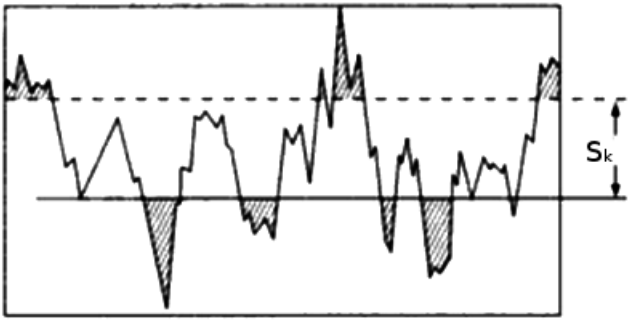

Figure 3.13: Core Roughness depth S_k.

in ISO/FDIS 25178-2. In particular, the S_k field parameter (core height) was employed as a measure of the surface roughness. S_k represents the core (or kernel) roughness of the surface over which a load may be distributed during most of the functional life of the surface. It is a measure of the nominal roughness and may be used to replace the mean roughness, Ra, and similar parameters. S_k, is a measure of the "core" roughness (peak-to-valley) of the surface with the predominant peaks and valleys removed, as shown in Figure 3.13. [83] It is more robust than R_a especially when localized singularities (e.g. very high peaks or deep pits) are present on the surface.

3.3.3 XPS analysis

Within the category of surface chemical analysis, the techniques being considered is the X-ray photoelectron spectroscopy (XPS). This method find various uses in adhesive bonding investigations, but there are several area of investigation. These include the assessment of surface properties, the removal of contamination, or the investigation of the chemistry of surface pre-treatments; the forensic analysis of adhesive bonding failures, the study of interfacial failure surfaces with the aim of identifying the presence of weak boundary layers or other phenomena responsible for failure and finally the direct probing of the interfacial chemistry responsible for adhesion itself. The last named presents perhaps the most challenging sce-

nario for surface analysis. The eventual aim is to engineer specific chemistry of an interface so as to provide specific properties in the adhesive joint.

XPS technique is based on low energy emitted electrons. It is the analytical use of low energy electrons that gives this technique its surface specificity, with analysis depth of $6nm$.

The XPS makes use of an X-ray beam (usually $AlK\alpha$ or $MgK\alpha$) and the spatial resolution attainable can vary, depending on the system specifications, from $1-0.5mm$ to $10\mu m$ for a high performance small area XPS system.

XPS is able to provide quantitative analysis of the surfaces of all materials providing they are stable within the Ultra-High Vacuum chamber of the spectrometer. It is the chemical specificity of XPS that has made it popular choice for surface analysis in adhesion science.

XPS (X-ray Photoelectron Spectroscopy) measurements were carried out in a Ultra-High Vacuum (UHV) chamber equipped for standard surface analysis with a base pressure in the range of $10^{-9}torr$. Non monochromatic $MG-K\alpha$ X-ray ($h\nu = 1253.4eV$) was used as excitation source. The XPS spectra were calibrated with the C1s peak of a pure carbon sample (energy position $284.6eV$). All XPS spectra have been corrected with analyzer transmission factor and the background was subtracted using the straight line subtraction mode. Moreover the XPS data were fitted assuming a Gaussian distribution for high resolution analysis. XPS measurements have been carried out by Barberio at the Department of Physics of University of Calabria.

3.3.4 Contact angle

Following the well known Young Equation:

$$\gamma_{sg} = \gamma_{sl} + \gamma_{lg}\cos\theta_c \tag{3.7}$$

representing the equilibria established by a sessile drop on a solid surface, a contact angle ($\theta_{\theta c}$) can be defined, as in Fig.3.14. This represents the angle of the tangent of the drop at the triple point between solid, liquid, vapour and the free energy of the solid substrate γ_{sg}, and the interfacial free energy of the liquid and the solid γ_{sl}. The surface free energy, or surface tension, of the liquid γ_{lg} will be known and θ_c provides a readily observed manifestation of the

interaction of a liquid with a solid. Thus, if we consider water as

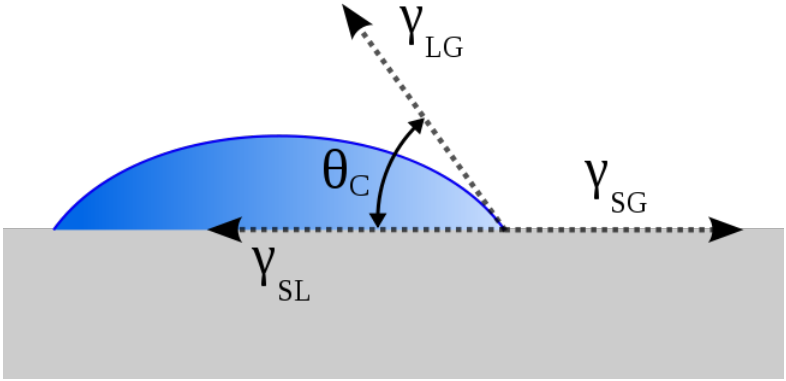

Figure 3.14: Thermodynamic equilibria of sessile liquid drop on a solid substrate.

the wetting liquid, a high surface energy substrate such as an oxide will wet fairly readily, while a low surface energy substrate such as a polymer will not wet so readily and the liquid will form a very high contact angle (perhaps even discrete spheres) on the surface. Thus, the simple expedient of observing the characteristics of a small drop of water on a solid substrate tells the observer much about the free energy and wettability of the solid surface. This can be important in two areas, the degreasing and the surface treatment of metals.

Although the Young Equation forms the underpinning basis for understanding the behavior of the solid/liquid interface and the spreading of liquids on a surface, there are several routine tests that find widespread use that merely offer a go/no-go situation and can be used quite satisfactorily for quality assurance purposes by untrained personnel.

Therefore, the contact angle can be very informative in order to assess the cleanliness of solid surface and to qualify the effectiveness of a surface pretreatment[3, 2]. Contact angle data determined by means of the sessile drop technique were used herein to track the evolution of surface wetting as a function of the laser parameters. A small drop of distilled water was placed on the metal substrates and the equilibrium contact angle was determined by drop shape anal-

ysis using a KSV NIMA Instruments Ltd CAM 200 optical contact meter. Each sample was measured twelve times to ensure data robustness. These measurements have been carried out by Alfano at the Department of Mechanical, Energetic and Management Engineering (DIMEG) of University of Calabria.

Chapter 4

Assessment of surface modifications

4.1 Surface and Topographic Analysis

The distributions of the Sk parameters, which are depicted in Fig.4.1 [64] for both materials, testify that below a precise threshold power level, the laser processing was not able to significantly modify surface morphology. Specifically, incident laser power levels equal to 12 W and 14 W represent the threshold levels for aluminum alloy and stainless steel substrates, respectively. Once the threshold level is reached, the Sk parameter exhibits a step-like, several-fold increase; beyond the threshold level, Sk displays an approximately constant value up to the system maximum power, that is, 20 W. It is also worth noting that the roughness induced by the laser process on aluminum alloy substrates was always below that recorded on the grit-blasted substrates (Fig.4.1(a)); on the other hand, the opposite was observed on stainless steel samples (Fig.4.1(b)). The surface profile of selected samples reported in Fig.4.2 [64] provides confirmation that laser processing gave rise to a variation in the surface topography with respect to the native (as produced condition) roughness of the metal substrates; the variation was significant once the power was set above the threshold level. The SEM pictures recorded across selected as-produced, and laser-irradiated aluminum alloy (upper row) and stainless steel (lower row) sub-

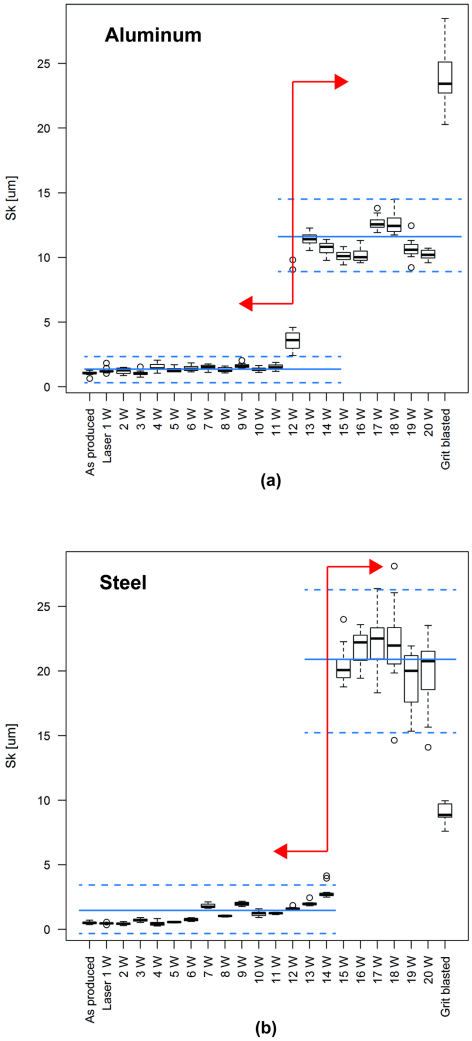

Figure 4.1: Distributions of the Sk parameters for (a) Al and (b) steel substrates. [64]

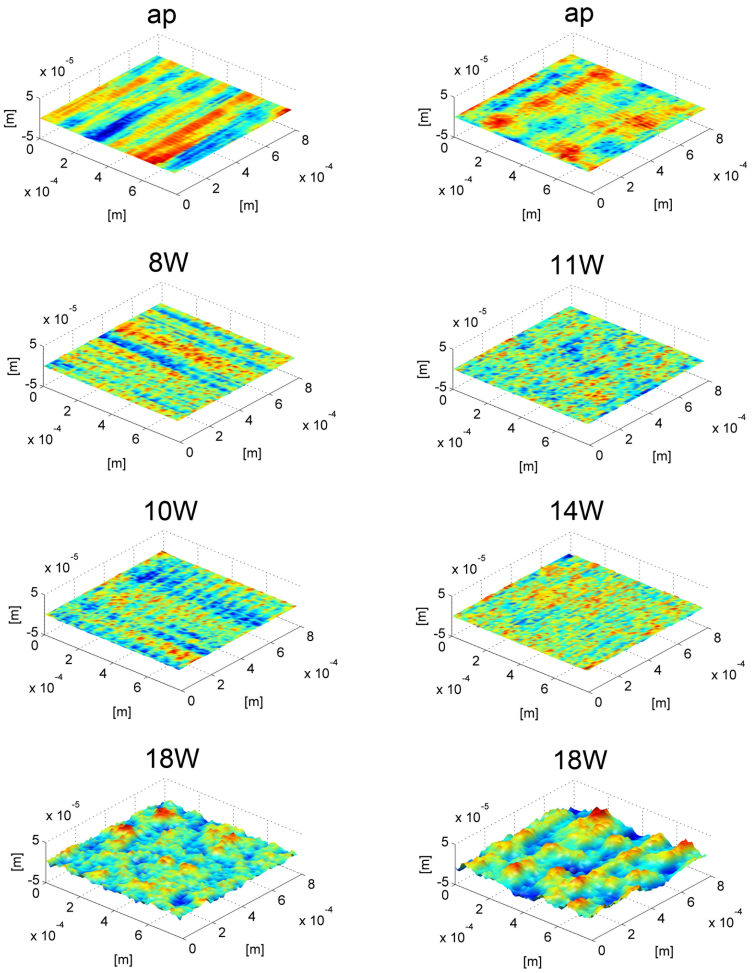

Figure 4.2: Results of 3D contact profilometry analyses showing surface morphology of aluminum (left column) and steel (right column) substrates for varying surface processing conditions. [64]

strates are given in Fig.4.3 [64]. As already shown through contact profilometry, for laser power below the threshold level, there was little modification of the surface morphology, although a certain degree of surface micro-waviness and patterning could be already observed. For higher power levels, large morphological modifi-

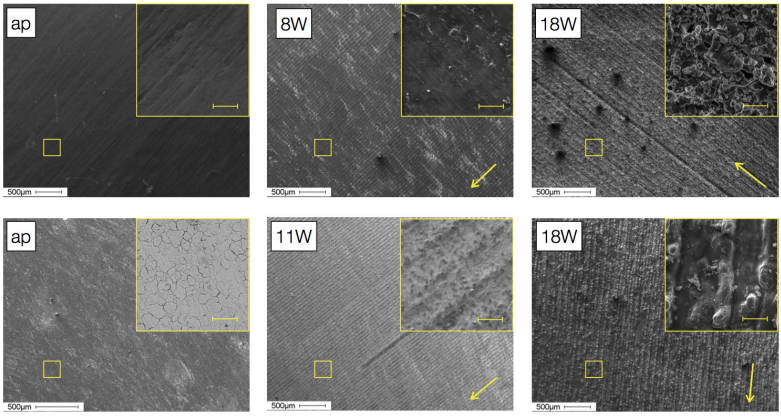

Figure 4.3: SEM observations of aluminum (upper row) and steel (lower row) substrates before and after laser irradiation and for varying level of the output power. The arrows demonstrate the lasing direction. The bars reported in the insert (rectangular box) indicate a $50\mu m$ spacing. [64]

cations occurred, with significant surface melting which led to a considerable increase in surface roughness. In both cases, surface patterning of the metal substrates was still apparent, although the intended pattern had been slightly distorted due to the considerable surface melting and oxidation. Globular micro-sized aluminum particles could be observed on aluminum substrates when the power level was set greater than the threshold value ($> 12W$). As already discussed in [49, 59], these particles formed through condensation of expanding gas or plasma during cooling. Oxide particles were not detected on steel substrates; instead, as a result of the laser ablation, extensive surface melting occurred, concurrent with a remarkable surface darkening. The related modifications of surface chemistry are investigated in the next section.

4.2 XPS Measurements

XPS spectra of the investigated surfaces along with a quantitative elemental analysis are reported in Figs4.4 and 4.5 [64]. The survey spectrum for the aluminum alloy surface, which is given in Fig.4.4 and Table4.1 [64], shows that aluminum and oxygen are present in the as-produced condition. In addition, contaminants such as carbon (C), tungsten (W), and fluorine (F) were also observed since the specimens were handled as received. This in order to keep

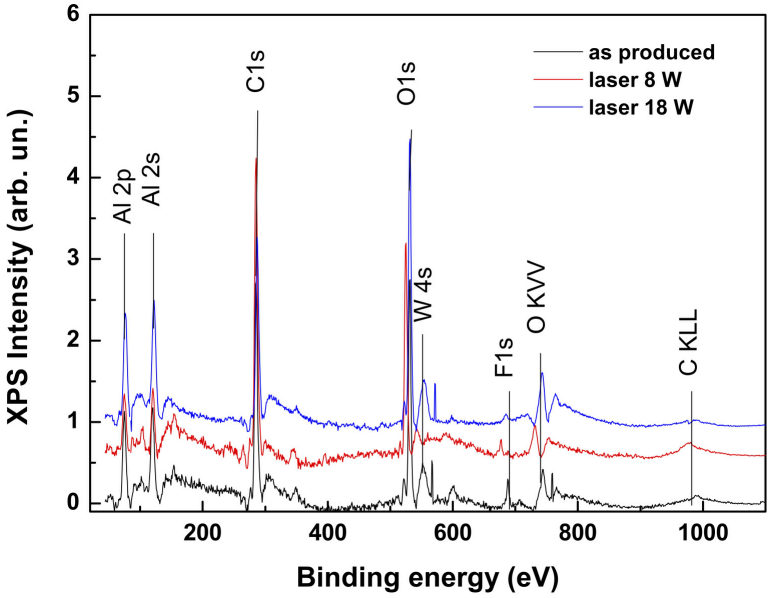

Figure 4.4: XPS spectra of as produced and laser treated AA6082T6 substrates. [64]

surface conditions similar to adhesive bonding of laser-treated substrates that was made on the as-received material as well. However, contamination can be also produced during laser irradiation as a result of sample surface carbonization that induces the formation of a thin CO_2 layer. The spectrum survey recorded after laser irradiation at power levels up to $11W$ showed a slight modification of surface composition, while contaminants were still retained on substrate surface.

Substrate	Element (at.%)							
AA 6082-T4	Al	Fe	O	C	Cr	W	F	
As produced	29.2	-	17.5	49.6	-	1.5	2.2	
Laser 8 W	29.7	-	19.3	47.6	-	1.3	2.1	
Laser 18 W	39.8	-	12.4	47.8	-	ND	ND	
AISI304	Al	Fe	O	C	Cr	W	F	Ca
As produced	-	0.22	9.46	89.86	0.43	-	-	0.03
Laser 11 W	-	0.3	11.47	85.0	3.23	-	-	-
Laser 18 W	-	0.65	16.77	78.14	0.43	-	-	0.43

ND, not detected.

Table 4.1: Elemental Composition of as Produced and Treated Substrates as Determined by XPS Analyses. [64]

However, when the power level achieved values higher than the threshold level, i.e., 18 W, a dramatic increase of aluminum and decrease of oxygen atomic percentages were recorded. On the other hand, the carbon content was retained after the surface treatment. It is worth noting that the carbon content on the analyzed surface can be originated during sample cutting, but also from adsorbed atmospheric contamination occurring during the process, as already observed earlier in this section [62, 67]. Moreover, high resolution XPS analyses allowed us to observe a shift in the Al 2p line peak from $75.6eV$ to $76.6eV$ when the samples were irradiated at laser power levels greater than $12W$.

It was then concluded that the Al_2O_3 layer, initially present on the as-received substrates, was replaced by an AlO oxide layer [75]. Therefore, laser power higher than the threshold level led not only to a variation of surface roughness, but also to a modification of the surface oxide layer. The survey spectra obtained on stainless steel substrates are given in Fig.4.5. In the as-received condition, surface composition included Fe, Cr, C, and O. A small atomic percentage of Ca, which was very close to the XPS detection limit (0.1%), was also recorded. It is believed that this contamination was accidentally introduced during sample handling and preparation process. Also the high carbon content can be attributed to the analysis of the samples in the as-received conditions, as in the case of aluminum alloy. After laser irradiation, the percentage of Fe and O increased

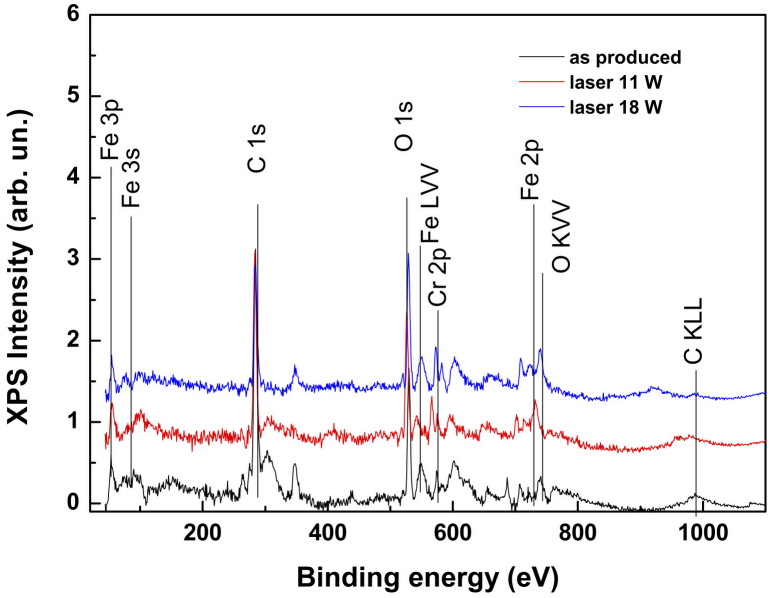

Figure 4.5: XPS spectra of as produced and laser treated steel substrates. [64]

while the percentage of C decreased. High resolution XPS analysis provided information on the chemical bonds between elements. In particular C1 s was asymmetric and could not be reproduced by one single Gaussian. Our best fit (Fig.4.6) indicated the presence of two well-distinguished peaks at 284.3 (main structure of C1 s) and 285.6eV that are typical of C–O chemical bonds [84]. Notice that a third peak at about 300eV is weakly visible in all spectra; this is due to plasma loss with both p and r characters and typical of all carbon structure. The intensity of C–O line increased with laser power indicating the formation of C–O bonds under laser irradiation. It is important to highlight that C–O are polar bonds and as such can potentially improve surface energy and wettability [3, 2]. Moreover, on all sample surface, Fe 3p and Fe 3s 2p lines present both a single main structure centered at about 56.6 and 92.8eV, respectively. Both these lines can be attributed to the presence of iron oxide (Fe_2O_3) [84] and indicate that laser ablation did not remove this oxide from the steel surface. The O1 s lines exhibit for all

samples a main structure at roughly $531eV$ that is usually assigned to oxygen bonded in O-metal states (Fig.4.6) [64]. Therefore, laser ablation of stainless steel substrates provided variation of surface morphology, but it did not substantially modify the surface oxide and led to the formation of C–O bonds which, in turn, are expected to improve surface wetting.

4.3 Contact Angle Measurements

The static water contact angle was analyzed to qualitatively assess the effectiveness of the investigated surface preparation techniques and their influence on surface wetting. The sessile drop technique was employed [3, 2]. Indeed, the simple observation of a small liquid drop on a solid substrate can provide useful information concerning the liquid–solid interaction. The obtained results for as-produced and selected laser-treated substrates are summarized in Fig.4.7 [64]. For the aluminum alloy substrate, it is shown that using a laser irradiation below $12W$ (i.e., $8W$), there was little or no effect on the contact angle since the recorded value was pretty similar to that observed on the as-produced surface. In other words, laser irradiation did not result in contact angles markedly different from the untreated surfaces as long as the power was lower than $12W$. Notice that, based on the previous XPS analyses, low power ablation did not modify the kind of surface oxide, and the Al_2O_3 layer present on the as-produced surface was retained. For power levels greater than or equal to $12W$ the water contact angle dramatically increased and the surface became super-hydrophobic. This behavior apparently conforms with the Wenzel wetting regime [3, 2], since the initially hydrophobic surface becomes more hydrophobic after the increase in surface roughness. However, it should be noted that the modification of the surface oxide ($Al_2O_3 \rightarrow AlO$) was concurrent to the variation of surface roughness. On the other hand, stainless steel substrates showed a different behavior. Indeed, the initial as-produced surface had a contact angle lower than 90 , and then it should be regarded as nearly hydrophilic. But when the roughness increased, the surface became super-hydrophobic, with a contact angle in excess of 160 . It is instead hypothesized that the more refined pattern on steel substrates induced liquid drop pinning on surface asperities and possibly induced air pockets immediately be-

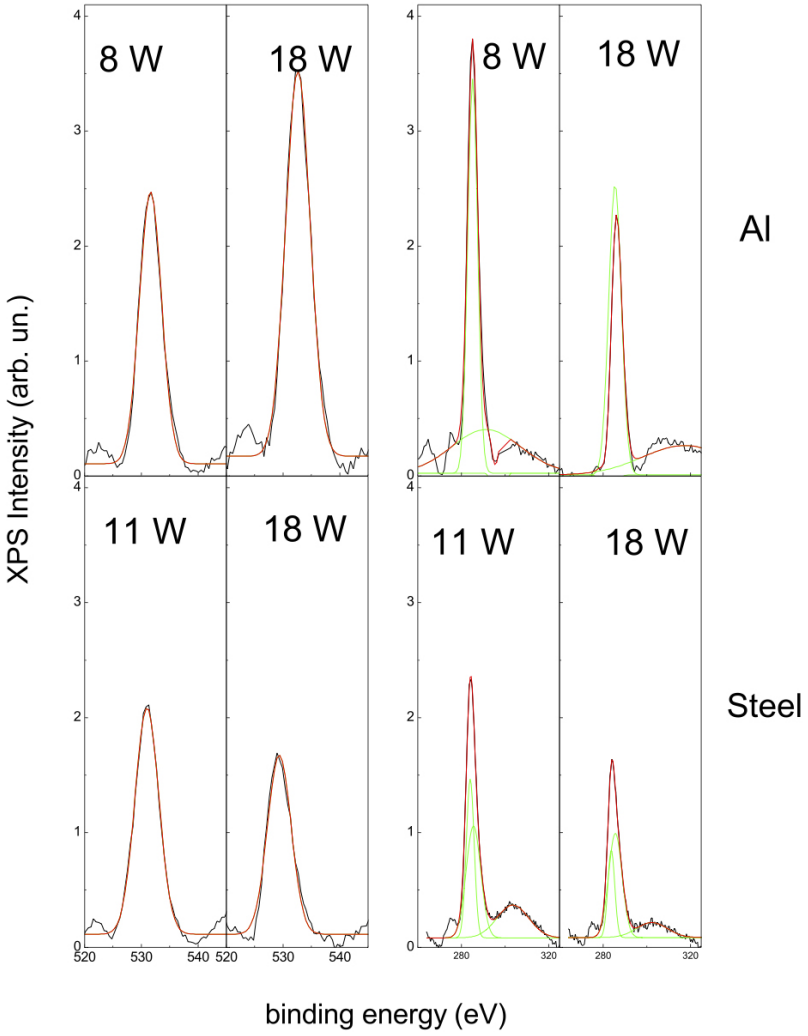

Figure 4.6: O1s spectra (left) and C1s spectra (right) of Al and Steel substrates. [64]

low the liquid. A similar behavior was already observed in [75] on aluminum alloy substrates, where a transition from Wenzel's to a metastable state, given by the combination of Wenzel's and Cassie-

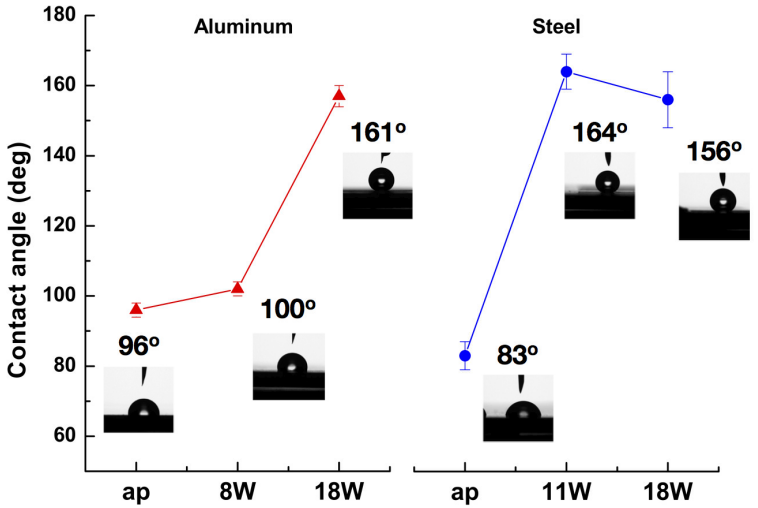

Figure 4.7: Evolution of contact angle as a function of surface conditions for aluminum (left) and steel (right) substrates. [64]

Baxter wetting state [85], was observed. The subsequent slight decrease of contact angle for higher power level might be related to the increased formation of C–O polar bonds that have been described in the previous section and which may increase the surface energy. Considering the small modifications of the surface oxide observed on steel samples, the water contact angle mostly depended on the modification of surface roughness. The higher power treatment provided the best performance in terms of pattern reproduction, surface morphology, and chemistry. For this reason, the subsequent analyses and mechanical testing were carried out by retaining the higher power level. As a result, samples were treated at $P = 18W$, $LS = 60\mu m$, and $V = 5mm/s$. The underlying hypothesis is that $18W$ pattern is representative of those obtained with powers above the threshold level. This assumption seems to be reasonable since the roughness exhibits a sharp increase beyond the threshold level, and after that it is fairly constant. Moreover, XPS analyses, not shown in the paper for brevity, have indicated that there are no significant variations in surface chemistry in that range. Indeed, the range of powers above the threshold that can be scanned is very

limited; therefore, significant changes could not be detected.

4.4 Analysis of Mechanical Interlocking

Since the water contact angle revealed an essentially hydrophobic behavior, additional investigations were carried out to assess the ability of the selected adhesive to interlock with the treated surfaces. It is indeed recognized that measurements of water contact angle by themselves do not account for additional important features of actual bonding procedures. For instance, it should be noted that the liquid epoxy adhesive has a lower surface tension compared to that of water; as a result, it may not be able to properly fill surface asperities. On the other hand, previous works have shown that surface wetting of the epoxy can be enhanced by surface roughness and change in surface chemistry, because of capillarity channeling and surface oxidation, respectively [53]. In order to assess whether or not the gap-filling capabilities of the adhesive may adversely affect the outcome of the present study, the metal/epoxy interfaces were observed using optical microscopy. To this purpose, ad-hoc samples were fabricated and then cut to display the related interfaces. Sample fabrication was executed using essentially the same procedures described in the previous chapter for the single-lap shear joints. Figure 4.8 [64] illustrates (a) AA6082-T4/epoxy and (b) AISI304/epoxy interfaces, respectively. Figure 4.8(a) testifies that there is little or no indication of mechanical keying in the aluminum joints, and that surface waviness is limited. This waviness is however compatible with the value S_k found in Fig.4.1(a) above $12W$.

Hence, it is not expected that mechanical keying will play a major role in determining the overall strength of these joints. On the other hand, surface patterns are quite apparent on the steel substrates, see for instance the micron sized pyramidlike structure in Fig.4.8(b). The adhesive seems to be able to fill the gaps between these micro-structures, although this information can only be confirmed by the outcome of the experimental tests where a larger interfacial area will be probed. It is also noted that the gap-filling capabilities of the adhesive were presumably enhanced thanks to the heat-assisted joint curing employed during fabrication, which lowers viscosity before polymerization favoring adhesive penetration inside the gaps. Indeed, the work reported in ref [75], which used the same

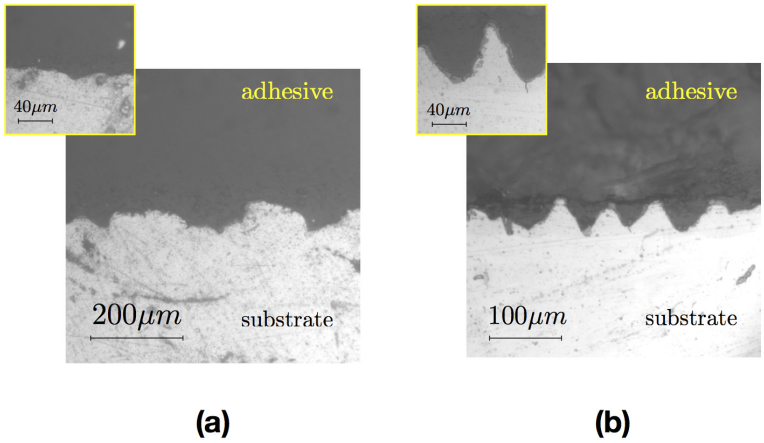

Figure 4.8: Cross-sectional views of the (a) aluminum/epoxy and (b) steel/epoxy interface (both treated at 18W), showing details of the morphological features interlocking with the epoxy adhesive. [64]

kind of adhesive, showed that cold curing could lead to an imperfect surface wetting. This problem occurs especially in presence of complex surface morphologies, since the adhesive may not fully penetrate the cavities created by the process and gels before a complete penetration.

Chapter 5

Mechanical testing results

In this work of thesis, the analysis around the effect of low power pulsed laser treatment has been focused in three directions: (i) the evaluation of two different material, in this case, austenitic stainless steel AISI304 and AA6082-T4 aluminum alloy; (ii) analysis of joint strength by using the Single Lap Shear (SLS) tests and the Thick Adherend Shear Tests (TAST); (iii) analysis and comparison of mode I fracture toughness of aluminum/epoxy joints by mean of Double Cantilever Beam (DCB) tests. For the sake of comparison, all laser ablated specimens has been compared with simple degreased and grit blasted adhesive joints.

5.1 Single Lap Shear tests

Failure loads of the single-lap aluminum/epoxy joints are reported in the column bars in Fig.5.1, where laser ablated aluminum joints are compared to simply degreased and grit-blasted ones [64]. Laser ablation consistently improved the strength of the joint with respect to simple degreasing, indeed a +100% increase was observed. The increased strength of aluminum alloy/epoxy joints might be related to the modification of the surface oxide layer which led to a better adhesive–substrate chemical interaction. This is in agreement with recent research carried out on the subject, where the oxide layer of

aluminum substrates for adhesive bonding was optimized by fiber laser ablation [66] or solid state laser ablation assisted by a process gas [67]. Anyway, surface oxidation might also have an adverse effect on the strength, since the oxide particles showed in the previous SEM analysis were weakly bonded to the Al substrates and could be easily detached under load.

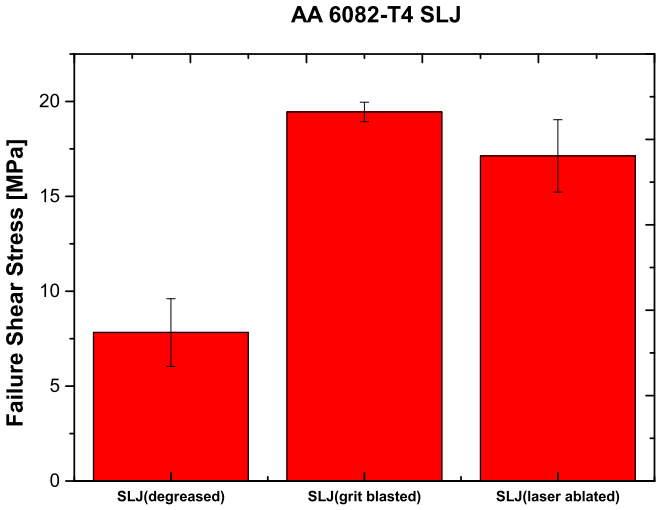

Figure 5.1: Failure shear stress for SLS aluminum/epoxy joints. [64]

On the other hand, steel/epoxy joints, showed a +25% improvement in strength with respect to simple degreasing as reported in Fig.5.3 [64]. It was not observed a sensible increase in the failure load for steel samples and it is, thus, apparent that a simple degreasing of steel surface enabled by itself a good adhesion strength. This point was also discussed in previous works [3, 2]. It is also worth noting that ablation did not greatly modify surface chemistry of steel substrates, it is then speculated that the +25% increase is mostly related to the increased surface roughness.

SEM images of typical fractured surfaces are reported in Fig.5.2 [64]. It is shown that laser ablation did not induce mechanical interlocking on aluminum alloy/epoxy joints. Indeed failure surfaces

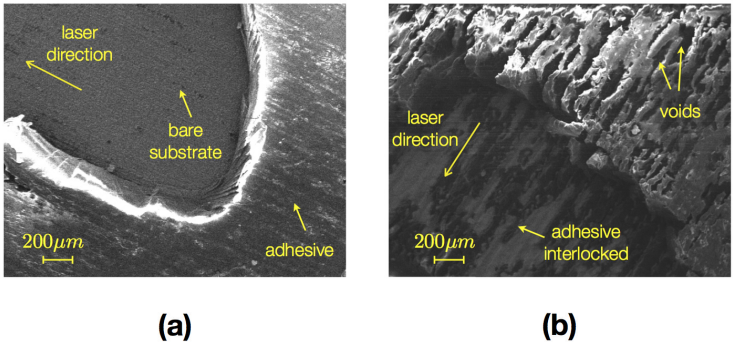

Figure 5.2: Cross-sectional views of the (a) aluminum/epoxy and (b) steel/epoxy interface (both treated at 18W), showing details of the morphological features interlocking with the epoxy adhesive. [64]

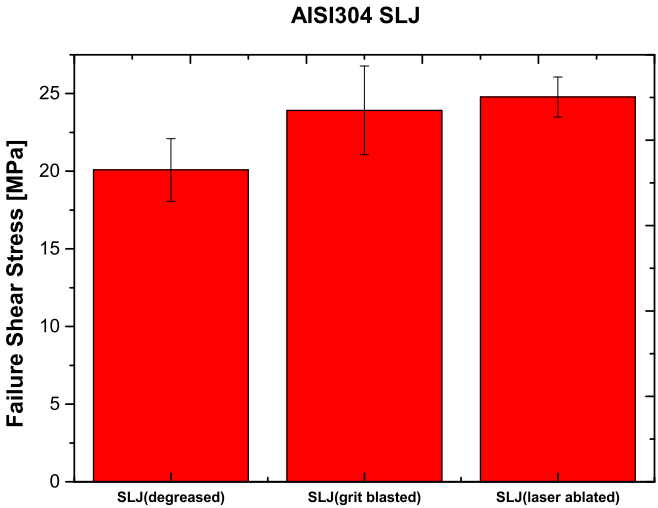

Figure 5.3: Failure shear stress for SLS stainless steel/epoxy joints. [64]

display a bare aluminum alloy substrate. On the other hand, failed stainless steel/epoxy joints showed some degree of mechanical interlocking, which was also expected based on the observation made earlier in the paper. However, voids are also shown, thereby leading to the conclusion that the filling of surface asperities was not always achieved throughout the interface of the sample. This may also explain the reduced increase in strength for that type of joints.

5.2 Thick adherend shear tests

The eccentric loading path and the relatively thin substrates employed for sample fabrication of SLS joints may induce large deflections and, more importantly, plastic deformations of the adherends. From this standpoint, it has been shown in [86] that adherend plasticity occurring during SLS tests may adversely affect the evaluation of lap-shear strength because it enhances local peeling deformations and increases the effect of mode I failure. Therefore, assessing the improvement of mechanical interlocking induced by the surface patterns through the SLS test coupon may be not very effective in these circumstances. In order to check to which extent the SLS test geometry affected the evaluation of the enhancement in joint strength, TAST specimens were also prepared and tested following essentially the same procedures employed for the SLS joints. It should be recognized that using the TAST sample configuration a significant enhancement of flexural and tensile stiffness of the adherends is achieved. As a result the TAST coupon allows to minimize the differential straining in the bonded portion of the substrates and allows to achieve a regularization of the stress fields within the bondline, which is expected to be essentially loaded in shear. In addition, it is also possible to rule out any adverse effect associated to adherends rotation and plasticity in the course of fracture. The failure shear stress for simply degreased, grit-blasted and laser ablated aluminum alloy/epoxy TAST samples are reported in Fig.5.4 [87].

Laser ablation was able to increase joint strength up to +20% in aluminum/epoxy with respect to simple degreasing and no adherend plastic deformation occurred on all sets of specimens after testing [87].

In order to resolve the mechanism of failure, SEM analyses of the failure surfaces were undertaken. Figure 5.5 [87] shows typical

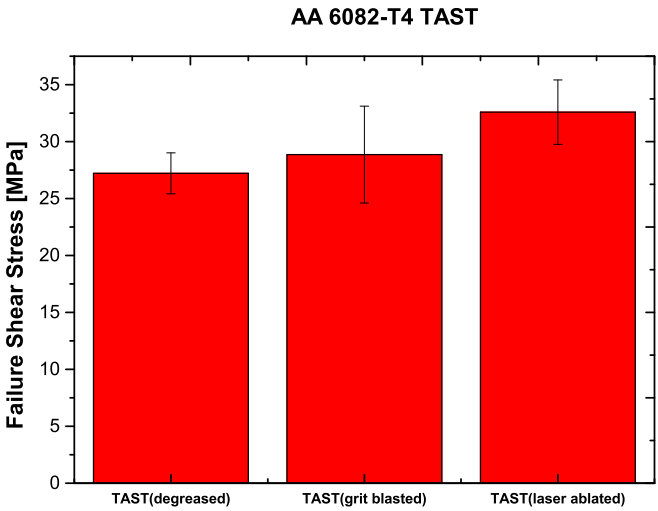

Figure 5.4: Failure shear stress for aluminum/epoxy joints obtained with the Thick Adherends Shear Test (TAST). [87]

fracture surfaces for a TAST sample In particular, Fig.5.5(a) shows the transition region where the failure path is diverted from the upper to the lower substrate; Fig.5.5(b) represent a magnification of such region displaying the cohesive failure of the adhesive, which appears to occur in conjunction with extensive inelastic shear deformations. The fracture surfaces across the transition region are reported in Fig.5.5(c) and (d). Figure 5.5(c) shows the top surface of the adhesive left on the substrate; inelastic deformations as well as small voids, likely associated to air entrapped during curing, are apparent. Inelastic deformations are due to the adhesive interlocked with the substrates which is torn apart in the course of failure. The adhesive residues within substrate asperities are highlighted by the white arrows reported in the SEM image given in Fig.5.5(d).

It is interesting to note that such interlocking was not observed in single lap joints with thinner adherends made up of similar adherends and same laser processing conditions [64]. This effect could be related to the use of the TAST specimens which enabled the ad-

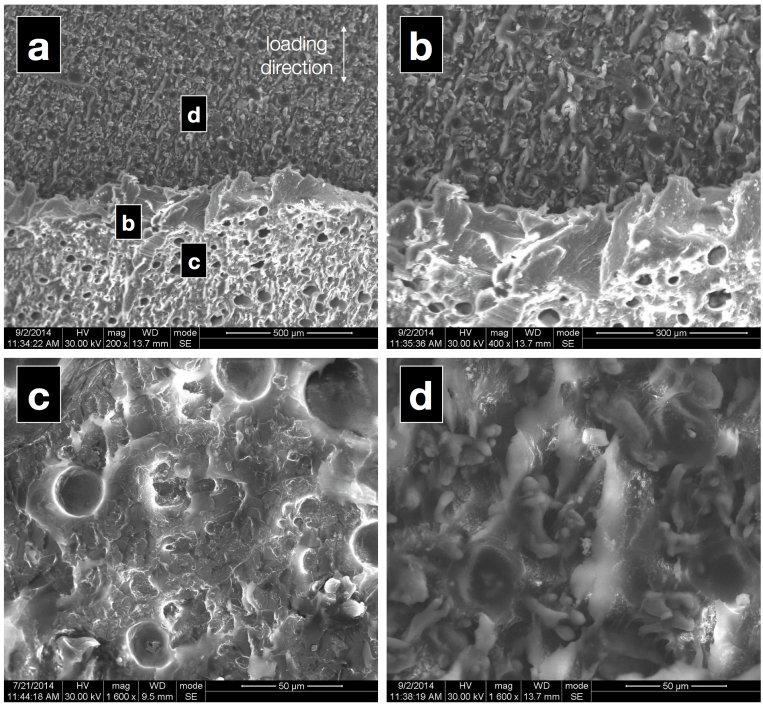

Figure 5.5: Scanning electron microscopy analyses of fracture surfaces associated to TAST samples. (a) Overview of the fracture surface at the transition region where the failure path is diverted from the upper to lower substrate. (b) Close-up image of the transition region where inelastic deformation led to cohesive failure of the adhesive. (c) High resolution image of the fractured surface from the adhesive side displaying inelastic deformations of the adhesive and air voids. (d) Detail of the failed surface displaying epoxy adhesive interlocked with substrate surface asperities (white arrows). [87]

hesive layer to be subjected to prevalent shear loading conditions. In addition, the modification of the surface oxide layer resulted in a better chemical interaction and in higher strength. This is in line with recent research on the subject, showing an optimization of the oxide layer of aluminum substrates carried out by fiber laser ablation [66]. Anyway, surface oxidation might also have an adverse

effect on the strength, since the oxide particles showed in the previous SEM analysis were weakly bonded to the Al substrates and could be easily detached under load.

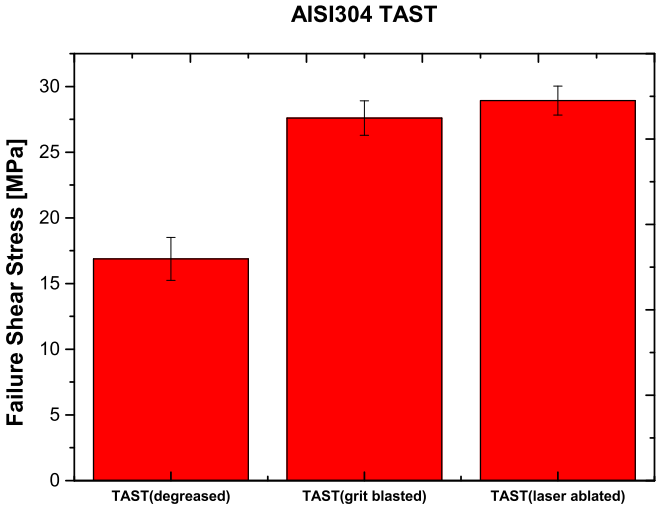

Figure 5.6: Failure shear stress for stainless steel/epoxy joints obtained with the Thick Adherends Shear Test (TAST). [87]

Interestingly, laser ablated AISI304/epoxy TAST joints showed a +77% increase of the failure shear stress with respect to simple degreased joints. In addition, for all three sets of samples there was no apparent plastic deformation after testing. The failure shear stress is reported in Fig.5.6 [87]. These results support the hypothesis made that the effectiveness of the mechanical interlocking effect induced by laser ablation depends on the stress state achieved in the bondline. The closer the stress distribution is to a uniform shear stress, the higher the increase in strength.

5.3 Mode I fracture toughness

Typical load-displacement responses recorded during DCB tests are reported in Fig.5.7 [87]. The global response of the degreased samples displayed some fluctuations in the post peak region (macroscopic crack propagation) if compared to the laser treated and grit-blasted ones, i.e. the response of the latter was indeed smoother.

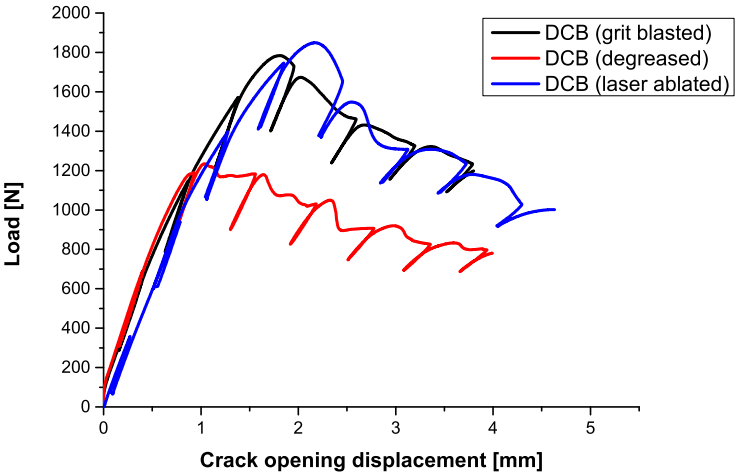

Figure 5.7: Typical load-displacement responses for DCB samples with as produced, grit blasted and laser treated substrates. [87]

The average strain energy release rate (G) was obtained using the procedure outlined earlier in the paper and the results are reported in Fig.5.8 [87] where the bond toughness of the T-peel joints was determined in an earlier work [88] on a similar Al/epoxy material system and using a cohesive zone model approach. It is possible to infer that the laser treatment consistently improved fracture toughness of the joints with respect to simple degreasing since an almost three-fold increase was recorded in conjunction with a lower scatter in the experimental data.

On the other hand grit-blasted specimens registered similar values of G. The increase in fracture toughness of the DCB samples was

concurrent with a shift of the crack path from interfacial (degreased samples) to full in-layer cohesive failure (in both laser ablated and grit-blasted specimens). Post failure visual examination of fracture surfaces displayed surface whitening typically associated with the occurrence of inelastic deformations within the adhesive layer.

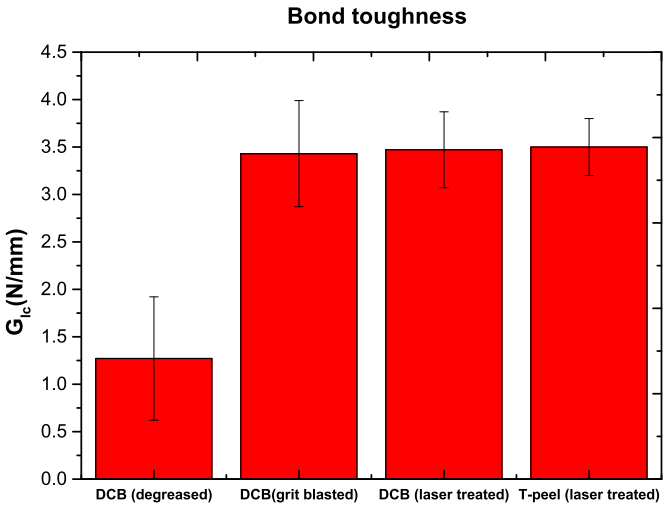

Figure 5.8: Comparison among obtained values of fracture energy for degreased, grit blasted and laser ablated substrates. [87][88]

This may be attributed to the enhancement of mechanical interlocking at the adhesive/substrates interface associated to surface morphological modifications induced by laser ablation. However, it is still not fully cleared if the observed surface oxide chemical modification may play a role on adhesion improvement, too. On the other hand, mechanical interlocking was not observed in as produced specimens since adhesive (interfacial) fracture occurred in all samples tested. SEM analyses of the fracture surfaces have been subsequently carried out. A low resolution image of a typical cohesive fracture occurred in laser treated specimens is shown in Fig.5.9(a) [87]. The SEM images display the air voids mentioned earlier. In addition the high resolutions pictures (b-d) also display

features of the inelastic deformation which led to surface whitening in the course of failure.

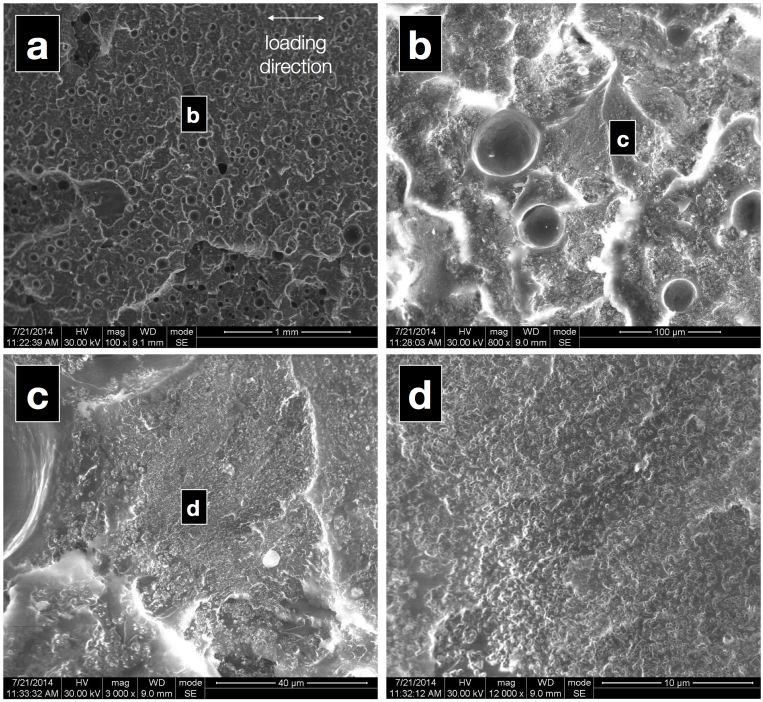

Figure 5.9: SEM images of fracture surfaces for a DCB sample with laser treated substrates. (a) Sample area of the fracture surface displaying air voids likely associated to adhesive mixing and spreading over the substrates. (b-d) High resolution images showing details of the fracture surface and of material deformations leading to cohesive failure. [87]

Despite the cohesive failure, fracture surface does not display an high degree of deformation likely because of a quasi brittle behavior of the adhesive. It is also worth noting that the obtained value of fracture toughness is in quite good agreement with that obtained in T-peel tests carried out on a similar material system in a previous study carried out by Alfano *et al.* [88]. In particular, the joints were bonded with the same epoxy adhesive and cohesive failure was observed; however, since debonding occurred concurrent with ex-

tensive plastic dissipation in the metal substrates, a cohesive model approach was employed to segregate fracture toughness from plastic dissipation.

Conclusions

In the present work, the effect of laser-induced surface patterning on the strength and bonding toughness of adhesive joints was analyzed. Laser ablation was carried out on aluminum alloy and stainless steel substrates using a pulsed Ytterbium fiber laser. An ytterbium-doped pulsed fiber laser was employed to perform laser ablation. The morphological and elemental modifications induced by the laser process were examined using surface profilometry, SEM, and XPS. Aluminum alloy and stainless steel substrates were affected to a different extent by the process. In both cases, there was a threshold value of the laser power after that a several-fold increase of surface roughness was recorded. Single-lap shear joints were then manufactured with a laser treatment at a power of 18 W, which is above the threshold value for both aluminum alloy and stainless steel. The obtained patterns were slightly distorted with respect to the intended ones, and an appreciable degree of mechanical interlocking was only achieved for the stainless steel substrates. The strength was then compared with that of joints with degreased and grit-blasted adherends. SEM observations of the fractured surfaces have shown some areas of imperfect wetting at the stainless steel/epoxy interface, and this might explain the reduced increase of adhesion strength for this joint type. On the other hand, the strength of aluminum alloy joints was enhanced and it was speculated that the modification of surface chemistry of aluminum alloy substrates improved the interactions at the adhesive/substrate interface [64]. Thick Adherend Shear Tests (TAST) were also manufactured and tested following essentially the same procedures employed for the SLS joints. Results demonstrated that laser ablation can effectively increase shear strength of Al/epoxy TAST joints. The obtained value of shear strength registered an average improvement

of about 20% with respect to as-produced adherends. Interestingly [87], AISI304 TAST samples showed a +77% increase of the average shear stress at failure with respect to simple degreasing. In addition, failure always occurred without any apparent plastic deformation. These results support the hypothesis made in the paper that the effectiveness of the mechanical interlocking effect induced by laser ablation depends on the stress state achieved in the bondline. The closer the stress distribution is to a uniform shear stress, the higher the increase in strength. Finally, mechanical tests were conducted on aluminum/epoxy Double Cantilever Beam (DCB) samples in order to evaluate the enhancement in bonding toughness. The results indicated that laser ablation can increase in a efficient manner the fracture toughness of adhesive bonded joints [87]. An almost three-fold increase in fracture toughness was recorded with respect to samples with degreased substrates. In addition, the obtained results are in good agreement with those obtained in past research work on Al/epoxy T-peel joint with laser treated substrates [88].

References

[1] ASTM D1002. Apparent shear strength of single lap joint adhesively bonded metal specimens by tension loading.

[2] Adams R D. *Adhesive Bonding; Science, Technology and Applications*. CRC Press, 2005.

[3] Kinloch A J. *Adhesion and Adhesives; Science and Technology*. Chapman & Hall, London, p. 1, 1987.

[4] Dillard D A. *Advances in Structural Adhesive Bonding*. CRC Press, 2010.

[5] Tabor D and Winterton R H S. *Proc Roy Soc*, (A312):435, 1969.

[6] Johnson K L, Kendall K, and Roberts A D. *Proc Roy Soc*, (A324):301, 1972.

[7] Knock K K and Locke M C. *Proceedings of the 159th Meeting of the American Electrochemical Society, Minneapolis, May*, 1981.

[8] Voyutskii S S. *Adhesives Age*, (5(4)):30, 1962.

[9] Voyutskii S S. *Autohesion and Adhesion of High Polymers, Wiley interscience, New York*, 1963.

[10] Voyutskii S S, Markin Yu I, Gorchakova V M, and Gul V E. *Adhesives Age*, (8(11)):24, 1962.

[11] Deryaguin B V. *Research*, (8):70, 1955.

[12] Deryaguin B V, Krotova N A, Kirillova Y M Karassev V V, and Aleinikova I N. *Proceedings of the 2nd International Congress on Surface Activity-III, Butterworths, London*, page 417, 1957.

[13] Deryaguin B V and Smilga V P. Adhesion, foundamentals and practice. *Mclaren and Son, London*, page 152, 1969.

[14] Pauling L. The nature of the chemical bond. *Cornell University Press, New York*, 1960.

[15] Good R J. Treatise on adhesion and adhesives. *Marcel Dekker, New York*, Vol. 1:15, 1967.

[16] Fowkes F M. Physicochemical aspects of polymer surfaces. *Plenum, New York*, Vol. 2:583, 1967.

[17] Volkersen O. Die nietkraftverteilung in zugbeanspruchten mit konstanten laschenquerschritten. *Luftfahrtforschung*, (15):41–47, 1938.

[18] Goland M and Reissner E. Stresses in cemented joints. *J Appl Mech (Trans ASME)*, (66):A17–A27, 1944.

[19] *Adhesives and Sealants*, volume 3. Engineered Materials Handbook, 1990.

[20] ASTM D 3433. Fracture strength in cleavage of adhesives in bonded metal joints.

[21] Adhesives Toolkit. `http://www.adhesivestoolkit.com/`.

[22] Plueddemann E P. Reminiscing on silane coupling agents. *J Mater Sci*, (4):261–277, 1991.

[23] Gerenser L J, Elman J F, Mason M G, and Pochan J M. ESCA studies of corona discharge treated polyethilene surfaces by use of gas phase derivitisation. *Polymer*, (26):1162–1166, 1985.

[24] Ayers R L and Shofner D L. Preparing polyolefin surfaces for inks and adhesives. *SPE Journal*, (28):51–55, 1972.

[25] Liston E M, Martinu L, and Wertheimer M R. Plasma surface modification of polymers for improved adhesion - a critical review. *J Adh Sci & Tech*, (7):1091–1127, 1993.

[26] Hall J R, Westerdahl C A L, Bodnar M J, and Levi D W. Effect of activated plasma treatment time on adhesive bondability of polymers. *J App Polym Sci*, (16):1465–1477, 1972.

[27] Critchlow G W and Brewis D M. Review of surface pretreatments for aluminium alloys. *Int J Adhesion and Adhesives*, (16):255–275, 1996.

[28] Bijlmer P F A. Adhesive bonding of anodised aluminium. *Metal Finishing*, (70(4)):30–34, 1996.

[29] Wegman R F. *Surface Preparation Techniques for Adhesive Bonding*. Noyes Pubblications, Park Ridge, NJ, 1989.

[30] Kock E, Muss V, Matz C, and De Wit F. Verfahren zur anodischen oxidation, Patent EP0607579 A1, 16 December 1993.

[31] Kwakernaak A. The importance of anodic oxide morphology in relation to adhesion and durability of bonded joints. In *Workshop in Bremen: Anodisation in the Aircraft Manufacturing Industry*. IFAM, Bremen, Germany, 15 April 2004.

[32] LamBert van Vugt Nanomaterials Science. `http://www.lambertvanvugt.com/`.

[33] Broockmann W "Steel adherends" in. *Durability of Structural Adhesives*. Kinloch A J (ed.), Elsevier Applied Science, London, Chapter 7, 306, 1987.

[34] Dahotre N and Harimkar S. *Laser Fabrication and Machining of Mate- rial*. Springer, 2008.

[35] Cullity B D. *Elements of X-ray Diffraction*. Addison-Wesley, Reading, MA, 1991.

[36] Corson D R Lorrain P. *Electromagnetic fields and waves*. WH Freeman, San Francisco, 1970.

[37] ISO 11146. Lasers and laser-related equipment - test methods for laser beam widths, divergence angles and beam propagation ratios, 2005.

[38] Pini S. *Study, automation and planning of micro-machining processes based on infrared pulsed Fiber Laser*. PhD thesis, University of Parma, 2011.

[39] RP Photonics Encyclopedia. `http://www.rp-photonics.com/`.

[40] N. Karube and H. Miura. Full-body laser scribing method of fragile material, March 22 2007. US Patent App. 11/520,020.

[41] Erbium-Doped Fiber Amplifier & CW Laser. `http://hank.uoregon.edu/`.

[42] Dubey A and Yadava V. Laser beam machining-a

review. *Int J of Machine Tools and Manufacture*, (48(6)):609–628, 2008.

[43] Canning J. Fibre lasers and related technologies. *Optics and Lasers in Engineering*, (44(7)):647–676, 2006.

[44] Steen W M and Mazumder J. *Laser Material Processing*. Springer, 2010.

[45] von Allen M. *Laser-beam Interactions with Materials*. Springer, Berlin, 1987.

[46] Bäuerle D. *Laser Processing and Chemistry*. Springer, Berlin, 2000.

[47] Baldan A. *J J Mat Sci*, (39):1, 2004.

[48] Critchlow G W and Brewis D M. *International J Adhesion Adhesives*, (16(4)):255, 1996.

[49] Alfano M, Ambrogio G, Crea F, Filice L, and Furgiuele F. Influence of laser surface modification on bonding strength of al/mg adhesive joints. *J Adhesion Sci Technology*, (25):1261–1276, 2010.

[50] Stammen E, Dilger K, Böhm S, and Hose R. Surface modification with laser: Pretreatment of aluminium alloys for adhesive bonding. *Plasma Processes and Polymers*, (4):39–43, 2007.

[51] Man H C, Zhang X M, Yue T M, and Lau W S. *J Mat Proc Tech*, (66 (1-3)):123, 1997.

[52] Man H C, Zhang X M, and Yue T M. *Materials Letters*, (30 (5-6)):327, 1997.

[53] Baburaj E G, Staikov D, Evans J, Shafeev G A, and Bensaoula A. *Int J Adhesion Adhesives*, (27 (4)):268–276, 2007.

[54] Jahani H R, Moffat B, Mueller R E, Fumo D, Duley W, North T, and Gu B. *App Surf Sci*, (127-129):767, 1998.

[55] Park J K and Mukherjee K. *Mat Manufact Proc*, (13 (3)):359, 1998.

[56] Wong R C P, Hoult A P, Kim J K, and Yu T X. Improvement of adhesive bonding in aluminium al-

loys using laser surface texturing process. *J Materials Processing Technology*, (63):579–584, 1997.

[57] Nonjof C J. *Material Processing with Nd Lasers*. Electrochemical Pubblications Ltd., London, 1988.

[58] Dolgaev S I, Lavrishev S V, Lyalin A A, Simakin A V, Voronov V V, and Shafeev G A. *App Phys A Mat Sci Proc*, (73(2)):177, 2001.

[59] Brailovsky A B, Gaponov S V, and Luchin V I. *Appl Phys Mat Sci Proc*, (61(1)):81–86, 1995.

[60] Adhesives Determination of tensile lap-shear strength of bonded assemblies. DIN EN 1465, 1995.

[61] Boehm S, Stammen E, Hose R, Horn-Solle H, Lammel C, and Dirscherl F. Integration eines laservorbehandlungssystems in eine moderne klebtechnische serienfertigung. *Abschlußbericht INTLASKLEB*, 2004.

[62] Rechner R, Jansen I, and Beyer E. Influence on the strength and aging resistance of aluminium joints by laser pre-treatment and surface modification. *Int J Adhes Adhes*, (30):595–601, 2010.

[63] Jansen I, Wust H, and Beyer E. *Adhäsion-Kleben und Dichten*, (4):44, 2006.

[64] Alfano M, Pini S, Chiodo G, Barberio M, Pirondi A, Furgiuele F, and Groppetti R. Surface patterning of metal substrates through low power laser ablation for enhanced adhesive bonding. *J Adhes*, (90):384–400, 2014.

[65] Palmieri F L, Watson K A, Morales G, Williams T, Hicks R, Whol C J, Hopkins J W, and Connel J W. In *Int SAMPE Tech Conf, Baltimore, USA*, 2012.

[66] Rechner R, Jansen I, and Beyer E. *J Laser Appl*, (032002):24(3), 2012.

[67] Langer M, Rechner R, Thieme M, Jansen I, and Beyer E. *Solid State Sci*, (14):926–935, 2012.

[68] Alfano M, Ambrogio G, Filice L, Furgiuele F, Gallus E, and D'Antuoni D. *Key Eng Mat*, (473):237–242, 2011.

[69] Galantucci et al. Surface treatment for adhesive-

bonded joints by excimer laser. *Composites Part A*, (27A):1041–1049, 1996.

[70] Baburaj et al. Enhancement of adhesive joint strength by laser surface modification. *Int J Adhesion & Adhesives*, (27):268–276, 2007.

[71] Spadaro et al. Laser surface treatments for adhesion improvement of aluminium alloys structural joints. *Radiation Physics and Chemistry*, (76):1441–1446, 2007.

[72] Man et al. Laser surface micro-drilling and texturing of metals for improvement of adhesion joint strength. *Applied Surface Science*, (256):3166–3169, 2010.

[73] Maressa et al. Effect of surface texture on the adhesion performance of laser treated ti6al4v alloy. *J of Adhesion*, (91(7)):518–537, 2015.

[74] Alfano M, Lubineau G, Furgiuele F, and Paulino G H. *Int J Fract*, (171(2)):139–150, 2011.

[75] Alfano M, Lubineau G, Furgiuele F, and Paulino G H. *Int J Adhes Adhes*, (39):33–41, 2012.

[76] da Silva L F M, Ferreira N M A J, Richter-Trummer V, and Marques E A S. *Int J Adhes Adhes*, (30(8)):735–743, 2010.

[77] Kim W S, Yun I, Lee J J, Jung H T, and Lee J J. *J Adhes*, (30):408–417, 2011.

[78] Lee M J, Kim W S, Jang C J, Kim K H, Cho T M, Lee B C, and Lee J J. *J Adhes*, (87):826–841, 2011.

[79] Cordisco F, Zavattieri P D, Hector L G, and Bower A F. *Eng Fract Mech*, (96):192–218, 2012.

[80] Goncalves Teixeira F and da Silva L F M. *J Adhes*, pages 671–687, 2011.

[81] UNI EN 14869-2. Determination of shear behaviour of structural bonds - part 2: Thick adherend shear test, 2004.

[82] Krenk S. Energy release rate of symmetric adhesive joints. *Engineering Fracture Mechanics*, (43(4)):549–559, 1992.

[83] ISO Standard 13565-2. Geometrical Product Specification (GPS) - surface texture: profile method; sur-

faced having stratified functional properties. Part 2: Height Characterization Using the Linear Material Ratio Curve, 1996. International Standard Organisation, Geneva, Switzerland.

[84] NIST XPS Database. `http://srdata.nist.gov/xps/`.

[85] Cassie A B D and Baxter S. *Trans Faraday Soc*, (40):546–551, 1995.

[86] Kafkalidis M S and Thouless M D. The effects of geometry and material properties on the fracture of single lap-shear joints. *Int J Solids Struct*, (39):4367–4383, 2002.

[87] Chiodo G, Alfano M, Pini S, Pirondi A, Furgiuele F, and Groppetti R. On the effect of pulsed laser ablation on shear strength and mode I fracture toughness of al/epoxy adhesive joints. *J Adhesion Sci Tech*, submitted for pubblication.

[88] Alfano M, Furgiuele F, Pagnotta L, and Paulino G H. Analysis of fracture in aluminum joints bonded

with a bi-component epoxy adhesive. *J Testing Eval*, (39(2)), 2011.

Ringraziamenti

Desidero ringraziare quanti, in modo più o meno diretto, mi hanno aiutato, ispirato o più semplicemente incoraggiato in questi tre anni di dottorato.

Ringrazio tutta la mia famiglia e in particolare mamma e papà, ai quali è dedicata la tesi. Grazie al Prof. Pirondi, al quale sono grato per gli insegnamenti e gli importanti suggerimenti ricevuti durante i tre anni di dottorato. Ringrazio il Dott. Ing. Alfano per la collaborazione nell'attività di ricerca e la Dott.ssa Barberio per aver effettuato le analisi SEM e XPS. Grazie a Stefano per il supporto ricevuto nella realizzazione dei trattamenti laser. Infine un ringraziamento a tutti i componenti del mio gruppo di ricerca: Fabrizio, al quale sono grato in particolare per avermi insegnato ad utilizzare le attrezzature in laboratorio, il mio collega di dottorato Gregorio, Enrico e Matteo.